Berichte des Deutschen Wetterdienstes

190

Model Calculations and Measurements of Chemically and Biologically Effective UV Radiation Reaching the Ground

Uwe Feister

Offenbach am Main 1994
Selbstverlag des Deutschen Wetterdienstes

Auf säurefreiem Papier gedruckt.

ISSN 0072-4130
ISBN 3-88148-302-0

Herausgeber und Verlag

Deutscher Wetterdienst
Zentralamt
Frankfurter Str. 135
63067 Offenbach am Main

Anschrift des Autors

Dr. Uwe Feister
Deutscher Wetterdienst
Observatorium Potsdam
Telegrafenberg
14473 Potsdam

Content page

Summary

Solar ultraviolet radiation ($\lambda < 400$ nm) affects the biosphere, some materials and the chemistry of atmospheric trace species. A change in atmospheric ozone, which absorbs part of the solar UV radiation, can influence UV radiation effects to man (e.g. erythema, carcinogenesis, eye damage) and plant life, and it also changes the photolysis rates of a number of atmospheric trace gases. The model used to simulate solar global UV radiation was compared with results of other model calculations and with measurements of spectral and broad-band UV irradiance. The differences are discussed in terms of the uncertainties in the input parameters to the model as well as to the uncertainties in the model and in the measurements.

Using this radiation model to simulate the spectral radiation reaching the lower atmosphere, Radiation Amplification Factors (RAF) were determined that describe the percentage increase in biologically and chemically effective radiation for a number of effects, when the total ozone amount is reduced by 1 %. The dependences of RAFs on the ozone amount and on solar zenith angle are shown to vary according to the shapes of their action spectra. A "saturation effect" is observed in some RAF values, i.e. with further increases in ozone mass the RAF can remain constant or even decrease. High values of RAF in the photolysis frequencies occur for the photodissociation of tropospheric ozone. The RAF of ozone photolysis is found to be 1.5 to 2.0 with zenith angles from 0° to 60°, i.e. a reduction of total ozone by 1 % enhances the photolysis of ozone and the subsequent OH production by 1.5 to 2 %.

The latitudinal and seasonal variation of the effective radiation for average conditions of total ozone and cloudiness was calculated. Ratios between effective UV radiation and total UV radiation, which are similar in their variations with zenith angle to the ratios between effective UV radiation and visible or photosynthetically active radiation (PAR), are almost constant in the seasonal course at low latitudes, while at higher latitudes these ratios show seasonal changes by 1 to 2 orders of magnitude. As ecosystems are adapted to the natural levels of those ratios, such as, for example, the ratio between plant damage in the UVB region and photosynthetic radiation in the visible region, consideration of the whole spectrum of radiation, not only the UVB region, should be a reasonable approach.

Ozone measurements at Potsdam had shown extremely low values in 1992 and 1993 with annual means of about 10 % below the long-term mean. Using the monthly mean ozone values monthly values of the biologically effective UV irradiation for clear sky conditions were modelled. It turned out that the biologically effective UV radiation must have been by 10 to 30 % above the long-term mean, with enhancements in the individual summer months of up to 40 %. Measurements of global radiation in the whole spectrum as well as in the UV region were used to estimate the effect of cloudiness on the biologically effective UV radiation for each month. The combined effect of ozone and cloudiness resulted in enhancements of the annual totals of biologically effective radiation at Potsdam by 10 to 30 % in 1992 and by 5 to 20 % in 1993.

Zusammenfassung

Die solare UV-Strahlung ($\lambda < 400$ nm) beeinflußt die Biosphäre, einige Materialien und die Chemie atmosphärischer Spurengase. Eine Mengenänderung des atmospärischen Ozons, das einen Teil der solaren UV-Strahlung absorbiert, kann zur Änderung der Wirkung der UV-Strahlung auf den Menschen (z.B. Erythem, Karzinogenese, Augenschäden) und auf Pflanzen führen und die Photolyseraten einer Reihe von atmosphärischen Spurengasen beeinflussen. Das hier benutzte Modell zur Simulation der solaren UV-Globalstrahlung wurde mit Ergebnissen anderer Modellrechnungen und mit spektralen sowie Breitband-Messungen der UV-Strahlung verglichen. Die Differenzen zwischen den verschiedenen Modellrechnungen und den Messungen werden im Hinblick auf Unsicherheiten der Eingansparameter des Modells, des Modells selbst sowie der Messungen diskutiert.
Durch Anwendung des Modells zur Berechnung der die untere Atmosphäre erreichenden spektralen Strahlung wurden Strahlungsvervielfachungsfaktoren (RAF) bestimmt, die die prozentuale Zunahme der biologisch und chemisch wirksamen Strahlung für verschiedene Wirkungen bei Abnahme des Gesamtozongehalts um 1 % beschreiben. Die Abhängigkeit der RAF vom Ozongehalt und vom solaren Zenitwinkel wird durch die Form des jeweiligen Wirkungsspektrums bestimmt. In den Werten einiger RAF zeigt sich ein "Sättigungseffekt", d.h. bei zunehmender Ozonmasse bleibt der RAF konstant oder nimmt sogar ab. Große RAF-Werte der Photolysefrequenzen ergeben sich für die Photodissoziation des troposphärischen Ozons. Der RAF der Ozon-Photolyse beträgt 1.5 bis 2.0 für Zenitwinkel von 0° bis 60°, d.h. die Verringerung des Gesamtozons um 1 % erhöht die Ozonphotolyse und die nachfolgende OH-Produktion um 1.5 bis 2 %.
Es wurden die Variationen der wirksamen Strahlung mit der geographischen Breite und mit der Jahreszeit für mittlere Bedingungen der Bewölkung und des Gesamtozons berechnet. Die Verhältnisse zwischen wirksamer UV-Strahlung und UV-Gesamtstrahlung, deren Variationen mit dem Zenitinkel den Verhältnissen zwischen wirksamer UV-Strahlung und sichtbarer oder photosynthetisch aktiver Strahlung (PAR) sehr ähnlich sind, erweisen sich in niederen Breiten als nahezu konstant im jahreszeitlichen Verlauf, während sie in höheren Breiten jahreszeitliche Änderungen um 1 bis 2 Größenordnungen zeigen. Da Ökosysteme an das natürliche Niveau dieser Verhältnisse angepaßt sind, sollte nicht nur der UVB-Bereich sondern das gesamte Spektrum in die Messungen und Modellierungen einbezogen werden.
Ozonmessungen in Potsdam hatten extrem niedrige Werte in den Jahren 1992 und 1993 gezeigt, wobei die Jahresmittelwerte um 10 % unter dem Langzeitmittelwert lagen. Mit den Monatsmittelwerten des Ozons wurden monatliche Werte der biologisch wirksamen Strahlung für wolkenlose Bedingungen berechnet. Es zeigte sich, daß die wirksame UV-Strahlung im Jahresmittel um 10 bis 30 %, in einzelnen Sommermonaten sogar um 40 % über den Langzeitmittelwerten gelegen haben muß. Anhand der Messungen der Globalstrahlung im gesamten Spektralbereich und im UV-Bereich wurde der Effekt der Bewölkung auf die biologisch wirksame UV-Strahlung abgeschätzt. Der kombinierte Effekt von Ozongehalt und Bewölkung dürfte zu einer Erhöhung der biologisch wirksamen UV-Strahlung in Potsdam um 10 bis 30 % im Jahre 1992 und um 5 bis 20 % im Jahre 1993 geführt haben.

1 Introduction

Solar UV radiation, which is defined as the radiation in the wavelength range 100 to 400 nm, affects the biosphere, damages materials and triggers the photodissociation of many atmospheric trace gases. Due to absorption by stratospheric ozone, solar UV radiation with wavelengths $\lambda < 290$ nm does not reach the lower atmosphere and the earth's surface, and radiation in the wavelength region from 290 to 340...350 nm is reduced depending on the absorbing ozone mass. Nevertheless, the remaining energy of solar radiation with $\lambda > 290$ nm is powerful enough to trigger biological processes and chemical reactions. The influence of UV radiation on human health manifests as immunosuppression reactions, erythema and carcinogenesis of the skin, and ocular damage. Growth and yield of many plants are reduced by UV radiation, and aquatic ecosystems such as phytoplankton, zooplankton and juvenile fish can be damaged as well by UV radiation (e.g. TITUS 1986, UNEP 1989, 1991, FREDERICK 1990, WHO 1994). Photochemical reactions of trace gases in the lower atmosphere are also driven by solar UV radiation. As an example, photolysis of ozone in the troposphere triggered by UV radiation with wavelengths $\lambda < 310$ nm is an important ozone loss mechanism, which accounts for more than half of the hydroxyl radical production in the troposphere. The subsequent attack of many atmospheric source gases by OH radicals triggers reaction chains for the destruction of those trace gases. On the other hand, the photochemical production of photooxidants such as ozone from nitrogen dioxide depends on UV radiation. In this way, chemical processes in the middle atmosphere such as stratospheric ozone loss due to chlorofluorocarbon release can affect the oxidizing capacity of the troposphere (e.g. LIU and TRAINER 1988, MADRONICH and GRANIER 1992).
A variety of models has been developed to solve the radiative transfer equation or to parameterize the processes of absorption and scattering of radiation, and they have been applied to simulate the spectral UV radiation reaching the lower atmosphere (e.g. HINZPETER 1955, 1956, 1957, CHANDRASEKHAR 1960, DAVE and FURUKUWA 1966, DEIRMENDJIAN 1969, McCULLOUGH 1970, LIOU 1973, BRASLAU and DAVE 1973a, b, SHETTLE and GREEN 1974, GREEN et al. 1974a, b, HALPERN and DAVE 1974, COAKLEY and CHYLEK 1975, MO et al. 1975, KERSHGENS et al. 1976, JOSEPH et al. 1976, PALTRIDGE and BARTON 1978, DOZIER 1980, ELANSKIJ et al. 1980, GREEN et al. 1980, ZDUNKOWSKI et al. 1980, GERSTL et al. 1981, 1983, HENSE et al. 1982, SCHIPPNICK and GREEN 1982, BJÖRN and MURPHY 1986, BIRD and RIORDAN 1986, MADRONICH 1987, NAKAJIMA and TANAKA 1986, SMITH et al. 1992, TSAY and STAMNES 1992, RUGGABER et al. 1993). Model simulations of solar UV radiation can be used to evaluate possible consequences that changes in atmospheric ozone, cloudiness and turbidity can have on the radiation and its effects to the biosphere and air chemistry. In this paper we focus on the results of model calculations that simulate biological and chemical effects of UV radiation and their changes. The model version is compared to irradiance measurements, and the differences between model calculations and measurements are discussed.

2 Model description

The model developed by GREEN et al. (1974 a, b, 1980) and SCHIPPNICK and GREEN (1982) including the modifications applied by RUNDEL (1986) was selected as the basic approach, because it has proven to be a good compromise between computer time and accuracy. The model was originally fitted to measurements of UV radiation by BENER (1972) and radiative transfer calculations using the discrete ordinate method by SHETTLE and GREEN (1974), and it was later improved by applying model calculations of BRASLAU and DAVE (1973 a, b), DAVE and HALPERN (1976), PETERSON (1976, 1977) and DEIRMENDJIAN et al. (1980).
In the present version, the spectral range of the model is extended to the wavelength region 250 to 400 nm with a stepwidth of 1 nm. In addition to the parameterized extraterrestrial radiation used in the original version

$$I(\lambda) = \frac{0.582}{R^2} \left(\frac{\lambda_0}{\lambda}\right)^5 \frac{\exp(9.102) - 1}{\exp\left(\frac{9.102\ \lambda_0}{\lambda}\right) - 1} \left\{ 1 + \sum_{i=1}^{6} a_i \exp\left[-\frac{(\lambda - b_i)^2}{2\ c_i^2}\right] \right\} \qquad (1)$$

where R is the distance sun-earth in astronomical units and a_i, b_i, c_i are coefficients, measurements of extraterrestrial radiation as given by the WMO Commision for Instruments and Methods of Observation (CIMO 1981, FRÖHLICH and LONDON 1986) have been used that correspond to a solar constant of 1367 W m^{-2}. Variations of the extraterrestrial radiation for wavelengths $\lambda > 300$ nm are smaller than 0.5 % within the 27 day solar rotation and less than 1 % within the 11 year solar cycle, but can extend to 6 % in a strong Fraunhofer absorption line (MO 1985, LEAN 1987). It can be assumed that the absolute uncertainty of measured values of extraterrestrial radiation is at least (5 ... 10) % (BRUCKNER et al. 1976, WHITE 1977, MOUNT et al. 1980, THEKAEKARA and DRUMMOND 1981, NICOLET 1980, 1989, MENTALL and WILLIAMS 1988). Another difference between the model version used here and the original one is the ozone absorption that can be calculated in our approach from measured ozone absorption coefficients taken from BASS and PAUR (1985) for stratospheric temperatures instead of the parameterization of ozone optical thickness (absorption coefficient times absorber amount) in the basic version

$$\tau_{O_3}(\lambda) = O_3 \frac{a\ (b + 1)}{b + \exp\left(\frac{\lambda - \lambda_0}{c}\right)} \qquad (2)$$

with O_3 the total ozone amount, $\lambda_0 = 300$ nm and a, b, c being constants (cf. RUNDEL 1986). We chose a = 9.788 atm-cm^{-1}, b = 0.0556 and c = 6.798 nm. The absolute uncertainty of the measured ozone absorption coefficients is estimated to be about (1 ... 2) % (DAUMONT et al. 1992). Note that the ozone absorption coefficients by BASS and PAUR (1985) applied in the model calculations described here are compatible with those used for regular measurements of total ozone in the stations network since 1992. The absorption coefficients, which have been in use in the Global Ozone Observing System since

January 1, 1992, provide ozone values being 2.7 % lower for ozone measurements derived from direct sun observations of the AD double wavelength pair than those derived before that date (HUDSON et al. 1991, KOMHYR 1991).
The optical thickness of molecular *Rayleigh scattering*

$$\tau_{AIR}(\lambda) = 1.221 \left(\frac{\lambda_0}{\lambda}\right)^{4.27} \quad (3)$$

was not changed, but the optical thicknesses of *scattering and absorption by aerosols* were changed according to the parameterization

$$\tau_{AER,S}(\lambda) = f \cdot 0.0804 \cdot \left(1 + 0.256 \frac{\lambda - \lambda_0}{\lambda_0}\right) \quad (4)$$

$$\tau_{AER,A}(\lambda) = f \cdot 0.0136 \left(1 - 0.441 \frac{\lambda - \lambda_0}{\lambda_0}\right) \quad (5)$$

(λ_0 = 300 nm). The constant f has been introduced to account for variable scaling of aerosol optical depths that have been observed to reach values between $\tau = 0.1$ and $\tau = 1$ at λ = 380 nm (GUŠČIN 1986, GABM 1989). Table 1 shows some examples of typical f values and the resulting optical thicknesses τ_{AER}.
Ratios between absorption by aerosols and scattering are held constant at 15 %. Model results obtained for a solar zenith angle of $\Theta = 0°$ and weak, strong and very strong aerosol extinction show global UV radiation to be lower by 3 %, 11 % and 25 %, respectively, than in an aerosol-free atmosphere. The corresponding reductions for zenith angles $\Theta = 60°$ are 5 %, 18 % and 39 %.
A generalized cosine function is used instead of the cosine of solar zenith angle to account for the curvature of the earth. Vertical profiles of optical depths for air, aerosols and ozone are parameterized as standard curves according to the formula given by GREEN et al. (1980).

Table 1 Aerosol optical depths for aerosol scattering and absorption ($\tau_{AER,S}$, $\tau_{AER,A}$) and selected constants f; for illustration, optical depths at the wavelength 550 nm were calculated with Angström's turbidity formula $\tau(\lambda) = \beta \lambda^{-\gamma}$ (λ in μm) assuming the frequently used value $\gamma = 1.3$

aerosol load	f	λ = 350 nm		λ = 550 nm	
		$\tau_{AER,S}$	$\tau_{AER,A}$	$\tau_{AER,S}$	$\tau_{AER,A}$
weak	1.00	0.084	0.013	0.047	0.007
strong	4.18	0.350	0.053	0.194	0.029
very strong	8.36	0.701	0.105	0.390	0.058

It must be mentioned that variations of the vertical ozone profile, particularly in the lower troposphere, can affect the model results, because scattering of radiation and thus absorption is stronger with higher air density in the lower atmosphere than with lower pressure in the higher atmosphere (BRÜHL and CRUTZEN 1989). This effect, which can not be accounted for in the model, may have contributed to the uncertainty of the model and the differences observed between model calculations and measurements. On the other hand, the calculations discussed here do not refer to long-term ozone variations that are of opposite direction in the troposphere and stratosphere. Therefore, for the present purpose, the vertical ozone distribution need not be changed. Table 2 shows some examples how the use of measurements of extraterrestrial radiation and ozone absorption coefficients instead of the original parameterizations affect the modelled UV radiation. We will designate the wavelength regions *UV* as $\lambda < 400$ *nm, UVB* as $280 < \lambda < 315$ *nm* and *UVA* as $315 < \lambda < 400$ *nm*.

It can be seen that the measured values of extraterrestrial radiation provide about (2 ... 4) % in the UVB and 7 % in the UVA region lower values of global UV radiation than the parameterization of eq. (1). The measured ozone absorption coefficients produce UVB radiation values being by (1 ... 11) % higher than those determined with the parameterization of eq. (2). If both measured values of extraterrestrial radiation and ozone absorption coefficients are used in combination, the differences in global UV radiation compared to the original parameterized version of the model are - 5 % in the UVA and +(5 ... 10) % in the UVB region.

Table 2 Percentage differences P in global UV radiation calculated for different ozone values and solar zenith angles

a) between UV radiation determined with measured values of extraterrestrial radiation (CIMO 1981) and UV radiation determined with the parameterization of eq. (1)

b) between UV radiation determined with ozone absorption coefficients by BASS and PAUR (1985) and UV radiation determined with eq. (2)

	P [%] $\Theta=0°$ $O_3=320$ D	**P [%] $\Theta=60°$ $O_3=320$ D**	**P [%] $\Theta=60°$ $O_3=600$ D**	**P [%] $\Theta=0°$ $O_3=160$ D**
a) UV ($\lambda < 400$ nm)	- 6.6	- 6.9	- 7.0	- 6.5
a) UVA ($315 < \lambda < 400$ nm)	- 6.7	- 6.9	- 7.0	- 6.7
a) UVB ($\lambda < 315$ nm)	- 4.0	- 3.3	- 1.8	- 3.6
b) UV	0.4	0.5	0.8	0.2
b) UVA	0.3	0.5	0.8	0.1
b) UVB	3.1	6.1	10.8	1.0

3 Comparison between model calculations and measurements

3.1 Calibration of instruments

Comparisons between the modelled irradiance and measurements of solar radiation can help to determine the range of uncertainty of the model results. In that case, one has to keep in mind that measurements do not provide the "true" value, but can also contain systematic and random errors. Measurements from two types of instruments have been available for comparison with the model. One of the instruments used is a spectroradiometer OL 752/10 by Optronic Laboratories. This instrument was calibrated with a 200 W tungsten halogen lamp operated at a constant current of 6.500 A. The lamp was calibrated at the National Institute of Standards and Technology (NIST) against an Eppley standard cell (SCHNEIDER and GOEBEL 1984). The uncertainties in the calibration level of the standard and its transfer result in a quoted spectroradiometric accuracy of the OL 752 instrument relative to the NIST standard source of $\pm$ (2 ... 4) % with an absolute wavelength accuracy of $\pm$ (0.2 ... 0.3) nm over the whole operating spectral range 250 nm to 800 nm. Frequent checks of the spectrometer's calibration level and wavelength stability can be made with a dual calibration and gain check source module consisting of a tungsten halogen source of 5 W and a mercury line source of 4 W. The spectrometer was used in such a configuration of entrance, middle and exit slits that a spectral half-band width (full width at half-maximum) of 1.5 nm was reached. A step width of 2 nm in the range 290 nm to 430 nm was selected for our measurements. Comparisons between the NIST 200 W standard lamp and a 1000 W quartz halogen lamp, which had been calibrated at the Physikalisch-Technische Bundesanstalt (PTB), showed that using the latter calibration level would have lowered the measured irradiance by 3 % at 400 nm to 7 % at 300 nm. It should be noted that the calibration level of the 1000 W source was confirmed within uncertainties of $\pm$ (1 ... 2) % by measurements with a 800 W lamp, which had been calibrated at the PTB and which was made available by KAASE (1993) from the Lichttechnisches Institut of the Technical University Berlin. The remaining overall uncertainty in the **absolute** calibration scale of the OL 752 instrument is estimated to be on the order of $\sim$ 5 %.

The instrument's cosine error, which was determined in our laboratory (Fig. 1), is eliminated from the measured spectra in the process of analysing the data. For that purpose, global and diffuse irradiance components are measured subsequently, the latter by using a shade disc, to determine direct irradiance. The direct irradiance is then cosine corrected and used to calculate a cosine corrected global irradiance (FEISTER 1994). Internal stray light in the spectrometer at the shortest wavelengths was reduced by extrapolating the irradiance for $\lambda < 295$ nm using the spectral irradiance in the region 295 nm $< \lambda <$ 300 nm instead of using the measured irradiances.

The second type of instruments used in the comparsion with model calculations is a filter instrument (FEISTER et al. 1992). Two spectral ranges with halfwidths corresponding to the wavelengths λ_1 = 310 nm and λ_2 = 320 nm (UV-S), and λ_1 = 295 nm and λ_2 = 387 nm (UV-L) were selected from the records. The nominal sensitivities shown in Fig. 2 refer to the whole filter sets and foreoptics including the spectral response of the photocell receiver.

The overall uncertainty of the instruments was estimated to be ± (5 ... 10) %. Their calibration procedure, which was carried out with a 200 W halogen lamp, was based on the effective half-width of the filter sets, i.e. the recorded irradiance data are considered to represent solar irradiance in the wavelength region of the filter halfwidth (FEISTER et al. 1992). To make the filter measurements comparable to the measurements taken with the spectrometer another approach was taken. For that purpose, the irradiance spectra taken with the OL 752 spectrometer on a cloudless day were weighted with the response curves of the filter instruments shown in Fig. 2. Those simulated filter measurements were used to determine scaling factors to the concurrent measurements taken with the filter instruments. The scaling factors turned out to be 2.25 for the UV-S instrument and 1.05 for the UV-L instrument. The high scaling factor for the UV-S instrument is due to the long-wave tail in the filter characteristics (Fig. 2). An approach other than described for the spectrometer was applied to eliminate the cosine error of measurements taken with the filter instruments. As only global irradiance of UV-S and UV-L and not the radiation components were recorded, the global irradiance was multiplied by constants F to eliminate the cosine error in the global irradiance

$$F(\Theta) = \frac{1}{X(\Theta)} \cdot \frac{E_B}{E} + \frac{E\downarrow}{E} \qquad (6)$$

(X (Θ): cosine error of UV-S or UV-L, E_B: direct irradiance, E↓: diffuse irradiance, E: global irradiance). The ratios between direct and global irradiance E_B/E and between diffuse and global irradiance E↓/E were taken from model calculations for classes of zenith angles $0° < \Theta < 85°$. The resulting F values are in the range $0.99 < F < 1.06$. It is mentioned that equation (6) is applicable for cloudless conditions only.

3.2 Input values to the model and results of the comparison

If the model is to be compared to measurements of spectral irradiance, the uncertainties in the input parameters to the model calculations need to be known. Atmospheric total ozone was determined from measurements taken with the Potsdam Dobson spectrophotometer #71 on the AD double wavelength pairs. Concurrent measurements with the Brewer spectrophotometer #30 were used to confirm the ozone observations taken with the Dobson instrument. Daily mean values of ozone derived from direct sun observations with Dobson instrument #71 and with Brewer instrument #30 at Potsdam were shown to be generally within ± (1 ... 2) % (FEISTER 1992), while the absolute uncertainty of direct sun ozone observations using a Dobson instrument is estimated to be ± (1 ... 3) % (BASHER 1982). The total ozone value on the day of the comparison (May 15, 1992) was determined from those measurements to be (336 ± 3) D[1], which is near to the overall long-term average of

[1] 1 D = 1 Dobson = 1 matm-cm = 2.1414 μg cm^{-2} = 2.6868 . 10^{16} cm^{-2} is defined as the length of a column of pure ozone at STP (0 °C, 101325 Pa).

ozone of 348 D at Potsdam. The surface albedo (dry grass) was determined from spectroradiometric measurements to increase from 2 % at 300 nm to 6 % at 430 nm. Therefore, the model calculations were carried out for a surface albedo of 5 %. The Angstrom turbidity coefficient for $\lambda < 625$ nm determined from 15 pyrheliometric measurements was $\beta = 0.179 \pm 0.025$. Using the Angstrom turbidity formula $\tau = \beta \cdot \lambda^{-\gamma}$ with the usual assumption of $\gamma = 1.3$ provides an optical thickness at the wavelength of 350 nm of $\tau_{350} = 0.70$, which was taken as input to the model calculations.

As an example of the comparison, Fig. 3 shows the ratios between a measured spectrum and the corresponding model calculation for May 15, 1992. Due to the greater stepwidth of 2 nm in the measurements as compared to the stepwidth of 1 nm in the model calculations the ratios show some scatter, but except at the shortest wavelengths ($\lambda < 310$ nm), where the measured irradiance is up to 10 % lower than the model result, there is no remarkable systematic difference between measured and modelled irradiance at longer wavelengths. Similar results have been found for the other spectra. It is noted that the original parameterization of the ozone absorption coefficients (see equation (2) for the optical thickness) instead of using measured ozone absoprtion coefficients by BASS and PAUR (1985) would have produced by (6 ... 8) % lower modelled irradiance values in the UVB region and thus much smaller differences between the measurements and model calculations in that spectral region. On the other hand, it might be speculated that part of the differences between the model and the measurements at the shortest wavelengths might be caused by tropospheric ozone that had a higher actual percentage on May 15, 1992 than is assumed in the model. Due to the stronger scattering of radiation, ozone molecules in the troposphere act as stronger absorbers of UV radiation than ozone molecules in the stratosphere, particularly at small solar zenith angles (BRÜHL and CRUTZEN 1989). This possible cause remains to be uncertain to explain the discrepancies between the model and the measurements, as ozone soundings at the nearby Observatory Lindenberg are not available on that day.

Figure 4 shows the percentage ratios of diffuse/global and direct/global irradiance components both from a measured and a modelled spectrum. The high percentage of scattered radiation (60 ... 80) % to global radiation is approximately reproduced by the model, except at the shortest wavelengths, where the modelled diffuse irradiance is somewhat higher than the measured irradiance. This discrepancy may at least partly be caused by instrumental stray light that becomes more relevant in the diffuse component, which has a lower intensity than the global irradiance. It should also be noted that the high percentage of diffuse radiation to global radiation in the UV region appreciably reduces the effect of the cosine error on global irradiance.

Figures 5 and 6 show a comparison between filter measurements of May 15, 1992, spectrometric measurements weighted for the filter response curves as well as model calculations. The short-time step increase in both types of measurements around noon time is due to a small cloud that moved over the observing site and led first to a decrease and later to an increase in irradiance probably by additional forward scattering of radiation. It is noted here that the measurements of the filter instruments were determined from hourly totals, while the irradiance spectra taken with the OL 752 instrument as well as the model

calculations refer to a shorter period of time. It can be seen in the Figures 5 and 6 that the model calculations reflect the measurements of UV-S with only small deviations, while they are about 5 % smaller than the values measured with the UV-L instrument. The cause of that discrepancy can be ascribed to the combined effect of uncertainties in the model and in the measurements.

4 Effective solar radiation

4.1 Biologically effective radiation

Effects of radiation are usually described by *action spectra* φ (λ) that define the normalized spectral response X of biological organisms (man, animal, plants etc.) or materials

$$E_X\ (\Theta,\ z,\ A,\ \tau) = \int_0^\infty \varphi\ (\lambda)\ \ E\ (\lambda,\ \Theta,\ z,\ A,\ \tau) \qquad d\lambda \qquad\qquad [W\ m^{-2}]_X \tag{7}$$

where E (λ, Θ, z, A, τ) is the spectral irradiance incident on a horizontal plane at the height z for the solar zenith angle Θ, the surface albedo A and the optical depth τ. The index X used in E_X and the unit $[W\ m^{-2}]_X$ is to indicate the *effective* (weighted with the action spectrum) quantity.

Photodissociation of atmospheric trace gases is analogously described by eq. (7). In that case, $J \equiv E_{AC}$ is the photolysis frequency in $[s^{-1}]$, $E^{\cap}$ (λ, Θ, z, A, τ) is the spectral radiation falling on a **sphere**, i.e. the "actinic flux" in photons $cm^{-2}\ s^{-1}\ nm^{-1}$, and

$$\varphi\ (\lambda) = \sigma\ (\lambda) \cdot \Phi\ (\lambda) \tag{8}$$

with σ (λ) being the absorption cross section of the photolyzed gas in cm^2 and Φ (λ) the dimensionless quantum yield of the photodissociation reaction. The product of photolysis frequency J and the number density of the photolyzed gas is called the photolysis rate or rate constant given in $cm^3\ s^{-1}$.

Hourly totals of effective irradiance, i.e. effective irradiation in $[J/m^2]_X$, were determined as sums of 6 values calculated for every 10 minutes and multiplied by 600. Daily totals were summed from the values of irradiation calculated between sunrise and sunset. Solar zenith angles, time equation and distance between sun and earth for each time and location were calculated from algorithms given by SONNTAG (1989). The uncertainty of the zenith angle calculated from that algorithm is estimated to be $\pm$ 55'' equalling $\pm$ 0.0153° for zenith angles $\Theta < 85°$ and thus much smaller than that of the most commonly used algorithms. A summary of that algorithm is given in Annex 1.

As an example of the ozone effect to global UV irradiance, Fig. 7 shows the spectral irradiance calculated at steps of 1 nm for a zenith angle of 0° and for different values of total ozone. The shift of the cut-off irradiance to smaller wavelengths with decreasing ozone

values can be readily seen. If total ozone becomes smaller than 100 D, the atmosphere becomes more and more transparent in the UVC region ($\lambda < 280$ nm) with decreasing ozone amount. Therefore, tropical and subtropical regions with both high noon time solar zenith angles and small natural amounts of stratospheric ozone would be particularly endangered, if atmospheric ozone decreased as a result of anthropogenic activities.

4.2 Comparison of the modelled effective radiation with results of other models

To assess the uncertainty and the ranges of the modelled values of effective irradiance, the model results were compared with results of model calculations taken from the literature. Fig. 8 shows the global UV radiation modelled for a total ozone value of 280 D and two different values of surface albedo and aerosol load (A = 5 %, τ_{350} = 0.4 and A = 25 %, τ_{350} = 0.1). The corresponding results taken from the literature are for the same ozone amount, but part of them is for slightly differing values of surface albedo and aerosol load. It can be seen in Figure 8 that, except at very high zenith angles, most of the results of other models are within the two curves provided by the model version applied in our study.
Another comparison of the model with additional model results is given in Table 3 for global UVB irradiance and for erythemal irradiance. Part of the differences in erythemal irradiance can be ascribed to different erythemal action spectra used by different authors. In the range of ozone values from 250 to 400 D and within the zenith angle region 30° to 75°, the present model produces irradiances that are by (5 ... 15) % higher than the values by DAVE and HALPERN (1976) as well as ZAVODSKA (1981), but by (20 ... 70) % lower than the model results of BELINSKIJ et al. (1968).
Another comparison of the model used in this study with results obtained by SMITH et al. (1992), who used an adding-doubling method in a multi-layer atmosphere, is shown in Table 4. Table 4 shows that the ratios UVB_1/UVA_1 are by 4 % for low albedo and by up to 11 % for high albedo higher than the results obtained by SMITH et al. (1992)[2]. In the wavelength region $\lambda < 308$ nm the differences between both models are still higher with values up to 20 %. A substantial part of these differences may be explained by the different ozone absorption coefficients used in both models and possibly the different values of extraterrestrial radiation. Looking back to Table 2 we recall that the ozone absorption coefficients used in our model provide values of UVB ($\lambda < 315$ nm) radiation being (3 ... 11) % higher than in the original version with the result that the ratios UVB/UVA are higher by that amount, in compliance with the results shown for UVB_1/UVA_1 in Table 4.

[2]In contrast to the UVB region from 280 nm to 315 nm, UVB_1 is defined here as the wavelength region 280 - 320 nm, while UVA_1 is the region 320 - 400 nm.

Table 3 Model calculated global irradiance (UVB and erythemal) compared to values taken from the literature (DH: DAVE and HALPERN (1976), ZA: ZAVODSKA (1981), BE: BELINSKIJ et al. (1968), all cited by SLOMKA and SLOMKA (1985), TS: this study with A=5 %, clear sky and aerosol optical depth τ_{350} = 0.4)

O_3 (D)	Ref.	E_{UVB} [W m^{-2}]			E_{ERY} [W m^{-2}]$_{ERY}$		
		θ=30°	θ=60°	θ=75°	θ=30°	θ=60°	θ=75°
250	DH	1.730	0.451	0.074	0.185	0.035	0.005
	ZA	-	-	-	0.179	0.037	0.006
	BE	2.250	0.630	0.120	0.360	0.070	0.010
	TS	1.879	0.497	0.079	0.213	0.040	0.005
300	DH	1.450	0.352	0.052	0.136	0.025	0.004
	ZA	-	-	-	0.139	0.027	0.003
	BE	1.920	0.510	0.080	0.272	0.051	0.007
	TS	1.617	0.406	0.059	0.161	0.029	0.004
350	DH	1.230	0.279	0.038	0.105	0.019	0.003
	ZA	-	-	-	0.111	0.021	0.003
	BE	1.660	0.420	0.060	0.212	0.039	0.003
	TS	1.406	0.335	0.045	0.126	0.023	0.003
400	DH	1.050	0.224	0.028	0.083	0.015	0.002
	ZA	-	-	-	0.090	0.017	0.002
	BE	1.460	0.360	0.050	0.170	0.030	0.004
	TS	1.232	0.279	0.035	0.101	0.018	0.002

The effects of changing ozone amounts on the *biologically effective* radiation strongly depend on the shape of the action spectrum, particularly its fall-off at the long-wavelength side. Some effects of UV radiation are shown in Table 5. Their action spectra such as erythema and pigmentation of human skin, photocarcinogenesis ("skin cancer"), photoconjunctivitis and photokeratitis of the eyes (CIE 1986 a, b), bactericide response, suppression of photosynthesis of plants and plant damage, DNA absorption and yellowing of plastics are shown in Fig. 9. It should be noted that for one and the same action action there are differences in the action spectra obtained by different authors. They reflect the experimental uncertainties, variations in living organisms as well as the historical progress of knowledge.

Table 4 Ratios between UVB_1 (defined here as the region 280 - 320 nm) and UVA_1 (320 - 400 nm) for a total ozone value of 360 D (left-hand columns) and ratios UVB_1/UVA_1 for two ozone values 180 D and 360 D (right-hand columns) in dependence of solar zenith angle Θ and surface albedo
(1) SMITH et al. (1992)
(2) this study

Θ	Albedo	UVB_1/UVA_1 for O_3=360 D			$(UVB_1:UVA_1)_{180}$ / $(UVB_1:UVA_1)_{360}$		
		(1)	(2)	(1)/(2)	(1)	(2)	(1)/(2)
45°	0.0	0.0454	0.0474	0.96	1.56	1.53	1.02
45°	0.5	0.0475	0.0475	0.92	1.58	1.52	1.04
45°	1.0	0.0511	0.0515	0.89	1.60	1.52	1.05
60°	0.0	0.0331	0.0346	0.96	1.71	1.62	1.06
60°	0.5	0.0347	0.0376	0.92	1.73	1.62	1.07
60°	1.0	0.0374	0.0422	0.89	1.75	1.63	1.07

As an example, Fig. 10 shows some erythemal action spectra taken from different references. The differences in the action spectra for one and the same effect result in different amounts of calculated erythemal irradiance. They become greater for higher ozone values and increasing solar zenith angle. Table 6 illustrates that the values of erythemal irradiance using different action spectra can be a factor of more than 2 different from each other, particularly with higher ozone values and greater zenith angles. It should be noted here that two general types of erythemal action spectra exist. While the older erythemal action spectra only refer to the UVB region with delayed tanning of the skin, the more recent action spectra such as those of BGBl (1987) and CIE (1987) have a long tail, which extends into the UVA and visible region, thus the latter include the effect of both immediate and delayed tanning (e.g. AMBACH and BLUMTHALER 1993).
Some of the effects summarized in Table 5 depend much more on the ozone amount than the erythemal radiation. Fig. 11 shows the percentage ratios between effective radiation calculated for total ozone amounts between 0 D and 600 D and referred to the irradiance for the ozone value of 300 D. While radiation in the whole UV region reaching the ground (UV = UVA + UVB) does not show any substantial change with changing ozone amount, the dependence of UVB radiation on ozone is remarkable. The latter is similar to that of photokeratitis. Photoconjunctivitis shows the most pronounced dependence on ozone. For example, an ozone decrease from 300 D to 100 D would enhance the radiation causing photoconjunctivitis by more than 17 times, and if there were no ozone in the atmosphere, the photoconjunctivitic radiation would be higher by a factor of 6280. Due to the non-linearity of the dependence between ozone column and effective UV radiation the same absolute ozone increase by 300 D from 300 D to 600 D results in a decrease of photoconjunctivitic radiation by a factor of only 0.086.

Table 5 Some effects of UV radiation to the biosphere and materials

Action	Abbr.	Comment
Erythema	ERY	inflammation, reddening and burning of human skin
Photocarcinogenesis	PHC	mutation of tissue resulting in skin cancer documented for hairless mice
Pigmentation	PIG	pigmentation of human skin
Photoconjunctivitis	CON	painful inflammation of the conjunctiva, the tissue coating the eyelid and part of the human eyeball
Photokeratitis	KER	painful inflammation of the cornea of the eye in primates
Bactericide response	BAC	killing bacteria and viruses
Plant response	PLR	damaging effect to proteins and DNA in plants
Suppression of photo-synthesis	SPH	suppression of photosynthesis in plants
DNA absorption	DNA	absorption spectrum of desoxyribonucleic acid
Yellowing of plastics	YEL	yellowing of polyvinylchloride and polycarbonate

Table 6 Ratios between the values of erythemal global radiation calculated from action spectra by different authors to erythemal radiation from BGBl (1987); for comparison, photocarcinogenesis is also shown

Action spectrum	O_3 = 250 D θ = 30°	O_3 = 400 D θ = 60°
ERY (BGBl 1987)	(0.2688 W m^{-2})	(0.03241 W m^{-2})
ERY (COBLENTZ and STAIR 1934)	0.87	0.54
ERY (BERGER et al. 1968)	0.73	0.49
ERY (CRIPPS and RAMSAY 1970)	0.74	1.13
ERY (KOMHYR and MACHTA 1973)	0.70	0.47
ERY (DIN 1979)	0.79	0.56
PHC (CIE 1986)	0.95	0.93

It is obvious that both components of global irradiance, the diffuse and direct radiation, contribute to global irradiance in a different manner that is mainly affected by varying solar zenith angle and wavelength. As wavelength decreases, the contribution of diffuse radiation to global radiation increases due to increasing scattering of radiation by air molecules and aerosol particles, while the contribution of direct solar radiation decreases at the same time due to that scattering and due to stronger absorption by atmospheric ozone. That effect, which is illustrated in Fig. 12, becomes more pronounced with higher zenith angles. When we consider the effective radiation, the contribution of effective diffuse radiation to global radiation is the greater, the more the spectral peak of the effective global radiation is shifted to shorter wavelengths. This effect is caused by the increase in scattering of radiation with decreasing wavelength. Fig. 13 illustrates the effect by showing the ratios of diffuse/global radiation at different solar height angles $h_\odot = 90° - \Theta$ for an average ozone amount of 300 D. Even if the sun is near the zenith, the diffuse solar radiation contributes (60 ... 70) % to global radiation for clear sky. With increasing zenith angles the contribution of diffuse radiation to global radiation further increases, until it reaches 100 % at zenith angles $\Theta > 80°$.

4.3 Radiation Amplification Factors

A parameter used to describe the dependence of effective UV radiation on ozone column amount is the *Radiation Amplification Factor (RAF)*. We define the RAF as the percentage increase in effective UV radiation E_X for a decrease of total ozone by 1 %. Fig. 14 shows some RAF values for different values of total ozone. UVB and the effective irradiance for all action spectra show RAF values between 0.5 and 4 %. It can also be seen that the RAF values are not constant, but change with increasing ozone amount. For lower ozone values, they increase with increasing ozone values, while the rate of increase becomes smaller with higher total ozone values. Particularly those effects, whose action spectra fall off more gradually at higher wavelengths, show a "saturation" effect with high total ozone, i.e. there is no further increase or even a decrease of the RAF with a further increase in total ozone. Fig. 15 demonstrates the changes in the RAF for different solar zenith angles. If the dependence of effective UV radiation on ozone becomes small at high zenith angles and/or high ozone values, because the action spectrum has a longwave tail, a further increase of the effective absorber mass produces a lesser increase in the effective UV radiation than it would produce for smaller absorber masses. While the changes in RAF with changing zenith angles are small for zenith angles between 0° and 60°, they can change appreciably for $\Theta > 60°$. Digital values of the RAF for two zenith angles are shown in Table 7. They were determined for average conditions of ozone, strong aerosol load, clear sky and a surface albedo of 5 %.

Table 7 RAF values for O_3 = 300 D, A = 5 %, strong aerosol load, clear sky and two solar zenith angles θ

Action spectrum	RAF (θ = 0°)	RAF (θ = 60°)
UVB (280 nm - 315 nm)	0.80	1.19
ERY (COBLENTZ and STAIR 1934)	1.63	1.83
ERY (BERGER et al. 1968)	1.52	1.77
ERY (CRIPPS and RAMSEY 1970)	1.12	0.72
ERY (KOMHYR and MACHTA 1973)	1.64	1.73
ERY (DIN 1979)	1.54	1.68
ERY (BGBl 1987)	1.32	1.28
ERY (CIE 1987)	1.23	1.08
PHC (CIE 1986)	1.32	1.30
PIG (DIN 1979)	0.03	0.00
PIG (CIE 1986)	0.05	0.00
CON (DIN 1979)	2.54	3.12
KER (DIN 1979)	0.87	1.12
BAC (DIN 1979)	2.33	2.48
BAC (BELINSKIJ et al. 1968)	0.62	0.44
DNA (SUTHERLAND and GRIFFIN 1981)	1.58	1.60
DNA (SETLOW 1974)	2.27	2.30
PLR (CALDWELL 1971)	1.54	2.09
SPH (SMITH et al. 1980)	0.12	0.12
YEL PVC (ANDRADY et al. 1989)	0.22	0.22
UVS instrument (FEISTER et al. 1992)	0.38	0.47
UVB instrument (FEISTER et al. 1992)	0.79	1.11

In an attempt to calculate the photochemically active radiation, a number of photolytic reactions have been selected that affect the photochemistry of the lower atmosphere. As solar UV radiation in the troposphere depends on the ozone mass in the stratosphere, a decrease of stratospheric ozone leads to higher photolysis frequencies, thereby accelerating the chemical decomposition of a number of atmospheric trace gases in the troposphere. The

RAF is defined anologously to the definition used for biological effects as the percentage increase of the photolysis frequency resulting from an ozone decrease by 1 %, which starts at 300 D. The absorption cross sections of gases and quantum yields of photolysis reactions were taken from FINLAYSON-PITTS and PITTS (1986), except the temperature dependent absorption cross sections of ozone, which are taken from BASS and PAUR (1985). The temperature dependent quantum yield of ozone photolysis is based on the parameterizations by DE MORE et al. (1983, 1985).
The calculations were carried out for a temperature of 20 °C. It should be noted, however, that quantum yields of a few reactions are still uncertain or even not known. In the latter cases, $\Phi \equiv 1$ was assumed. Whether this assumption is justified or not, would not affect the RAF values, as long as Φ is not wavelength dependent. Table 8 shows the RAF values determined for a number of photolysis reactions and two solar zenith angles ($\Theta = 0°$ and $\Theta = 60°$).
The greatest RAF values of 1.50 ... 1.96 within the range of zenith angles $0° < \Theta < 60°$ occur for the ozone photodissociation by UVB radiation

$$O_3 + h\nu \dashrightarrow O\,(^1D) + O_2\,(^1\Delta_g) \qquad \lambda < 310\ nm\ . \qquad (9)$$

A reduction of stratospheric ozone by 1 % should thus lead to an increase of ozone photolysis near the surface by 1.5 % to 2 %. This reaction with the subsequent reaction of singlet O atoms and water

$$O\,(^1D) + H_2O \dashrightarrow 2\ OH \qquad (10)$$

accounts for about 40 % of the production of hydroxyl radicals in the free troposphere (RIDLEY et al. 1992). Another 17 % and 3 % of tropospheric OH radicals are produced by the photolysis of hydrogen peroxide (H_2O_2) and methyl hydroperoxide (CH_3OOH), respectively. Both latter reactions are dependent on the overhead ozone column to a lesser degree than the O_3 photolysis (Table 8).
Second greatest values of RAF $\approx$ 1 can be seen for the photolysis of nitric acid (HNO_3), methyl nitrate (CH_3ONO_2) and acetaldehyde (CH_3CHO). Some reactions such as the photolysis of nitrogen dioxide (NO_2), which is an important chain link in the tropospheric ozone production in NO_X rich environments,

$$O\,(^3P) + O_2 \dashrightarrow O_3 \qquad (11)$$

hardly depend on column ozone ($RAF_{NO2} = 0.02 \ldots 0.03$).

Table 8 Radiation Amplification Factors for photolytic reactions of trace gases as determined from model calculations with O_3 = 300 ---> 297 D, A = 5 %, very strong aerosol load and a temperature of 20 °C

PHOTOLYTIC REACTION		RAF Θ=0°	RAF Θ=60°
$O_3 + h\nu$ ---> $O(^1D) + O_2(^1\Delta_g)$	ozone	1.50	1.96
$NO_2 + h\nu$ ---> $NO + O(^3P)$	nitrogen dioxide	0.02	0.03
$N_2O_5 + h\nu$ ---> $NO_3 + NO_2$	dinitrogen pentoxide	0.31	0.32
$HONO + h\nu$ ---> $OH + NO$	nitrous acid	0.00	0.02
$HNO_3 + h\nu$ ---> $OH + NO_2$	nitric acid	0.93	1.00
$CH_3NO_2 + h\nu$ ---> $CH_3 + NO_2$	nitromethane	0.29	0.32
$C_2H_5NO_2 + h\nu$ ---> $C_2H_5 + NO_2$	nitroethane	0.32	0.34
$CH_3ONO_2 + h\nu$ ---> $CH_3O + NO_2$	methyl nitrate	0.77	1.01
$C_2H_5ONO_2 + h\nu$ ---> $C_2H_5O + NO_2$	ethyl nitrate	0.44	0.55
$H_2O_2 + h\nu$ ---> $OH + OH$	hydrogen peroxide	0.33	0.31
$CH_3OOH + h\nu$ ---> $CH_3O + OH$	methyl hydroperoxide	0.31	0.31
$CH_3OOCH_3 + h\nu$ ---> $CH_3O + CH_3O$	dimethyl peroxide	0.31	0.37
$(CH_3)_3COOC(CH_3)_3 + h\nu$ ---> $2\ (CH_3)_3CO$	di-tert-butyl peroxide	0.42	0.45
$HCHO + h\nu$ ---> $H + HCO$	formaldehyde	0.36	0.43
$HCHO + h\nu$ ---> $H_2 + CO$	formaldehyde	0.11	0.13
$CH_3CHO + h\nu$ ---> $CH_3 + HCO$	acetaldehyde	0.83	1.06
$C_2H_5CHO + h\nu$ ---> $C_2H_5 + CHO$	propionaldehyde	0.47	0.53
$n\text{-}C_3H_7CHO + h\nu$ ---> $n\text{-}C_3H_7 + CHO$	n-butyr-aldehyde	0.41	0.49
$iso\text{-}C_3H_7CHO + h\nu$ ---> $iso\text{-}C_3H_7 + CHO$	isobutyraldehyde	0.38	0.42
$CH_3COCH_3 + h\nu$ ---> $CH_3 + CH_3CO$	acetone	0.64	0.76
$C_2H_5COC_2H_5 + h\nu$ ---> $2\ C_2H_5 + CO$	diethyl ketone	0.78	0.92
$CH_3COC_2H_5 + h\nu$ ---> $CH_3CO + C_2H_5$	methyl ethyl ketone	0.67	0.74
$CH_3CO(CH_2)_3CH_3 + h\nu$ ---> ?	methyl-n-butyl-ketone	0.61	0.76
$H_2O_2 + h\nu$ ---> $OH + OH$ (liq.phase)	hydrogen peroxide	0.38	0.37
$HONO + h\nu$ ---> $OH + NO$ (liq.phase)	nitrous acid	0.05	0.02
$HNO_3 + h\nu$ ---> $OH + NO_2$ (liq. phase)	nitric acid	0.93	1.00
$NO_2^- + h\nu$ ---> $(NO_2^-)^*$ ---> $NO + OH + OH^-$	nitrite ion	0.02	0.06
$NO_3^- + h\nu$ ---> $NO_2^- + O$ ---> $NO_2 + O^-$	nitrate ion	0.46	0.60

4.4 Photolysis of ozone

Photolysis frequencies of the ozone photolysis according to eq. (9) were compared with modelled and measured values taken from other authors. A comparison of the dependence of the calculated ozone photolysis frequencies on column ozone is shown in Fig. 16. The calculated photolysis frequencies, even those with a high albedo of 80 % and weak aerosol absorption, decrease with increasing total ozone in a very similar way as do the results obtained by BLACKBURN et al. (1992), but the absolute level of photolysis frequencies in this study is somewhat lower than that shown by the results of BLACKBURN et al. (1992), even if we assume a high surface albedo of 80 % and weak aerosol load in our calculations. On the other hand, filter radiometer measurements of ozone photolysis carried out by HOFZUMAHAUS et al. (1992) during a ship's expedition over the Atlantic Ocean in 1988 provide results that are similar to the results of our model calculations, but show a slightly different dependence on total ozone than the model calculations. At least part of the observed differences can be explained by the approximation of the effective absorbing ozone mass, i.e. the product between total ozone (in Dobson) and the relative slant path through the ozone layer. To a rather crude approximation the latter is sometimes replaced by sec Θ. Such an approach of an effective ozone mass would be justified for direct sun radiation, because in that case the Lambert Bouger law is valid. However, for global radiation it is not necessarily applicable. As an illustration, Fig. 17 shows results of a model run, in which only the solar zenith angle was varied and total ozone was held at a constant value of O_3 = 300 D. The model results compare much better with the measurements of J_{O1D} which reflect to a greater extent the variation in Θ than the variation in column O_3. Comparisons between model calculations and measurements should, therefore, preferably be made separately for definite total ozone values and zenith angles. Despite the uncertainties inherent in the measurements and the model as well as the uncertainties of input parameters to the model calculation, the differences between model simulation of J_{O1D} and the results of measurements given in two different polynomial parameterizations by HOFZUMAHAUS and BRAUERS (1991) and HOFZUMAHAUS et al. (1992) are small (Fig. 11).

Using the described model, the dependence between O_3 photolysis frequency and temperature turns out to be approximately linear in the temperature range -30 °C ... +30 °C. A temperature increase of 1 °C results in an increase of J_{O1D} of 0.95 %. Fig. 18 compares the ratios of J_{O1D} determined at the temperature t and the corresponding value for t = 0 °C with results obtained by DICKERSON et al. (1982) and BLACKBURN et al. (1992). It can be seen that the results of the model described here are between the results of the temperature dependence of J_{O1D} from both groups of authors.

The dependences of J_{O1D} on total ozone and on height are shown in Fig. 19. A temperature decrease from 20 °C at ground level to -10 °C at a height of 5 km is chosen in the calculations. It can readily be seen that J_{O1D} depends much stronger on ozone than on height. The change of J_{O1D} with height is most pronounced in the lowest height layer from 0 km to 1 km, where the photolysis frequency almost doubles, and the increase of J_{O1D} is reduced to (3 ... 7) % in the layer 4 to 5 km.

5 Latitudinal and seasonal variation of effective solar radiation

The model was used to determine the latitudinal and seasonal distribution of the biologically effective global UV radiation reaching the ground at sea level. The calculations were made for the 15th day of each month in time steps of 10 minutes from sunrise to sunset.
Monthly and zonal averages of cloudiness were taken from MATVEEV and MATVEEV (1984), and total ozone values were taken from PEROV and KHRGIAN (1985) as input values to the model calculation (see Fig. 20). It should be noted that the parameterization of cloud cover by a cloudiness factor

$$F = 1 - 0.56 \cdot C_A \qquad (12)$$

with C_A being the cloud cover in tenths (0 ... 1) in the original model version is an average curve of UV radiation measurements published by BÜTTNER (1934). While AMBACH et al. (1991) determined a smaller reduction of UV radiation due to clouds by a similar relation

$$F = 1 - 0.4 \cdot C_A \qquad (13)$$

from UV radiation measurements taken on the mountain Jungfraujoch, BAIS et al. (1993) found a non-linear relation of the cloud factor from Brewer spectrometer measurements (290 - 325 nm) taken at Thessaloniki in Greece for $\Theta = 50°$

$$F = 1 + 0.06\ C_B - 0.02\ C_B^2 \qquad (14)$$

with the cloud cover $3 \leq C_B \leq 8$, and $F = 1$ for $C_B \leq 2$. Fig. 21 compares the three curves of cloudiness factors. It should be noted that the three parameterizations can only reflect average conditions, while in individual cases deviations from these curves occur due to different optical thicknesses of the clouds (DEHNE 1988). For example, opaque cloudiness can reduce global UV irradiance down to ~ 10 % of its clear sky value (FEISTER 1991). In addition to that, it is important for global UV radiation, whether the sun is obscured by clouds, or whether it is not. In the calculations described here the cloud factor by BÜTTNER (1934) was used.
The results of the calculations for erythemal irradiation on the 15th day of each month (daily totals) at 4 latitudes (75°, 55°, 35°, 15° N) are shown in Fig. 22 for clear sky and for latitudinal and seasonal averages of cloud cover. Due to the increasing absorption of erythemal radiation with increasing solar zenith angles, its seasonal variation is much higher at high latitudes than at lower latitudes. The *Minimal Erythemal Dose (MED)* needed to produce a faint reddening of the skin is between 210 and 750 $(J\ m^{-2})_{ERY}$ depending on the skin type (BGBl, 1987). Fig. 22 shows that even for average cloudiness the MED is exceeded several times per day in the tropics and subtropics during the whole year, and to a lesser degree at mid- to high latitudes during the summer months. As the seasonal variation of total UV radiation ($\lambda < 400$ nm) and also of visible radiation is smaller than the variation of the effective radiation, the ratios between effective radiation affected by atmospheric ozone, and total UV radiation, which is nearly independent of ozone, should

hardly vary at low latitudes, but should show substantial seasonal changes at higher latitudes. Figures 23 a and b show the seasonal variations of the ratios between erythemal radiation and UV radiation as well as between plant damaging radiation and UV radiation. Similar seasonal changes can be expected to occur for the ratios between plant damaging radiation and photosynthetic active radiation (PAR).

It is interesting to look at the effects that occur in the effective radiation due to the pattern of the natural global ozone distribution and the distribution of cloudiness. As an example of those effects, Fig. 24 shows the global distribution of UV radiation effective for plant response (PLR) modelled for average conditions. It is noted that the ozone distribution is based on ozone observations carried out before 1980, so the Antarctic ozone "hole" is not included in the observations. Despite that anthropogenic effect, which became obvious during the eighties, the natural conditions of ozone and cloudiness lead to somewhat higher levels of calculated UV radiation in the Southern hemisphere as compared to the Northern hemisphere. The effect of ozone and cloudiness can be seen in Table 9, which shows the zonal average ratios of UV radiation between the Northern and Southern hemisphere. The ratios for UVA and clear sky conditions between Northern and Southern latitudes are equal to 1, except for the latitude belt of 60° to 70°, where it was assumed in the calculations that the surface is covered with snow or ice, while it was assumed to be ice free in the Northern hemisphere in summer. The cloud cover being smaller in the Northern than in the Southern hemisphere, except over the Antarctic continent, leads to (10 ... 15) % higher values of UVA in the Northern as compared to the Southern hemisphere. Tropical regions are an exception, because the ozone values in the tropical belt of the Northern and Southern hemisphere are very similar. When we look at the UVB region, the results are quite different. The average ozone values are greater in the Northern than in the Southern hemisphere leading to higher values of UVB radiation for clear sky in the Southern hemisphere as compared to the Northern hemisphere. It is noted again that latitudinal differences in the vertical ozone distribution are not taken into account in our calculations.

The combined effect of cloudiness and ozone results in average values of UVB radiation that are around 10 % higher in the Northern hemisphere. An exception are high latitudes where the Southern hemisphere should receive more UVB radiation even for "undisturbed" conditions due to a lesser ozone amount. The photoconjunctivitic radiation also shown in Table 9 is more affected by ozone variations than the UVB radiation, but it is affected by clouds to the same extent. Therefore, even for cloudy conditions the ratios of CON radiation between Northern and Southern hemisphere are stronger influenced by the ratios of ozone than those of clouds.

Fig. 25 shows the percentage increase in plant response that can be expected for an ozone decrease by 10 %. The irradiaton effective for plant response would increase by 18 to 20 % in the tropics and up to 40 % at high latitudes in winter. The greatest absolute increase can be expected to occur at low latitudes, where the natural radiation level is highest.

Table 9 Ratios between global radiation at x degrees northern latitude and y degrees southern latitude for clear sky and for average cloudiness

Ratio	UVA clear sky	UVA av. cl.	UVB clear sky	UVB av. cl.	CON clear sky	CON av. cl.
85°N/85°S	1.00	0.80	0.92	0.72	0.87	0.67
75°N/75°S	0.65	0.58	0.46	0.40	0.41	0.35
65°N/65°S	1.00	1.18	0.96	1.11	0.96	1.10
55°N/55°S	1.00	1.17	0.95	1.10	0.88	1.01
45°N/45°S	1.00	1.17	0.97	1.14	0.93	1.09
35°N/35°S	1.00	1.14	0.95	1.09	0.85	0.98
25°N/25°S	1.00	1.10	1.01	1.11	1.01	1.11
15°N/15°S	1.00	1.07	1.00	1.08	1.00	1.07
5°N/ 5°S	1.00	0.97	1.00	0.97	1.00	0.97

Latitudinal and seasonal changes were also calculated for other effects. While the erythemal and photocarcinogenic radiation show increases by 18 % at low latitudes throughout the year and 20 % at high latitudes in winter, when ozone is decreased by 10 %, the photoconjunctivitic radiation reveals the highest increase by 30 % in the tropics and subtropics, and up to about 60 % at high latitudes in winter.

The results of calculations for all biological effects considered cannot be shown here. Table 10 shows a summary of the percentage increases in the average daily totals of effective UV radiation determined by model calculations for an ozone decrease by -(3 ... 5) %, which has occurred at mid-latitudes of the Northern hemisphere from 1970 to the present (WMO 1992). Increases in biologically effective irradiation are between 4 and 25 %. A decrease of ozone by 50 %, which has occurred in the months September and October over the Antarctic continent since the mid-seventies (STOLARSKI et al. 1992) should have resulted in an increase of irradiation by 120 % and 880 %. The non-linearity in the changes of effective UV radiation can be recognized in Table 10.

A comparison between the Tables 7 and 10 clearly shows that the results of the model calculations are different from those that would have been obtained by using only RAF values to estimate the effects of ozone decreases for the effective irradiance.

Table 10 Percentage increase of effective UV radiation for a change of total ozone by - (3 ... 5) % at mid-latitudes in individual months and -50 % in the Antarctic in September/October

	O_3 = - (3 ... 5) % at mid-latitudes	O_3 = - 50 % in the Antarctic
UVB	4 ... 10	120 ... 280
ERY	5 ... 10	190 ... 220
PHC	6 ... 10	210 ... 230
CON	11 ... 25	710 ... 880
KER	4 ... 8	120 ... 170
BAC	8 ... 20	460 ... 510
PLR	7 ... 20	320 ... 470
YEL PVC	1... 2	30 ... 45

6 Higher effective irradiation at mid-latitudes in 1992 and 1993

6.1 Effect of low ozone values

Total ozone measurements in large regions of the Northern hemisphere showed extremely low values in 1992 and in 1993. We will not discuss the possible causes such as the eruption of Mt. Pinatubo on Northern Luzon in the Philippines in 1991 and the abnormal atmospheric circulation in 1992 and 1993 (e.g. PITARI and RIZI 1993), but only try to estimate the enhancements of effective UV radiation as a consequence of the low ozone values. Figures 26 and 27 show the daily ozone values measured at the Potsdam Observatory in 1992 and in 1993. Long-term averages of ozone and its standard deviations σ are also shown. They were determined from TOMS satellite data for Potsdam, because the long-term record of ground-based ozone observations using Dobson spectrophotometers at Potsdam for the period 1964 to 1990 is being re-evaluated and can, therefore, not yet be used for that purpose. It can be seen that total ozone values at Potsdam are below the long-term average minus 1 σ for most of the time in 1992 and 1993, and even below the average minus 2 σ in shorter time periods. Extremely low ozone values were observed in January 1992 and February 1993. The monthly mean ozone value in January 1992 was 20 % below the long-term average, and the monthly mean ozone value in February 1993 was almost 30 % below the long-term average.

Two model runs were performed using in the first run the long-term monthly mean values of total ozone and in the second run the monthly mean values of total ozone for the individual months in 1992 and 1993. Under the assumption that only the ozone values have

changed and the other atmospheric conditions, particularly cloudiness and turbidity, have remained the same, the ratios between the values of UV irradiation calculated for actual and average conditions provide estimates of the changes in the UV irradiation. Figure 28 shows the calculated ratios of UV irradiance for 1992 and 1993 as compared to the radiation for long-term averages of ozone and clear sky. Greatest increases in the effective UV radiation can be seen in the winter months of January and February, but the summer months also show values of the effective irradiation higher than the long-term mean by 10 to 30 %. It is obvious that the summer months are of particular importance to the annual total UV irradiation at mid-latitudes, because they contribute the greatest portion to the annual total. To quantify this well-known observation the percentage contribution of the effective irradiation in individual months to their annual totals was calculated. Fig. 29 shows that the effective UV irradiation at 50° N during the half-year period from April to September contributes (89 ... 94) % to the annual total irradiation, while the irradiation for the whole UV region ($\lambda < 400$ nm) during the summer period contributes only 76 %. At higher latitudes the contribution of effective UV irradiation during the summer period is still higher. At 75° N the contribution of clear sky irradiation to the annual total in the period April to September is (98.8 ... 99.8) % for the effective irradiation and 94 % for total UV irradiation (Fig. 30).

6.2 Combined effect of ozone and cloudiness

It is obvious that the ratios between the actual UV irradiation in 1992 and 1993 on the one hand, and their long-term averages on the other hand can have been affected not only by ozone, but also other atmospheric conditions, in particular cloudiness and aerosols, in both years. To assess the effect that cloudiness did exert on UV irradiation in 1992 and 1993 we did not use one of the cloud parameterizations (12) to (14), but applied another approach. This approach, which accounts for possible changes of aerosols, takes advantage of the records of measurements of global UVA[3] irradiance (315 ... 391) nm) (FEISTER et al. 1992, FEISTER and GRASNICK 1992) taken at Potsdam. It is mentioned that UVA is almost independent of atmospheric ozone, but is affected by clouds and aerosols in a similar way as the biologically and chemically effective UV radiation, because scattering and absorption of radiation by aerosols and clouds are only weakly dependent on wavelength. Ratios between monthly averages of UVA measured in 1992 or 1993 and their long-term averages should reflect the effect of cloudiness and aerosols on global UV irradiance, e. g.

$$C = \frac{UV_{1992}}{UV_{1978-1991}} \qquad \textbf{(15)}$$

that can be used as correction factors to the effective UV radiation simulated with the model

[3]In this case, UVA means the wavelength region of filter instruments with the effective halfwidth of 315 to 391 nm.

for clear sky conditions. As the UV irradiance measurements at Potsdam do not date back to 1978, i.e. $UV_{1978\text{-}1991}$ does not exist, we used the ratios between measured UV radiation and total global radiation G (380 - 2800 nm), which has been recorded at Potsdam for more than six decades, to determine the cloud correction factors

$$C = \frac{UV_{1992}}{UV_{1988-1992}} \cdot \frac{G_{1988-1992}}{G_{1978-1991}} \quad . \qquad \textbf{(16)}$$

Equations (15) and (16) can analogously be applied to 1993. The ratios between total global irradiation in 1992 and 1993, respectively, and the long-term average (1978 - 1991) are shown in Fig. 31. It can be recognized that the values of total global irradiation during the first three months of 1992 were by 10 to 20 % lower than their averages, while they were higher than the average up to 30 % from May to July 1992.

The modelled ratios of UV irradiation including the cloud effect are shown in Fig. 32. It can be seen that the anomalies in cloud cover enhanced or diminished the UV irradiation depending on the time period. For example, in the spring and early summer of 1992 the cloud cover, which was lower than normal, led to further enhancement of the global UV irradiation, which was already above normal, with the result that UV irradiation from May to July 1992 and in September 1992 was by (30 ... 50) % higher, and in March and April 1993 it was by even (40 ... 80) % higher than the long-term average. In the winter months January to March of 1992 and in February 1993, clouds with amounts higher than normal reduced the effect of low ozone values on UV irradiation at the ground.

Estimates of the annual totals of effective UV irradiation are given in Fig. 33. Due to the much higher contribution of irradiation received in the summer months to the annual totals, the ratios between annual totals in both years to the long-term averages are very similar to the results obtained for the summer months. For clear sky conditions the annual totals of effective UV irradiation are by (8 ... 26) % and by (12 ... 32) % higher than the long-term average in 1992 and in 1993, respectively, due to lower than normal ozone values. The cloud cover modulated the ozone effect to UV radiation. While in 1992 lower than normal cloud cover further enhanced the UV irradiation to (11 ... 32) % above the average, the greater than normal cloud cover in 1993 reduced the ozone effect with values of effective UV irradiation being only (4 ... 22) % higher than the average.

For those biological actions that depend on ratios of irradiance in different spectral regions the effect of ozone (without the cloud effect) can also be important. An example for that is the UV radiation causing plant damage (PLR). It is enhanced, when atmospheric ozone decreases. If cloud cover decreases at the same time, UV radiation is further increased. Photosynthetic active radiation in the visible region is increased due to a diminished cloud cover. These changes in the irradiation levels of both spectral regions create conditions for the plants different to those, when only the irradiance responsible for plant damage would shift. An increase in cloudiness might thus more than balance the adverse effect of decreasing ozone values to the plant, even if the UVB radiation is increased due to diminished ozone values.

The model can also be applied to determine predictions of the expected effective UV irradiance, if forecasts of the atmospheric ozone value, cloud cover and turbidity are

available. To show the expected variability due to ozone variations we consider the erythemal irradiation at one site on a cloudless mid-summer day at 52° N. Fig. 34 shows the erythemal irradiation expressed in MED per hour (1 MED = 250 $(J\ m^{-2})_{ERY}$) calculated for the station Potsdam for three different ozone values that are 1 σ and 2 σ apart from the long-term average ozone value of 372 D for June. The daily totals of "accumulated" MED are between 12.6 MED for the ozone average value of 372 D and 15.2 MED for the extremely low ozone value 316 D. If we consider only the four noon hours from 10.00 to 14.00 local time, the corresponding figures are 6.9 MED for the ozone average, 7.6 MED for the average minus 1 σ and 8.4 MED for the average minus 2 σ ozone value, i.e. 1.5 MED more than the average number of MED on cloudless days can be expected to be incident on a horizontal surface during the four hours around noon time in cases with extremely low ozone amounts. It is mentioned that the calculated hourly values of the MED refer to skin, which is not pre-radiated, i.e. they do not include an adaptation effect, which can occur by thickening of the epidermis as a result of UVB radiation.

The relative enhancement in erythemal irradiation due to diminished ozone values is shown in Fig. 35. It can be readily seen that the relative enhancement is greatest around noon time and decreases in the morning and afternoon hours. The maximum relative enhancement of erythemal UV irradiation is 10 % for ozone values, which are lower by 1 σ than the average ozone, and it is 22 % for ozone values, which are lower by 2 σ than the average ozone. These numbers correspond to a RAF value of about 1.2, in close correspondence to the result given in Table 7 for small zenith angles.

An impression of the spatial differences, which can be expected on a sunny day in June within Germany for erythemal irradiation, can be gained from Fig. 36. This Figure shows the number of MED per hour at the three sites Westerland on the island of Sylt in the North Sea, Potsdam near Berlin in the central part and Hohenpeissenberg south of Munich in the southern part of Germany. The sites are at the latitudes of 54.9° N, 52.4° N and 47.8° N. The distance between Potsdam and Westerland is 422 km, and between Potsdam and Hohenpeissenberg it is 813 km. While the stations Westerland and Potsdam are almost at sea level, the height of the site Hohenpeissenberg is 975 m asl. Average ozone values in June for Hohenpeissenberg (346 D) and Potsdam (372 D) were taken from the records of observations, while for Westerland the average ozone value from TOMS ozone data for Copenhagen (373 D) was applied (ERICKSEN 1993). The higher irradiation at Westerland as compared to Potsdam is due to the lower aerosol optical thickness, which was used as input to the model calculation to account for the cleaner air there. If we had used the same optical thickness for both sites, the UV irradiation at Westerland would have been slightly smaller than at Potsdam due to the greater solar zenith angles at Westerland. The resulting difference in erythemal irradiation between Potsdam and Westerland amounts to about 2 MED, i.e. 17 %. A bigger difference of more than 5 MED can be seen between the irradiation calculated for Potsdam and the one calculated for Hohenpeissenberg. This difference is due to the lower latitude and the higher elevation of the latter site.

In the preceding chapter, examples of the latitudinal and seasonal variations of the biologically effective irradiation were given, while variations of atmospheric ozone in time at one site have been the focus of this chapter. As an example of the spatial variations, Fig.

37 shows the erythemal irradiation that travellers from Germany to other regions of the globe can expect to receive. The hourly totals of UV irradiation for Potsdam on a cloudless day are compared to the results obtained for a site at 40° N, which should reflect the conditions in the Mediterranean region (Spain, Italy, Greece etc.) in the middle of June and for the latitude of 15° N (South East Asia, Africa, Carribean etc.) on January 1. It can be seen that travelling from 52° N to 40° N in June results in an increase of the daily erythemal dose by more than 5 MED (41 %). Due to the higher sun angle at noon at 40° as compared to 52° N, the values of erythemal irradiation in the four hours around noon are even 51 % higher at 40° N (10.6 MED from 10 to 14 local time) than at 52° N (7.0 MED from 10 to 14 local time). A similar daily variation of erythemal UV irradiation, though with a lower amplitude, as at the latitude of 40° N in the middle of June occurs at 15° N in the beginning of January. The daily total erythemal irradiation with 12.4 MED at 15° N in January is similar to the erythemal dose at 52° N in June, but during the 4 hours around noon time 27 % more erythemal irradiation is received at 15° N as compared to 52° N (8.9 MED at 15° and 7.0 MED at 52°). Calculations of this kind are considered to be useful to provide advice to travellers, who plan to visit places at other latitudes. Combined with additional recommendations about the reasonable behaviour of people, the values of biologically effective radiation, or parameters derived from them such as a UV index (e.g. WEATHERHEAD and McNEELY 1994), can help to reduce the risk of adverse effects to the skin and the eyes. This is of particular importance for people who live outside the tropics, if they travel to low latitudes in the winter and spring months, when their skin is not adapted to high levels of UVB radiation.

7 Measurements of spectral UV irradiation

Measurements of spectral UV irradiance with MKII Brewer spectrophotometer #30 were used to determine effective irradiances at Potsdam. The Brewer instrument has been used for regular global UV irradiance measurements at Potsdam since August 31, 1993. Spectral scans in the region 290 to 325 nm are made at fixed solar zenith angles, which correspond to time differences between consecutive individual spectral scans of about half hourly intervals from sunrise to sunset. The spectral stepwidth is 0.5 nm with a spectral resolution (full width at half maximum) of 0.5 nm. The calibration of the instrument as well as results of comparisons with other Brewer spectrophotometers and with different types of spectroradiometers as well as with model calculations are described in detail by FEISTER and DEHNE (1994).

Daily totals of the erythemally effective irradiation derived from the Brewer measurements with the erythemal action spectrum by CIE (1987) for the period 31 August 1993 to 16 April 1994 are shown in Fig. 38. As the spectral range of the Brewer instrument ends at 325 nm, the remaining part of erythemal radiation contributed by UVA radiation, which is on the order of about 8 % for low ozone values and small zenith angles and 30 % for high ozone values and greater zenith angles, is extrapolated from the spectral irradiances measured in

each scan at wavelengths $\lambda < 325$ nm. This drawback of the instrument does not apply to effects with action spectra such as photoconjunctivitis that do not have long-wave tails. The irradiation is given here in daily numbers of MED for a threshold value of 1 MED $\equiv$ 250 $(J\ m^{-2})_{ERY}$. In addition to the measured irradiation, Fig. 38 also shows the results of model calculations, which were carried out for the 15th day of each month, for clear sky conditions and the long-term monthly mean values of ozone. The resulting modelled values of erythemal irradiation were interpolated for each day of the month (dashed curve). Both the seasonal variation due to solar zenith angle and the high day to day variability due to cloudiness, atmospheric ozone and aerosol load can be recognized in the erythemal irradiation. Triangles designate those days with ratios between diffuse and global total irradiation less than 0.3, i.e. days with a high percentage of direct solar radiation. Peak values in the measured erythemal irradiation are mainly caused by small amounts of cloudiness and/or low ozone values. For illustration, the curve on top of Fig. 38 shows the ratios between daily mean values of atmospheric ozone as measured by Dobson spectrophotometer #71, and long-term mean values of ozone at Potsdam. Triangles are used again to designate days with ratios of diffuse/global total irradiation of less than 0.3. It can be seen that the majority of peaks in the erythemal irradiation occur on days with low ratios diffuse/global irradiation and/or low ozone values, but that there are also a few occasions when this is not the case. The ozone effect on the effective UV irradiation can be recognized somewhat more pronounced in the photoconjunctivitic irradiation, which is shown in Fig. 39, because this effective UV radiation is more weighted by the irradiances of shorter wavelengths than the erythemal radiation.

It is important to note that the model calculations are in some way idealised, because they were made for only one average turbidity and for the monthly mean ozone values. Furthermore, it must be taken into account that cloudiness affects UV irradiance in a different way than it affects total global irradiance. Even if two days show the same ratio of diffuse to global total irradiation, differences in the diurnal variations of the clouds on both days can affect the hourly values of UV irradiance in a different manner with the result that differences in the daily sums of UV irradiation occur. Finally, the total ozone amount can change over the day, and daily mean ozone values are determined from measurements, which need not be evenly distributed over the day. All these factors contribute to the uncertainty of the model results. Nevertheless, despite these uncertainties, which have to be considered, the calculations are thought to provide useful approximate estimates for the biologically effective UV irradiation for average atmospheric conditions with clear sky.

8 Conclusions

A modified version of the basic UV radiation model by SCHIPPNICK and GREEN (1982) was applied to calculate effective irradiances for a number of biological actions and the photolysis frequencies of some chemical reactions. Measured values of extraterrestrial radiation and ozone absorption coefficients instead of the parameterizations in the original model were used. Differences between the results of the model calculations presented here and other models can, at least in part, be traced back to these modifications in the model.
A comparison between model calculations and spectral measurements as well as broad-band filter measurements shows differences on the order of ~ 10 %. They are due to uncertainties in the input values as well as parameterizations applied in the model, and uncertainties in the measurements including the calibration of instruments.
Radiation Amplification Factors for some biological effects and chemical reaction rates were determined. Their non-linear changes with atmospheric total ozone and solar zenith angle illustrate the ranges in which they can be assumed to be approximately constant.
RAF values, which were calculated for a number of photolysis reactions, show the greatest values for the photolysis of ozone, nitric acid, acetaldehyde and methyl nitrate. The RAF values for a specific action mainly depend on the ozone amount and solar zenith angle. Though there are certain ranges in total ozone and zenith angles, for which the RAF values of biological and chemical actions can be assumed to be nearly constant, the consequences of ozone changes to the effective radiation can better be determined by direct model calculations.
The differences between modelled values of the O_3 photolysis frequency and measurements taken from the literature are small, as soon as the total ozone value and the zenith angle are used separately instead of using the effective ozone mass (O_3 . sec Θ). It is also shown that total ozone affects the photolysis rate of O_3 and other gases having similar RAFs much more than their variation with height.
Model calculations carried out to estimate the consequences of the extremely low ozone values observed at mid-latitudes in 1992 and 1993 on the effective UV irradiance showed enhancements of about 10 to 30 % in the annual totals referred to the long-term mean values for clear sky conditions. If the cloud effect is taken into account, the enhancement in effective UV irradiance is even slightly higher in 1992 than the enhancement calculated for cloudless conditions, but it is reduced by the clouds to 5 to 20 % above normal in 1993.
A combination of model calculations and broad-band UV measurements can thus be helpful in providing estimates of the actual levels of global UV irradiance. It will be interesting to see, whether future measurements of spectral solar UV radiation will reflect the changes that are predicted by the model simulations. First results of measurements of the spectral UV irradiance at Potsdam are encourageing in that respect.

References

AMBACH, W., M. BLUMTHALER (1993), Biological effectiveness of solar UV radiation in humans, Experientia 49, 747 - 753

AMBACH, W., M. BLUMTHALER, G. WENDLER (1991), A comparison of ultraviolet radiation measured at an Arctic and Alpine site, Solar Energy 47, No. 2, 121 - 126

ANDRADY, A.C., A.TORIKAI, R.K. FUEKI (1989), Photodegradation of rigid PVC formulations. I. Wavelength sensivity to light-induced yellowing by monochromatic light, J. Appl. Polymer Sci. 37, 935 - 946

BASHER, R.E. (1982), Review of the Dobson spectrophotometer and its accuaracy, WMO Global Research and Monitoring Project Report No. 13

BASHER, R.E. (1987), The calculation of solar ultraviolet radiation and its sunburning effect under clear skies, Scientific Report 26, ISSN 0112-2398, New Zealand Meteorological Service, PO Box 722, Wellington

BASS, A.M., R.J. PAUR (1985), The ultraviolet cross-section of ozone, Atmospheric Ozone, D.Reidel Publishing Comp. Dordrecht Boston Lancaster, 606 - 616

BELINSKIJ, V.A., M.P. GARADŽA, C.M. MEŽENNAJA, E.I. NEZVAL (1968), Ultravioletovaja radiacija solnca i neba, Izdatel'stvo Moskovskogo universiteta.

BENER, P. (1972), Approximate values of intensities of natural UV radiation for different amounts of atmospheric ozone, Final Technical Report, U.S. Army DAJA 37.68. C 1017, Davos 1972

BERGER,D., F. URBACH, R.E. DAVIS (1987), The action spectrum of erythema induced by ultraviolet radiation, Proc. 13. Congressus Internationalis Dermatologicae, Munich 1967

BGBl (1987), Empfehlungen zur Begrenzung gesundheitlicher Strahlenresistenz bei der Anwendung von Solarien und Heimsonnen, Bundesgesundheitsblatt 30 (Nr. 11, 19 - 31)

BIRD, R.F., C. RIORDAN (1986), Simple solar spectral model for direct and diffuse irradiance on horizontal and tilted earth's surface for cloudless atmospheres, J. Climate Appl. Meteorol. 25, 87 - 92

BLACKBURN, T. E., S.T. BAIRAI, D.H. STEDMAN (1992), Solar photolysis of ozone to singlet D oxygen atoms, J. Geophys. Res. 97, D9, 10,109 - 10,117

BRASLAU, N., J.V. DAVE (1973 a), Effect of aerosols on the transfer of solar energy through realistic model atmospheres, Part I: Non absorbing aerosols, Part II: Partly-absorbing aerosols, J. Appl. Meteorol. 12, 601 - 619

BRASLAU, N., J.V. DAVE (1973 b), Effect of aerosols on the transfer of solar energy through realistic model atmospheres, Part III: Ground level fluxes in the biologically active band 2850 - 3700 microns, IBM Research Report, R Ci 4308

BÜTTNER, K. (1938), Physikalische Bioklimatologie, Akademische Verlagsgesellschaft Leipzig, 13f

CALDWELL, M.M. (1971), Photophysiology (ed. by A.C. Giese), Vol. 6, 131 - 177, Academic Press New York

CHAMEIDES, W. L., F. FEHSENFELD, M.O.RODGERS, C. CARDELINO, J. MARTINEZ, D. PARRISH, W. LONNEMANN, D.R. LAWSON, R.A. RASMUSSEN, P. ZIMMERMAN, J. GREENBERG, P. MIDDLETON, T. WANG (1992), Ozone precursor relationships in the ambient atmosphere, J. Geophys. Res. 97, D5, 6037 - 6055

CHANDRASEKHAR, S. (1960), Radiative transfer, New York

CIE (1986 a), Division G, Budapest 1986, Personal communication by U. Amlong

CIE (1986 b), Research note, Photoconjunctivitis, CIE Journal 5, 24 - 28

CIE (1986 c), Research note, Photoakeratitis. CIE Journal 5, 19 - 23

CIE (1987 a), Research Note: A reference spectrum for ultraviolet induced erythema in human skin, CIE Journal 6, 17 - 22

CIE (1987 b), Publ. No. 17.4

CIMO (1981), Abridged Final Report of the eight's Session, Mexico City, 19-30 October 1981, WMO - NO. 590

COAKLEY, J. A., P. CHYLEK (1975), The two-stream approximation in radiative transfer: Including the angle of the incident radiation, J. Atmosph. Sci. 32, 409 - 418

COBLENTZ, W.W., R. STAIR (1934), Data on the spectral erythemic reaction of the untanned human skin to ultraviolet radiation, Bureau of Standards Journal of Research 12, 13 - 14

CRIPPS, D.J., C. A. RAMSEY (1970), Br. J. Derm. 82, 584 - 592

DAUMONT, D., J. BRION, J. CHARBONNIER, J. MALICET (1992), Ozone spectroscopy I: Absorption cross-sections at room temperature, J. Atmosph. Chem. 15, 145 - 155

DAVE, J. V., P.M. FURUKUWA (1960), Scattered radiation in the ozone absorption bands at selected levels of a terrestrial Rayleigh atmosphere, Meteorol. Monographs 7, No. 29, Boston Americ. Meteorol. Soc., 1 - 353

DAVE, J.V., P. HALPERN (1976), Effect of changes in ozone amount on the ultraviolet radiation received at sea level of a model atmosphere, Atmosph. Environm. 10, 547 - 555

DEHNE, K. (1991), Personal communication

DEHNE, K. (1988), Zur Variation von Absolut- und Relativwerten der UV-Globalstrahlung, Laufener Sem.beitr. 3/88, 13 - 26

DEIRMENDJIAN, D. (1969), Electromagnetic scattering on spherical poly-dispersions, American Elsevier, New York

DEIRMENDJIAN, K.L., K.L. SCHERE, J.T. PETERSON (1980), Theoretical estimates of actinic (spherically integrated) flux and photolytic rate constants of atmospheric species in the lower troposphere, Adv. Environ. Sci. Technol. 10, 369 - 459

De MORE, W.B., J.J. MARGITAN, M.J. MOLINA, R.T. WATSON, D.M. GOLDEN, R.F. HAMPSON, M.J. KURYLO, C.J. HOWARD, A.R. RAVISHANKARA (1985), Chemical kinetics and photochemical data for use in stratospheric modeling, Evaluation No. 7, JPL Publication No. 85 - 87

DE MORE, W.B., M.J. MOLINA, R.T. WATSON, D.M. GOLDEN, R.F. HAMPSON, M.J. KURYLO, C.J. HOWARD, A.R. RAVISHANKARA (1983), Chemical kinetics and photochemical data for use in stratospheric modeling, Evaluation No. 6, JPL Publication No. 83 - 92

DICKERSON, K.R., D.H. STEDMAN, A.C. DELANY (1982), Direct measurements of ozone and nitrogen dioxide photolysis rates in the troposphere, J. Geophys. Res. 87 (C7), 4933 - 4946

DIN (1979), Strahlungsphysik im optischen Bereich und Lichttechnik. Größen, Formeln und Kurzzeichen für photobiologisch wirksame Strahlung, DIN 5031, Teil 10, November 1979, 1 - 8

DOZIER, J. (1980), A clear-sky spectral solar radiation model for snow-covered mountainous terrain, Water Resources Research 16, 709 - 718

ELANSKIJ, N.F., JU.C. TRUTCE, E.A. USTINOV (1980), Potoki ul'trafioletovoj radiacii v nižnej atmosfere, Akademija Nauk SSSR, VINITI

ERICKSEN, P. (1993), Private communication

FEISTER, U. (1991), Messungen und Modellrechnungen der pflanzenwirksamen UV-Globalstrahlung in Potsdam, BMFT-Workshop, August 1991, Insel Vilm, 57 - 69

FEISTER, U. (1992), Comparison between Brewer spectrometer, M124 Filter Ozonometer and Dobson spectrophotometer, Quadrennial Ozone Symposium of IAMAP, Charlottesville, Virginia, June 1992, (to be published)

FEISTER, U. (1994), Measurements of chemically and biologically effective radiation reaching the ground, accepted for publication in J. Atmosph. Chem.

FEISTER, U., K.-H. GRASNICK (1992), Solar UV radiation measurements at Potsdam, Solar Energy 49, No. 6, 541 - 548

FEISTER, U., K.-H. GRASNICK, R. GREWE (1992), Instruments for broad-band UV radiation measurements, Solar Energy 49, No. 6, 535 - 540

FEISTER, U., K. DEHNE (1994), Intercomparison of UV spectrometers at the Meteorological Observatory Potsdam, June 1993, (to be published as DWD Abt. Forschung, Arbeitsergebnisse)

FREDERICK, J.E. (1990), Trends in atmospheric ozone and ultraviolet radiation: mechanisms and observations for the Northern hemisphere, Photochemistry and Photobiology 51, No. 6, 757 - 763

FRÖHLICH, C., J. LONDON (ed.) (1986), Revised instruction manual on radiation instruments and measurements, WCRP Publications, Ser. No. 7, WMO - TD No. 149

FINLAYSON-PITTS, B.J., J.N. PITTS, Jr. (1986), Atmospheric Chemistry, Fundamentals and experimental techniques, John Wiley & Sons, New York

GABM (1989), Global Atmospheric Monitoring for selected environmental parameters BAPMON data for 1986, Environmental Pollution Monitoring and Research Programme No. 57, Vol. 1

GERSTL, S.A.W., R.D. EDMOND, G.Z. WHITTEN (1987), Tropospheric ultraviolet radiation assessment of existing data and effects on ozone formation, EPA 600/3-87/047, Research Triangle Park, North Carolina

GERSTL, S.A.W., A. ZARDECKI, H.C. WISER (1981), Biologically damaging radiation amplified by ozone depletions, Nature 294, No. 5839, 352 - 354

GERSTL, S.A.W., A. ZARDECKI, H.C. WISER (1983), UV-B Handbook, Vol. I., Los Alamos National Laboratory, CA - UR - 83 - 728

GREEN, A.E.S., K.R. CROSS, L.A. SMITH (1980), Improved analytic characterization of ultraviolet skylight, Photochemistry and Photobiology 31, 59 - 65

GREEN, A.E.S., T. SAVADA, E.P. SHETTLE (1974a), The middle ultraviolet reaching the ground, Photochemistry and Photobiology 19, 251 - 259

GREEN, A.E.S., T. MO., J.H. MILLER (1974b), A study of solar erythema radiation doses, Photochemistry and Photobiology 20, 473 - 482

GUŠČIN, G.P. (1986), Obščee soderžanie atmosfernogo ozona i spektralnaja prozračnost atmosfery, Leningrad, Gidrometeoizdat 1986

HALPERN, P., J.V. DAVE (1974), Sea-level solar radiation in the biologically active spectrum, Science 186, 1204 - 1208

HENSE, A., M. KERSCHGENS, E. RASCHKE (1982), An economical method for computing the radiative energy transfer in circulation models, Quart. J. Roy. Meteorol. Soc. 108, 231 - 252

HINZPETER, H. (1955, 1956, 1957), Einfache Messungen und Rechnungen zur Globalstrahlung und zur diffusen Himmelsstrahlung, Z. Meteorol. 1955: 308 - 315; 1956: 100 - 110, 1957: 1 - 10

HOFZUMAHAUS, A., T. BRAUERS (1991), Die Oxidationsfähigkeit der Atmosphäre: Experimentelle Messungen der Ozon-Photolysefrequenz im UV-B auf dem Atlantik zwischen 50° N und 30° S, BMFT-Tagung Solare UV-B-Änderungen: Ursachen, Ausmaß, Wirkungen, 28. - 31. 8. 1991, Insel Vilm

HOFZUMAHAUS, A.,T. BRAUERS, U. PLATT, J. CALLIES (1992), Latitudinal variation of measured O_3 photolysis frequencies $J(O^1D)$ and primary OH production rates over the Atlantic Ocean between 50°N and 30°S, J. Atmosph. Chemistry 15, 283 - 298

HUDSON, R.D., W.D. KOMHYR, C.L. MATEER, R.D. BOJKOV (1991), Guidance for use of new absorption coefficients in processing Dobson and Brewer spectrophotometer total ozone data beginning 1 January 1992, Letter to operators at ozone stations, December 1991

JOSEPH, J.H., W.J. WISCOMBE, J.A. WEINMAN (1976), The Delta-Eddington approximation for a radiative flux transfer, J. Atmosph. Sci. 33, 2452 - 2459

KAASE, H. (1993), Private communication

KOMHYR, W.D. (1991), New Bass and Paur ozone absorption coefficients for use with Dobson spectrophotometers, Paper presented at the International Instrument Data Workshop held in Lanham, Maryland, September 11 - 13, 1991

KOMHYR, W.D., L. MACHTA (1973), The perturbed troposphere of 1990 and 2020, 28 Feb. - 3 March, 1973, Vol. IV, CIAP, Department of Transportation, Washington, D.C.

KERSCHGENS, M., E. RASCHKE, U. REUTER (1976), The absorption of solar radiation in model atmospheres, Beitr. Physik Atmosph. 49, 81 - 97

LEAN, J. (1987), Solar ultraviolet irradiance variations, A review, J. Geophys. Res. 92, 839 - 869

LIOU, K.-N. (1973), Transfer of solar irradiance through cirrus cloud layers, J. Geophys.Res. 78, 1409 - 1418

LIU, S.C., M. TRAINER (1988), Responses of the tropospheric ozone and odd hydrogen radiances to column ozone change, J. Atmosph. Chemistry 6, 221 - 233

MADRONICH, S. (1987), Photodissociation in the atmosphere, 1. Actinic flux and the effects of ground reflections and clouds, J. Geophys. Res. 92, No. D8, 9740 - 9752

MADRONICH, S., C. GRANIER (1992), Impact of recent total ozone changes on tropospheric ozone, photodissociation, hydroxyl radicals and methane trends, Geophys. Res. Lett. 19, No. 5, 465 - 467

MATVEEV, JU. C., L.T. MATVEEV (1984), Fiziko - statističeskij analiz global'nogo polja oblačnosti, Izvest. Akad. Nauk SSSK, Fiz. Atmosf. Okeana 20, 11, 1042 - 1054

McCULLOUGH, E.C. (1970), Qualitative and quantitative features of the clear day terrestrial solar ultraviolet radiation environment, Physics in Medicine Biology 15, 723 - 734

McPETERS, R. (1992), Private communication

MENTALL, J.E., D.E. WILLIAMS (1988), Solar ultraviolet irradiance on December 7, 1983 and December 10, 1984, J. Geophys. Res. D1, 735 - 746

MOUNT, G.H., G.J. ROTTMANN, J.G. TIMOTHY (1989), The solar spectral irradiance 1200 - 2550 A at solar maximum, J. Geophys. Res. 85, 4271 - 4274

MO, K. (1985), A review of solar irradiance measurements between 270 and 480 nanometers, Atmospheric Ozone, D. Reidel Publishing Company, Dordrecht / Boston / Lancaster, 661 - 665

MO, T., G.P. KEZWER, A.E.S. GREEN (1975), The use of the modified two-stream approximation to represent a multistream numerical solution of the radiative transfer equation, J. Geophys. Res. 80, 2072 - 2676

NAKAJIMA, T., M. TANAKA (1986), Matrix formulations for the transfer of solar radiation in a plane-parallel scattering atmosphere, J. Quant. Spectr. Radiat. Transfer 35, 13 - 21

NICOLET, M. (1980), Solar UV radiation and its absorption in the mesosphere and stratosphere, PAGEOPH, 118, 3 - 19

NICOLET, M. (1989), Solar spectral irradiance with their diversity between 120 and 900 nm, Aeronomica Acta, A, 338 - 1989

OPTRONICS (1991), Optronic Laboratories, Inc. OL 752 High Accuracy UV-visible spectroradiometer manual No. M000039, Revision D, March 1991

PALTRIDGE, G.W., I.J. BARTON (1978), Erythemal ultraviolet radiation distribution over Australia - the calculations, detailed results and input data including frequency analysis of observed Australian cloud cover, Division of the Atmospheric Physics Technical Paper No. 33, Commonwealth Scientific and Industrial Research Organization, Australia

PEROV, S.A., A.KH. KHRGIAN (1980), Sovremennye problemy atmosfernogo ozona, Leningrad. Gidrometeoizdat

PETERSON, J.T. (1976), Calculated actinic fluxes (290 - 700 nm) for air pollution photochemistry application, EPA-600/4-76-025, June 1976

PETERSON, J.T. (1977), Dependence of the NO_2 photodissociation rate constant on altitude, Atmosph. Environment 11, 689 - 695

PITARI, G., V. RIZI (1993), An estimate of the chemical and radiative perturbation of stratospheric ozone following the eruption of Mt. Pinatubo, J. Atmosph. Sci. 50, No. 19, 3260 - 3276

RIDLEY, B. A., S. MADRONICH, R.B. CHATFIELD, J.G. WALEGA, R.E. SHETTER, M.A.CARROLL, D. MONTZKA (1992), Measurements and model simulations of the photostationary state during the Mauna Loa Observatory Photochemistry Experiment: Implications for radical concentrations and ozone production and loss rates, J. Geophys. Res. 97, No. D10, 10,375 - 10,388

RUGGABER, A., R. FORKEL, R. DLUGI (1993), Spectral actinic flux and its ratio to spectral irradiance by radiation transfer calculations, J. Geophys. Res. 98, No. D1, 1151 - 1162

RUNDEL, R. (1986), Computation of spectral distribution and intensity of solar UV-B radiation, Stratospheric Ozone Reduction, Solar Ultraviolet and Plant life. NATO ASI Series G: Ecological Scienes, 8, Springer-Verlag, Berlin, Heidelberg, New York, Tokyo, 49-62

SCHIPPNICK, P.F., A.E.S. GREEN (1982), Analytical characterization of spectral actinic flux and spectral irradiance in the middle ultraviolet, Photochemistry and Photobiology 35, 89 - 101

SCHNEIDER, W.E., D.G. GOEBEL (1984), Standards for calibration of optical radiation measurement systems, Reprint from Laser Focus Electro Optics, September 1984

SETLOW, R.B. (1974), The wavelengths in sunlight effective in producing skin cancer: A theoretical analysis, Proc. Nat. Acad. Sci. USA 71, No.9, 3363 - 3366

SHETTLE, E.P., A.E.S. GREEN (1974), Multiple scattering calculation of the middle ultraviolet reaching the ground, Appl. Optics 13, No.7, 1567 - 1581

SLOMKA, J., K. SLOMKA (1984), Participation of ultraviolet in the global solar radiation, Publs. Inst. Geophys. Pol. Acad. Sc. D-20, (178), 59 - 69

SMITH, R.A., K.S. BAKER, O. HOLM-HANSEN, R. OLSON (1980), Photoinhibition of photosynthesis in natural waters, Photochemistry and Photobiology 31, 585 - 592

SMITH, R.C., Z. WAN, K.S. BAKER (1992), Ozone depletion in Antarctica: Modelling its effects on solar UV irradiance under clear-sky conditions, J. Geophys. Res. 97, C5, 7383 - 7397

SONNTAG, D. (1989), Formeln verschiedenen Genauigkeitsgrades zur Berechnung der Sonnenkoordinaten, Abh. des MD der DDR 143

STOLARSKI, R., R. BOJKOV, L. BISHOP, C. ZEREFOS, J. STAEHELIN, J. ZAWODNY (1992), Measured trends in stratospheric ozone, Science 256, 342-349

SUTHERLAND, J.C., K.P. GRIFFIN (1981), Absorption spectrum of DNA for wavelengths greater than 300 nm, Radiation Research 86, 399 - 409

THEKAEKARA, M.P., A.J. DRUMMOND (1971), Standard values for the solar constants and its spectral components, Nature Physical Science 229, 6-9

TITUS, J.G. (ed.) (1986), Effects of changes in stratospheric ozone and global climate, US EPA UNEP Report, August 1986

TSAY, S.-C., K. STAMNES (1992), Ultraviolet radiation in the Arctic: The impact of potential ozone depletions and cloud effects, J. Geophys. Res. 97, D8, 7829 - 7840

UNEP (1989), Environmental Effects Panel Report Pursuant to Article 6 of the Montreal Protocol on Substances that Deplete the Ozone Layer under the Auspices of the United Nations Environment Programme UNEP, November 1989

UNEP (1991), Environmental Effects of Ozone Depletion: 1991 Update. Panel Report Pursuant to Article 6 of the Montreal Protocol on Substances that Deplete the Ozone Layer under the Auspices of the United Nations Environment Programme (UNEP), November 1991

WEATHERHEAD, E.C., C. McNEELY (1994), Considerations on establishing a Ultraviolet Index, (submitted for publication by Photochemistry and Photobiology)

WHITE, O.R. (ed.) (1977), The solar output and its variation, Colorado Associated University Press, Boulder

WMO (1992), WMO/UNEP Scientific Assessment of Stratospheric Ozone 1991, WMO Ozone Report # 25

ZAVODSKA, E. (1981), Biologisch wirksame ultraviolette Strahlung, Contr. Geophys. Inst. Slovak. Acad. Sci., Ser. Meteor. 3, 33 - 49

ZDUNKOWSKI, W.W., R.M. WELCH, G. KORB (1980), An investigation of the structure of typical two-stream-methods for the calculation of solar fluxes and heating rates in clouds, Beitr. Phys. Atmosph. 53, 147 - 166

Annex

Algorithm to determine solar zenith angle θ and excentricity factor 1/ R^2 sun/earth (after Sonntag 1989)

B latitude (°)
L longitude (°)
L_Z longitude of time zone (°)
Y, M, I year, month, day
UTC universal time coordinated (L_Z = 0°)

TEH: time equation (h)
ZT: zonal time (h)
TST: true solar time (h)
UTC = ZT - L_Z/15 (h)
ZT = TST - TEH - L/15 + L_Z/15
TEH = TE/15 (± 3 s)

1. Day number from January 1, 2000, 12 h

$$n = INT[365.25(2000-Y)] + INT\left(\frac{275\,M}{9}\right) - INT\left(\frac{9+M}{12}\right) + [1 - INT\left(\frac{9+M}{12}\right)]\left[INT\left(\frac{Y+2-4\,INT\left(\frac{Y}{4}\right)}{3}\right) + I - 31.5 + \frac{UTC}{24}\right.$$

2. Geometric, geocentric average longitude of the sun including aberration (°)

$$L_\odot = 280.458532° + 0.985647323\ n \qquad \pm 0.79''$$

3. Average anomaly of the sun (°)

$$M_\odot = 357.5277233 + 0.985600279\ n \qquad \pm 0.10''$$

4. Numerical excentricity of the earth's path (rad)

$$e = 0.016709114 - 1.1473 \cdot 10^{-9}\ n \qquad \pm 2 \cdot 10^{-8}$$

5. Average curtosis of the ecliptic (°)

$$\epsilon_m = 23.4392811 - 3.56035 \cdot 10^{-7}\ n \qquad \pm 0.001''$$

6. Geocentric, ecliptical longitude of the sun (°)

$$\lambda_\odot = L_\odot + \frac{180}{\pi}\left(2e \sin M_\odot + \frac{5}{4}\, e^2 \sin 2M_\odot\right) \qquad \pm 60.455''$$

7. Geocentric rectascension of the sun (°)

$$\tan \alpha_\odot = \frac{\cos \epsilon_m \ \sin \lambda_\odot}{\cos \lambda_\odot} \qquad \pm 65.5''$$

8. Geocentric declination of the sun (°)

$$\sin \delta = \sin \epsilon_m \sin \lambda_\odot \qquad \pm 35''$$

9. Time equation (°)

$$TE = L_\odot - \alpha_\odot \qquad \pm 45''$$

10. Hour angle of true sun (°)

$$t_\odot = 15\ (UTC + \frac{L}{15} + TE \pm 12) \qquad \pm 45''$$

11. Azimuth of the sun (°)

$$\tan a_\odot = \frac{-\sin t_\odot}{\cos B \tan \delta - \sin B \cos t_\odot} \qquad \pm 77''$$

12. Zenith angle of the sun (°) $\theta = 90° - h_\odot$

$$\sin h_\odot = \sin B \sin \delta + \cos B \cos \delta \cos t_\odot \qquad \pm 55''$$

13. Radiusvector Earth/Sun in Astronomical Units (Excentricity $1/R^2$)

$$R = 1 + \frac{1}{2} e^2 - (e - \frac{3}{8} e^3) \cos M_\odot - (\frac{e^2}{2} - \frac{e^4}{3}) \cos 2M_\odot - \frac{3}{8} e^3 \cos 3M_\odot - \frac{e^4}{3}$$

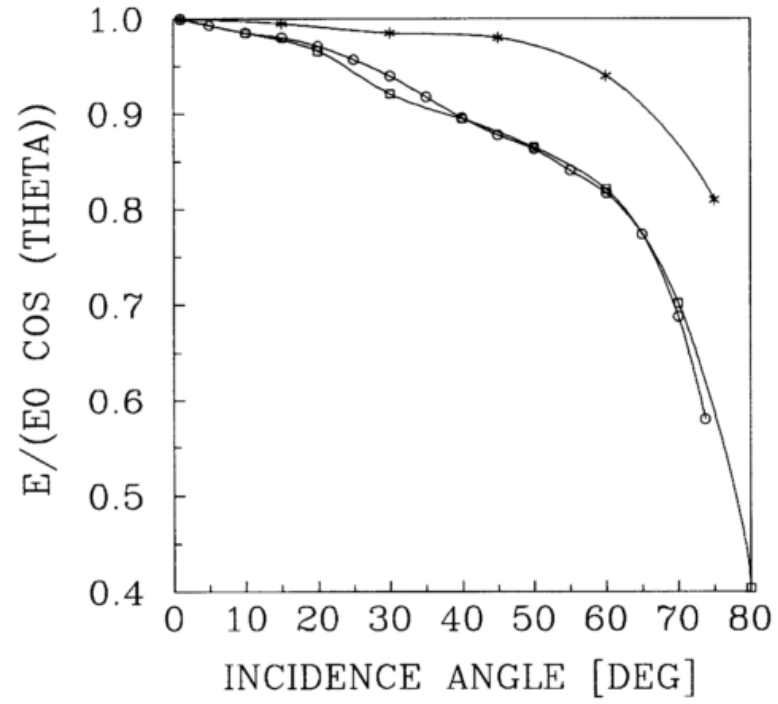

Fig. 1 Cosine error of the spectrometer OL 752/10
○○○ measured at Potsdam
□□□ measured by DEHNE (1992)
*** given by OPTRONICS (1991)

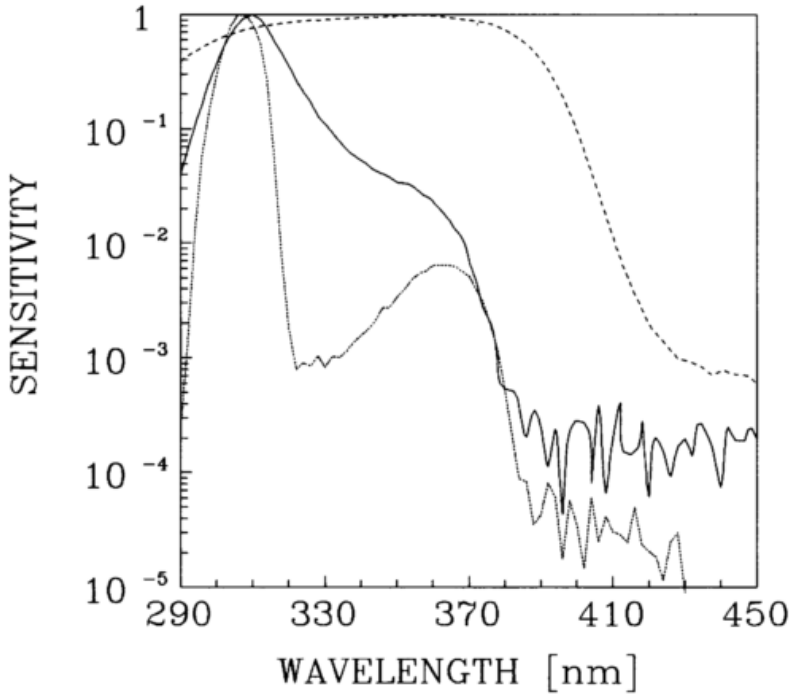

Fig. 2 Nominal sensitivities of the filter instruments UV-S (solid line), UV-L (dashed line) and UV-B (dotted line). The latter instrument was not used in the intercomparison.

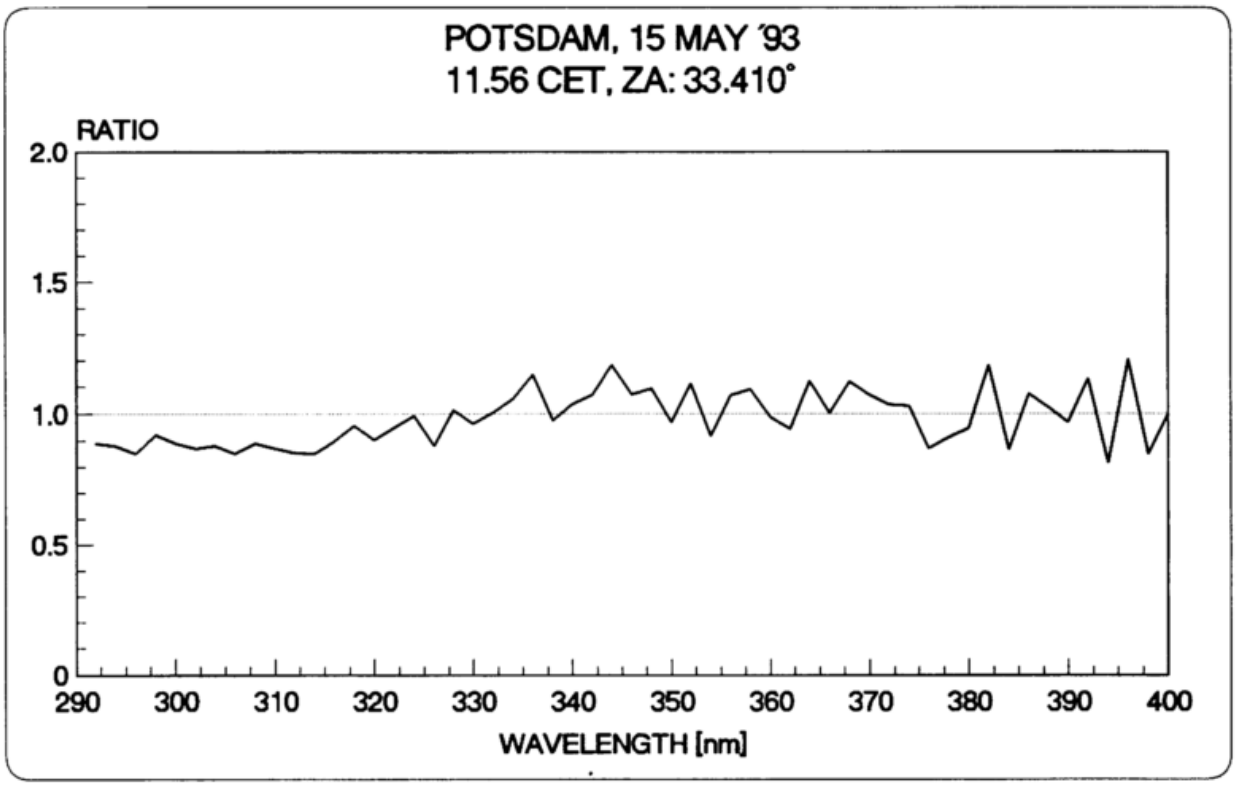

Fig. 3 Ratio between a measured spectrum and the corresponding model calculation for May 15, 1992 (Θ = 33.410°, O_3 = 336 D, τ_{350} = 0.7, A = 5 %)

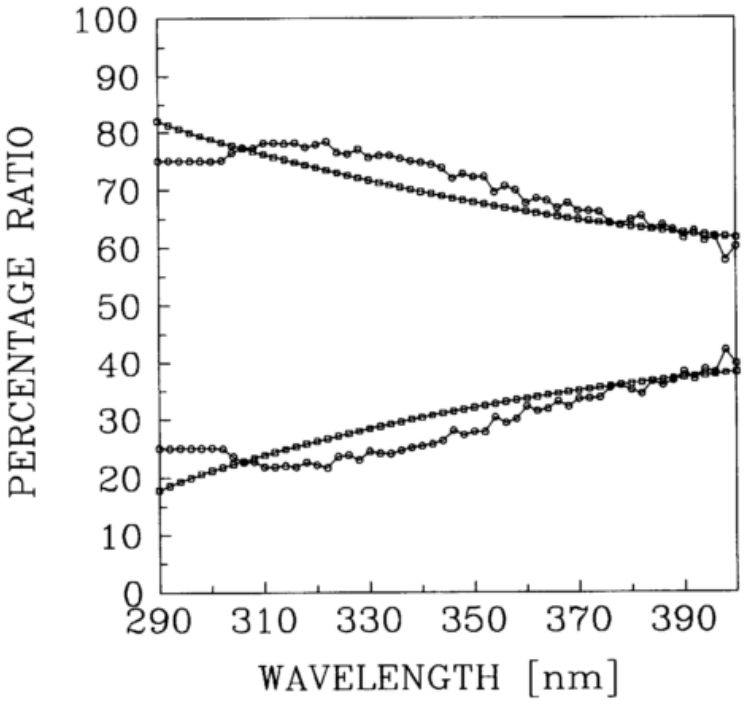

Fig. 4 Ratio between diffuse and global radiation (upper curves) and between direct and global radiation (lower curve)
□□□ model calculation ○○○ measurement on May 15, 1992, Θ = 33.410°

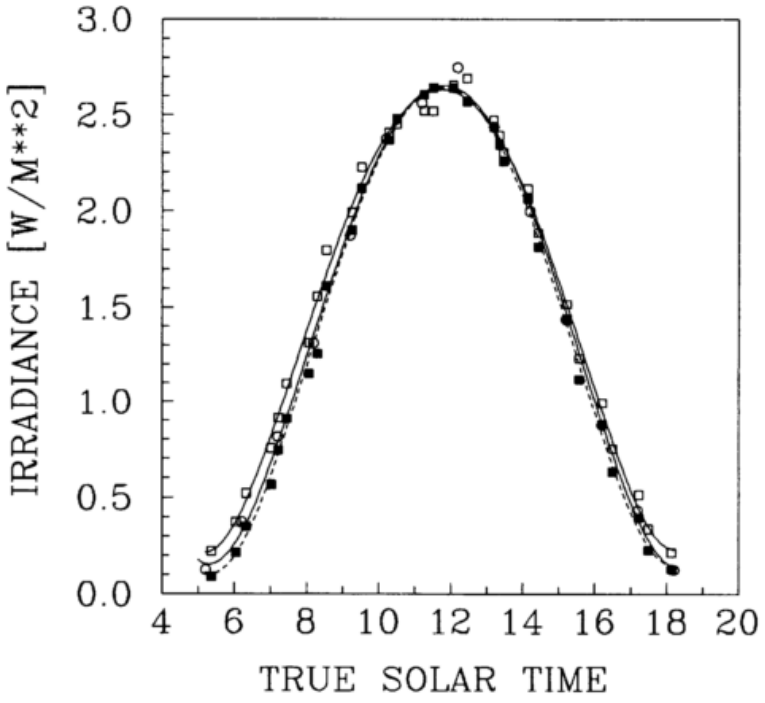

Fig. 5 Measured and modelled irradiance for UV-S on May 15, 1992

○○○ filter instrument UV-S (derived from hourly totals), new calibration scale

□□□ spectra from OL 752/10 weighted for the UV-S sensitivity

■■■ model calculations weighted for UV-S sensitivity

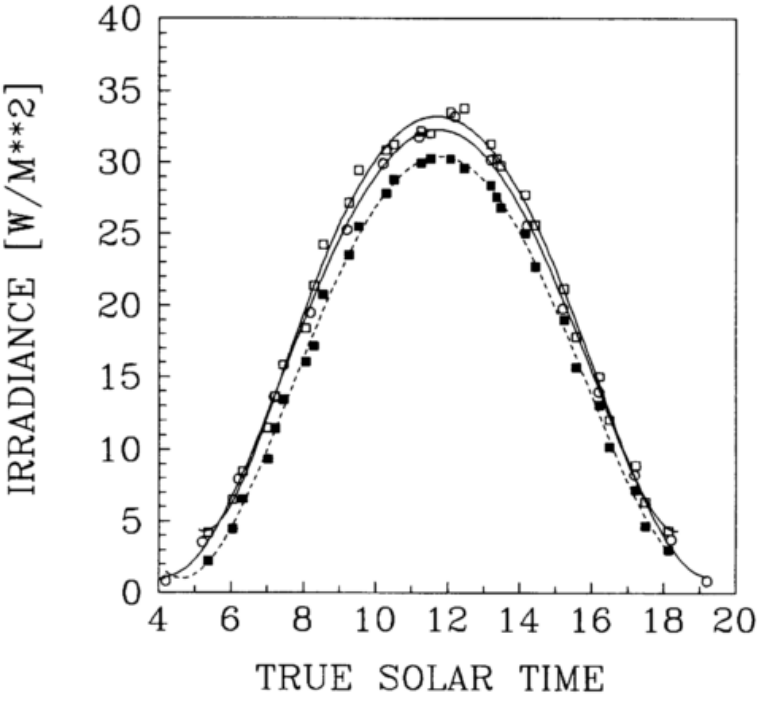

Fig. 6 Same as Fig. 5, but for UV-L

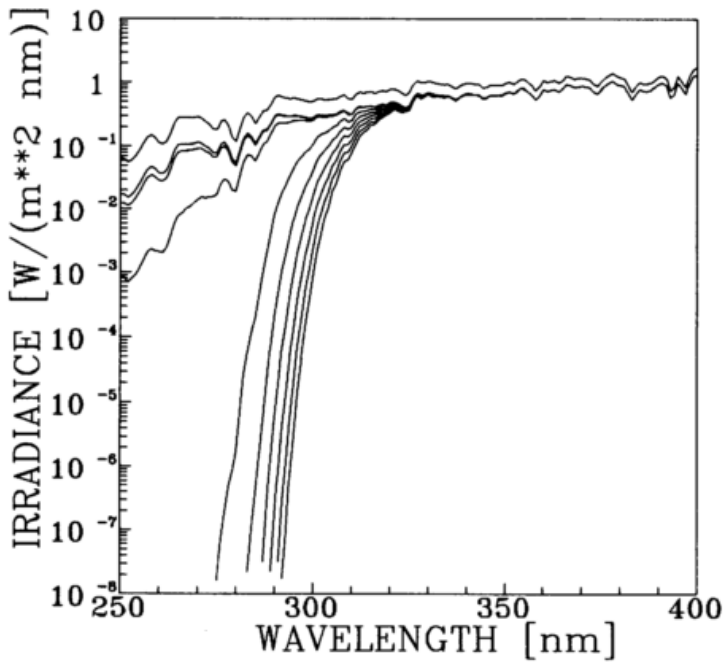

Fig. 7 Global UV irradiation for a zenith angle of $\Theta = 0°$, strong aerosol load (Table 1), surface albedo of A = 5 % and cloudless conditions at sea level for different values of total ozone; the curves from top to bottom are

1 extraterrestrial radiation (CIMO 1981)

2 O_3 = 0 D, i.e. only Rayleigh scattering + aerosol extinction

3 O_3 = 1 D

4 O_3 = 10 D

5 O_3 = 100 D

6 O_3 = 200 D

7 O_3 = 300 D

8 O_3 = 400 D

9 O_3 = 500 D

10 O_3 = 600 D

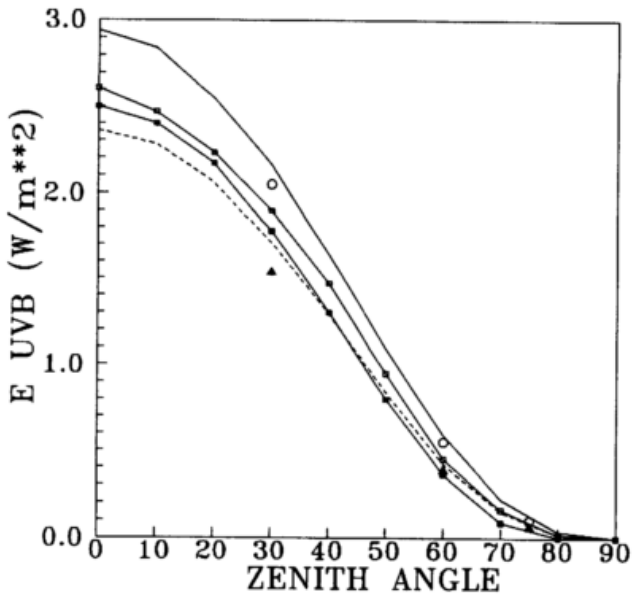

Fig. 8 Modelled clear sky global UVB radiation ($280 < \lambda < 315$ nm) as compared to calculated irradiances from other models

———	this model, O_3 = 280 D, A = 25 %, aerosol: $\tau_{350} = 0.1$
- - -	this model, O_3 = 280 D, A = 5 %, aerosol: $\tau_{350} = 0.4$
○○○	BELINSKIJ et al. (1968), O_3 = 280 D
□□□	GERSTL et al. (1983), O_3 = 278 D, A = 0 %, $\tau_{350} = 0.0$
■■■	CHAPMAN (1987), O_3 = 280 D, A = 25 %, aerosol: $\tau_{350} = 0.4$
▲▲▲	DAVE and HALPERN (1976), O_3= 280 D

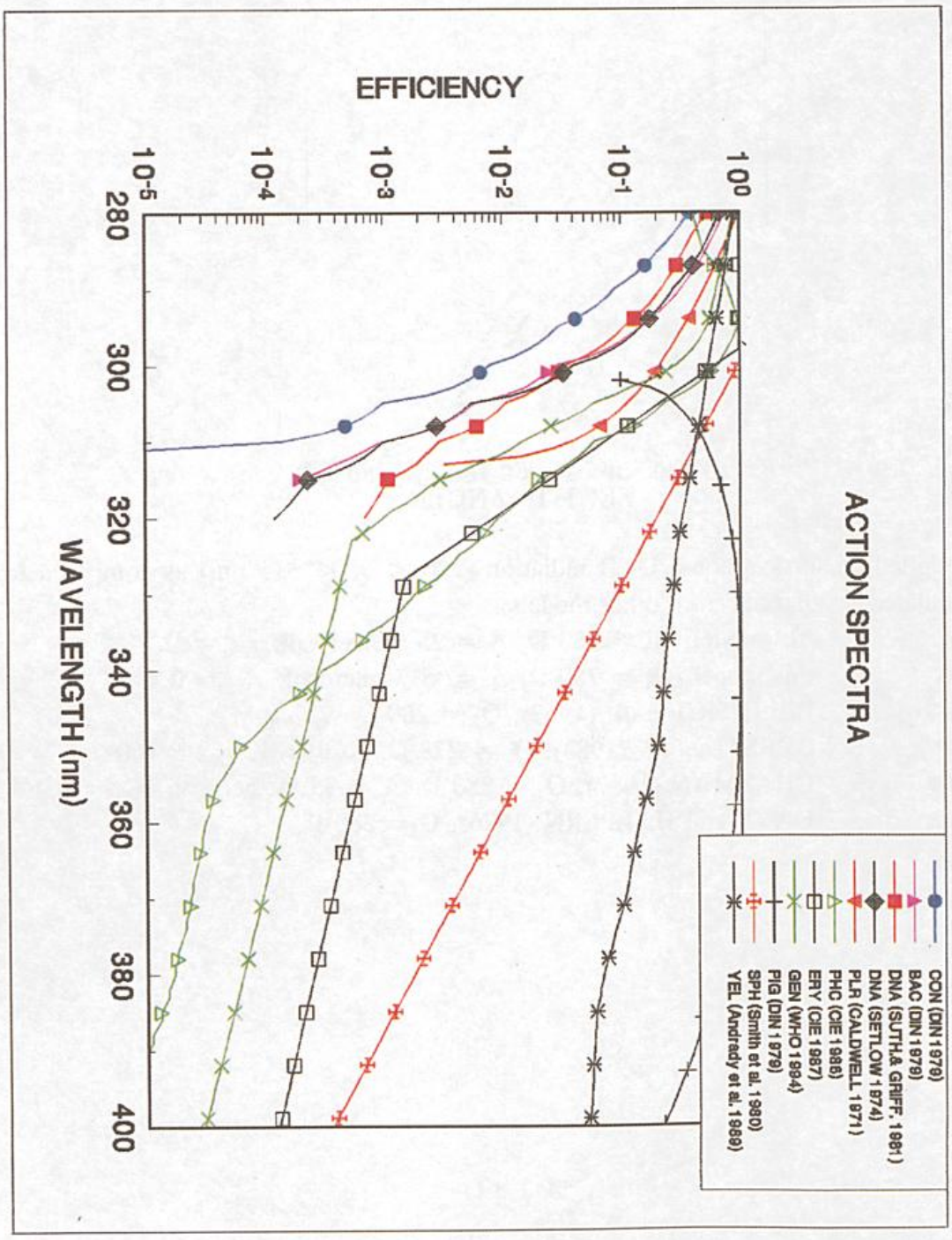

Fig. 9 Action spectra of UV radiation effects to the biosphere and materials

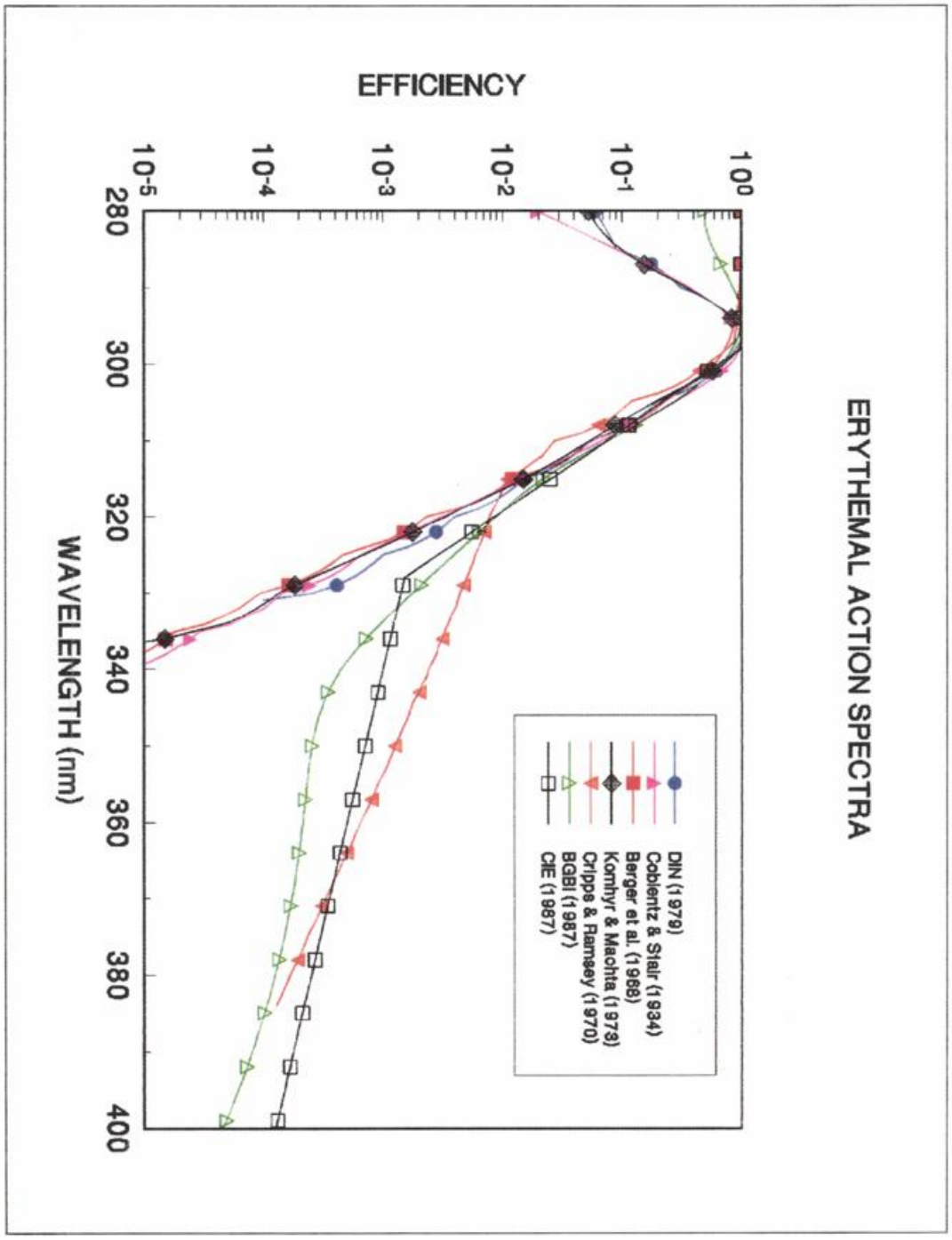

Fig. 10 Erythemal action spectra

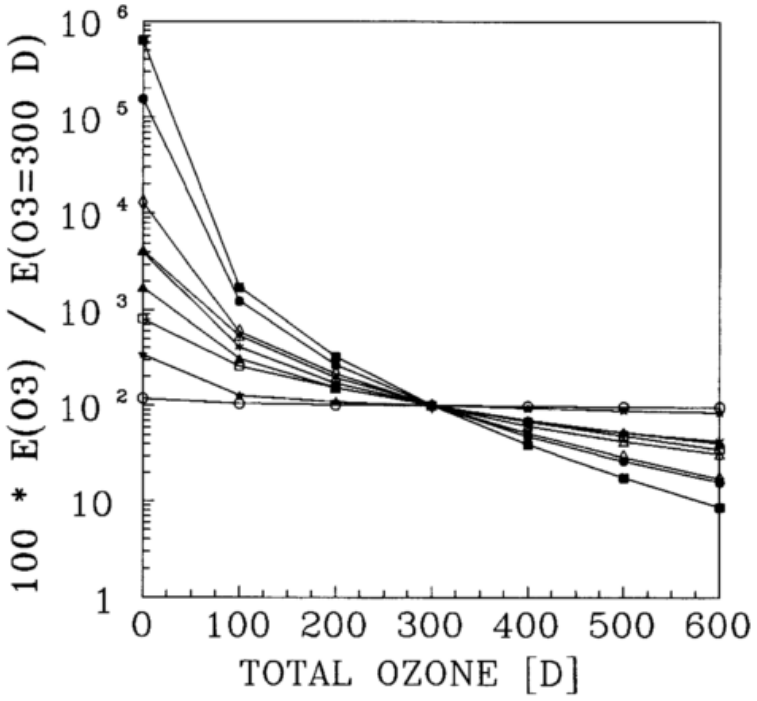

Fig. 11 Ratios between effective UV radiation for changing total ozone values referred to the radiation at O_3 = 300 D (Θ = 60°, A = 5 %, strong aerosol load, clear sky)

○○○	UV = UVA + UVB	▲▲▲	KER
□□□	UVB	●●●	BAC
△△△	ERY (DIN 1979)	◇◇◇	PLR
***	PHC	★★★	YEL PVC
■■■	CON		

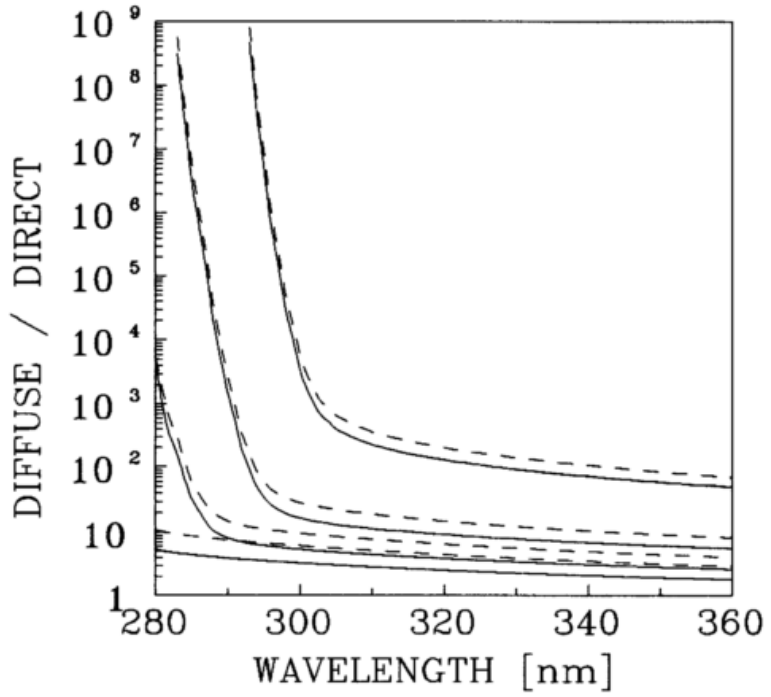

Fig. 12 Ratios between diffuse and direct solar irradiance for different solar zenith angles (from top to bottom) Θ = 75°, 60°, 45° and 30° (O_3 = 300 D, very strong aerosol load, clear sky)

____ A = 0 %

- - - - A = 100 %

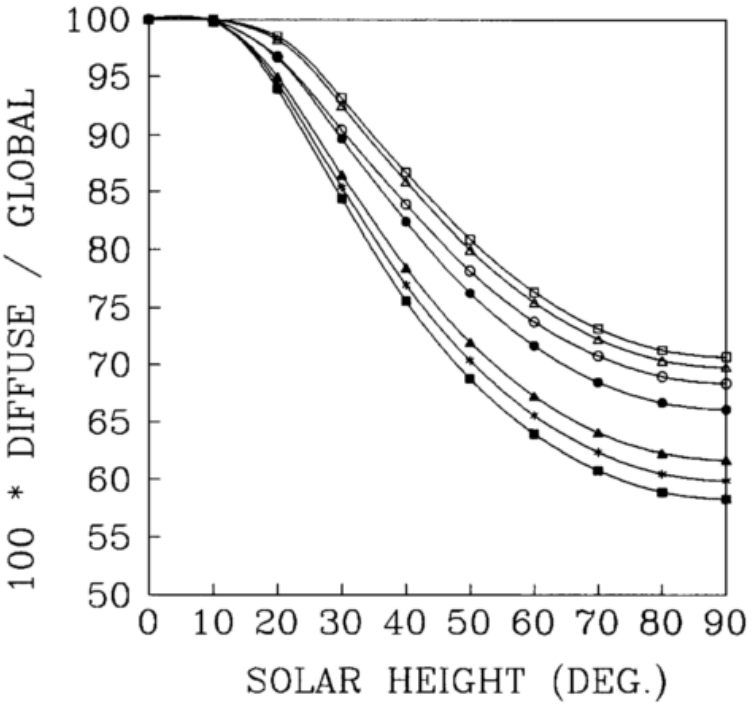

Fig. 13 Percentage ratios between diffuse and global radiation for some effects in dependence on solar zenith angle (O_3 = 300 D, A = 5 %, very strong aerosol load); for comparison, spectral characteristics of UV radiation instruments are shown

□□□ photoconjunctivitic radiation (DIN 1979)
△△△ plant response (CALDWELL (1971)
○○○ erythema (CIE 1987)
●●● sensitivity of the UV-S instrument (FEISTER et al. 1992)
▲▲▲ suppression of photosynthesis (SMITH et al. 1980)
* * * sensitivity of the UV-L instrument (FEISTER et al. 1992)
■■■ pigmentation (CIE 1986)

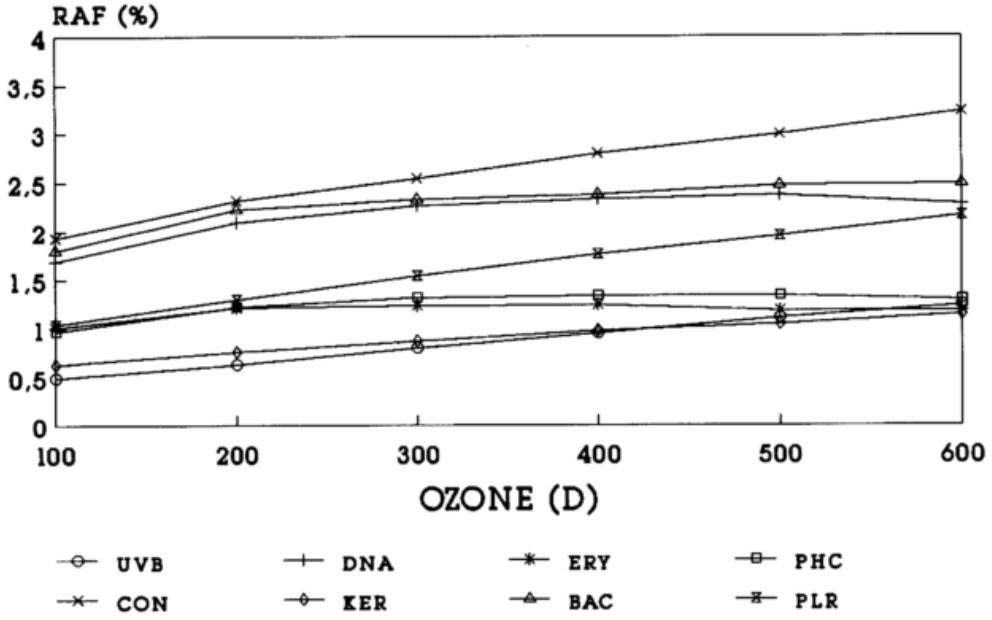

Fig. 14 Radiation Amplification Factors (RAF) for some biological effects of UV radiation ($\Theta = 0°$, strong aerosol load, clear sky) in dependence on ozone

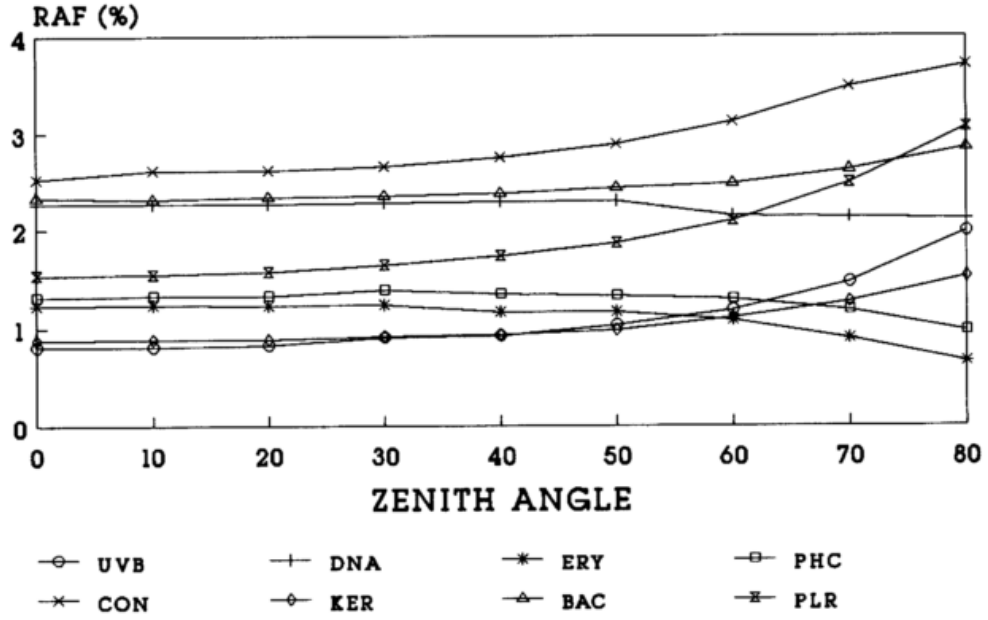

Fig. 15 Radiation Amplification Factors for some biological effects at different zenith angles (O_3 = 300 D, A = 5 %, strong aerosol load, clear sky)

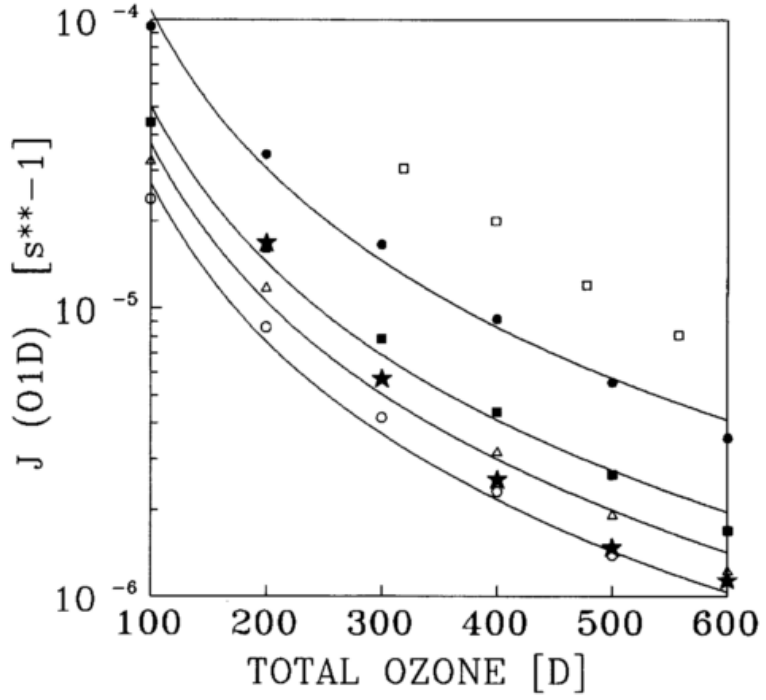

Fig. 16 Ozone photolysis frequencies in dependence on overhead column ozone for a zenith angle of $\Theta = 60°$ and a temperature of $t = 20$ °C

○○○ 1 this study, A = 5 %, very strong aerosol load: $J_{O1D} = 0.12061 \cdot O_3^{-1.82351}$

△△△ 2 this study, A = 5 %, weak aerosol load: $J_{O1D} = 0.16164 \cdot O_3^{-1.81872}$

■■■ 3 this study, A = 80 %, very strong aerosol load: $J_{O1D} = 0.21476 \cdot O_3^{-1.81363}$

●●● 4 this study, A = 80 %, weak aerosol load: $J_{O1D} = 0.48515 \cdot O_3^{-1.82570}$

□□□ 5 BLACKBURN et al. (1992)

★★★ 6 measurements by HOFZUMAHAUS et al. (1992) according to their relation

$J_{O1D} = \exp \{-8.02 - 8.8 \cdot 10^{-3} \cdot O_3 \sec \Theta + 3.4 \cdot 10^{-6} \cdot (O_3 \sec \Theta)^2\}$

(given for $t = 22$ °C and $28° < \Theta < 60°$, calculated at $\Theta = 60°$)

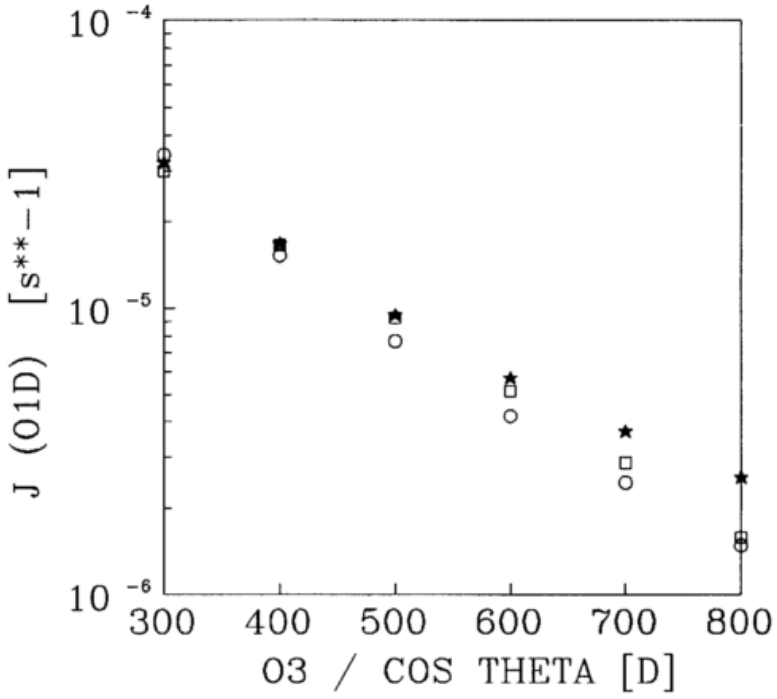

Fig. 17 O_3 photolysis frequencies in dependence on the *effective* ozone mass O_3 . sec Θ

○○○ this model calculated for constant O_3 = 300 D and varying zenith angle Θ (A = 5 %, strong aerosol load, temperature t = 20 °C)

□□□ results of measurements by HOFZUMAHAUS and BRAUERS (1991): $J_{O1D} = 1.74 \cdot 10^{-4} \exp \{-5.87 \cdot 10^{-3} \cdot O_3 \cdot \sec \Theta\}$

★★★ results of measurements by HOFZUMAHAUS et al. (1992) according to the parameterization given in Fig. 16

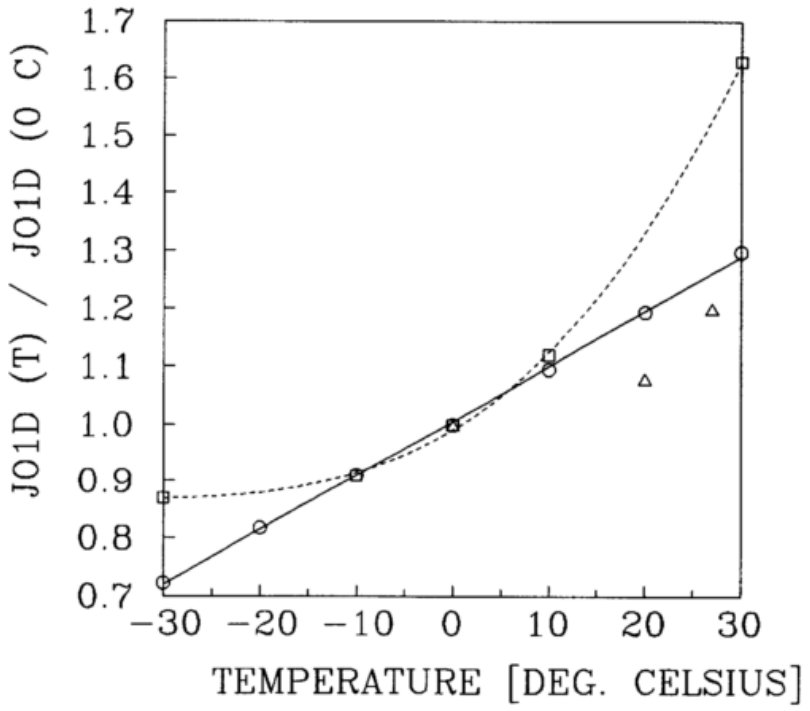

Fig. 18 Ratios between O_3 photolysis frequency at temperature t and O_3 photolysis frequency at t = 0 °C

○○○ this study for O_3 = 300 D, A = 5 %, Θ = 60° and strong aerosol load

□□□ measurements by DICKERSON et al. (1982)

△△△ measurements by BLACKBURN et al. (1992)

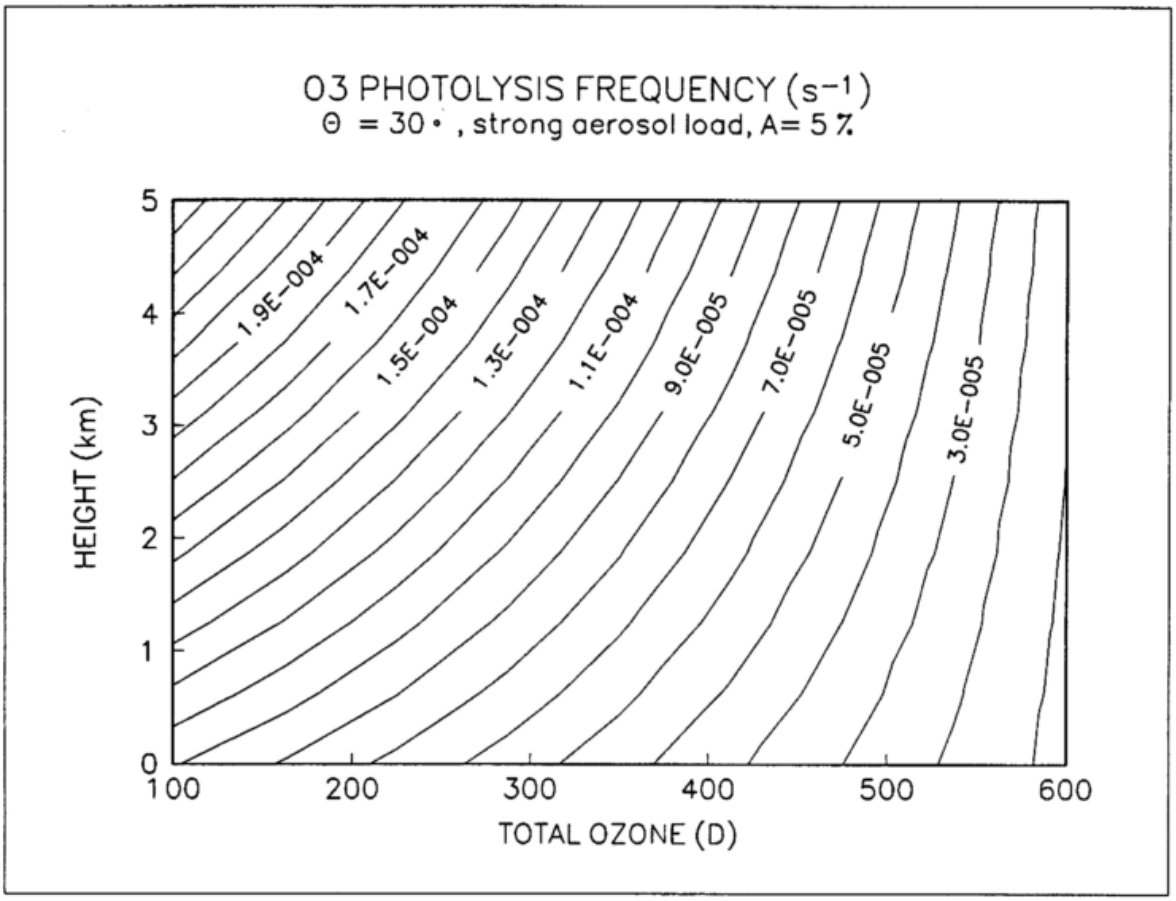

Fig. 19 Modelled photolysis frequencies of ozone J_{O1D} in s^{-1} for a solar zenith angle of $\Theta = 30°$, heights between 0 and 5 km, and total ozone values from 100 to 600 D (A = 5 %, clear sky, strong aerosol load)

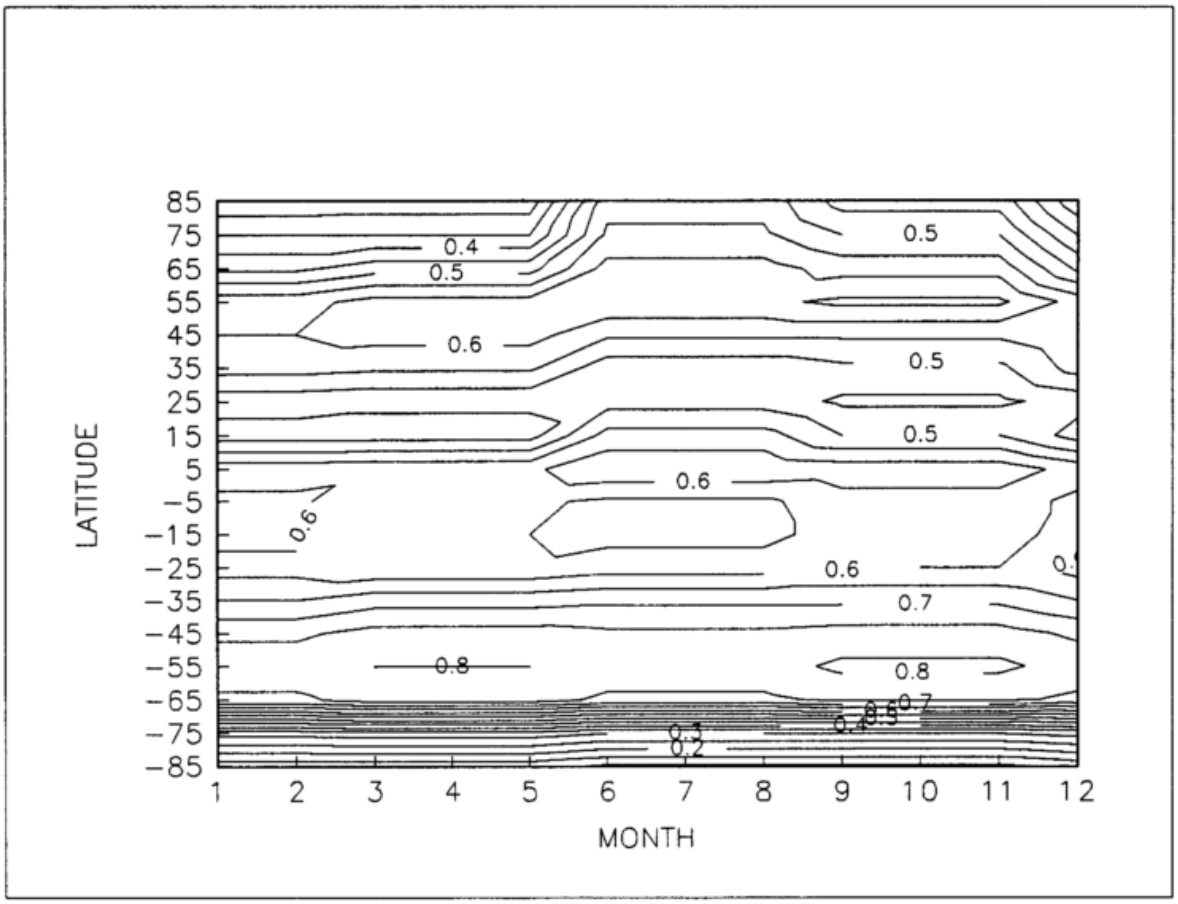

Fig. 20 Zonal and seasonal distribution of cloud cover in tenths (after MATVEEV and MATVEEV 1984) (top) and of total ozone in D (after PEROV and KHRGIAN 1980)

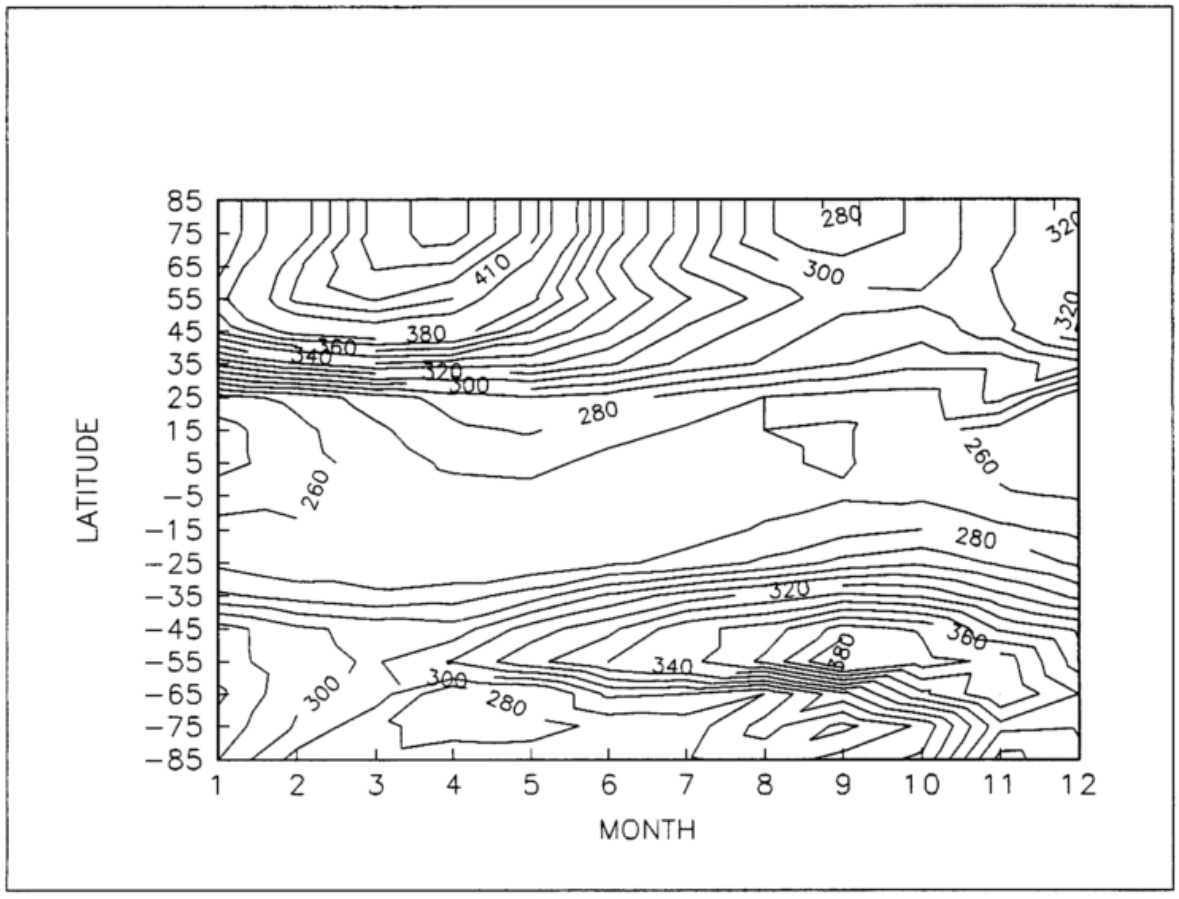

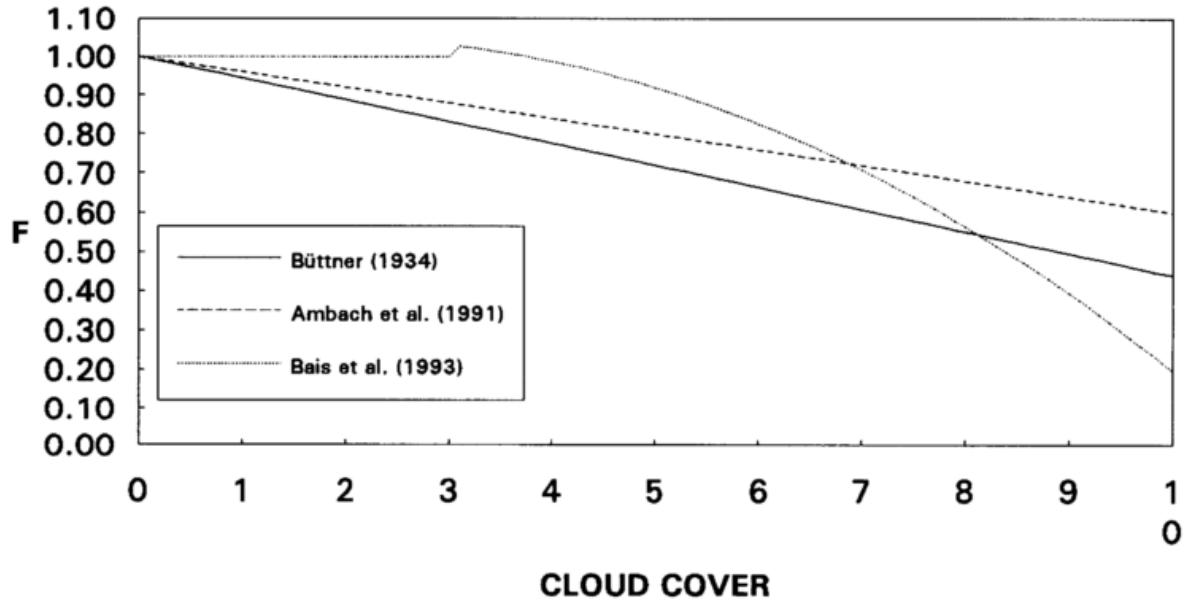

Fig. 21 Cloudiness factor F in dependence on total cloud cover (0 ... 10) according to three references

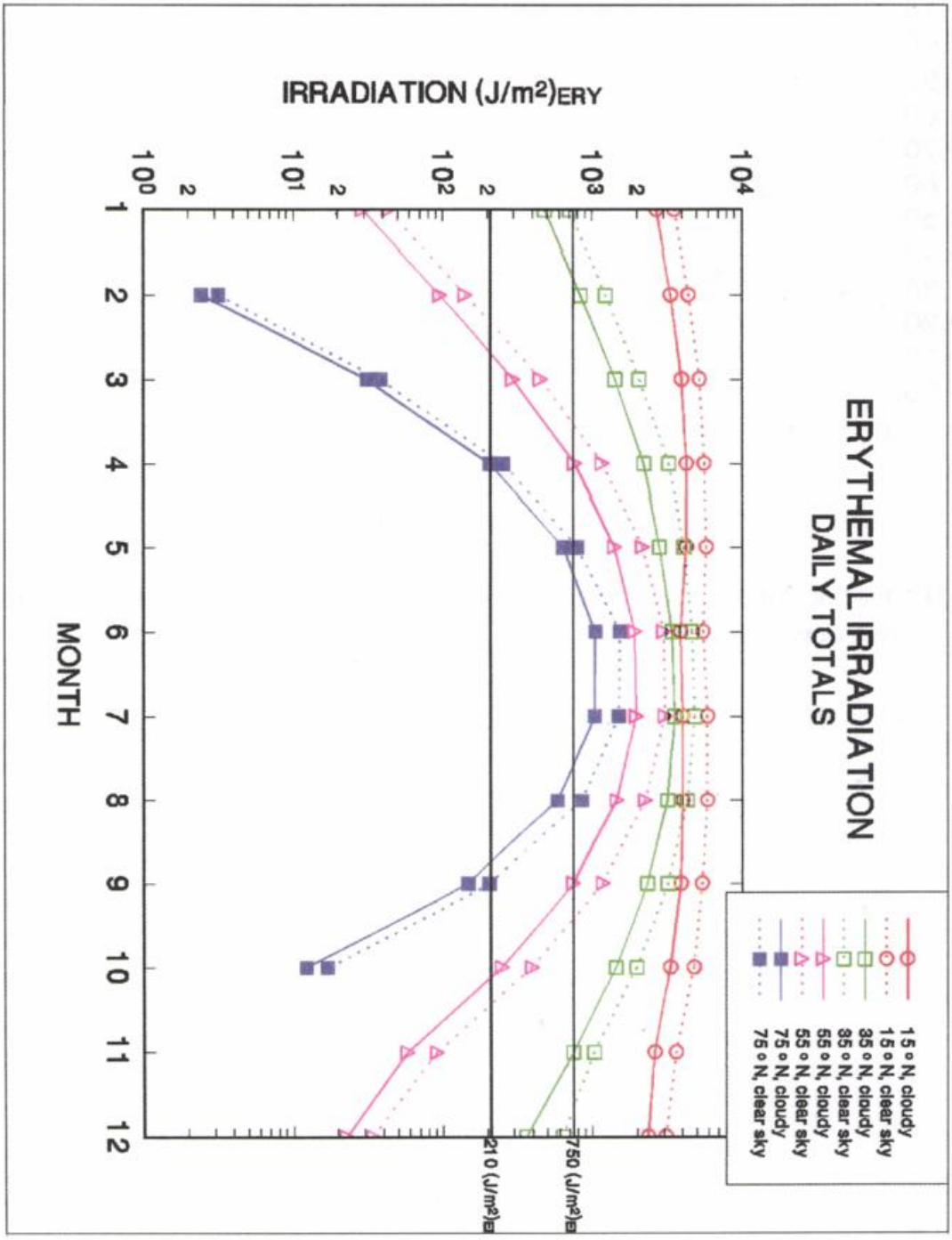

Fig. 22 a Daily totals of erythemal global irradiation (action spectrum from DIN 1979) for the 15th of each month for clear sky conditions (---) and average cloudiness (___) at the following latitudes

○○○ 15° N △△△ 55° N

□□□ 35° N ■■■ 75° N

Limits of the MED (210 … 750) $(J\ m^{-2})_{ERY}$ are shown as horizontal lines

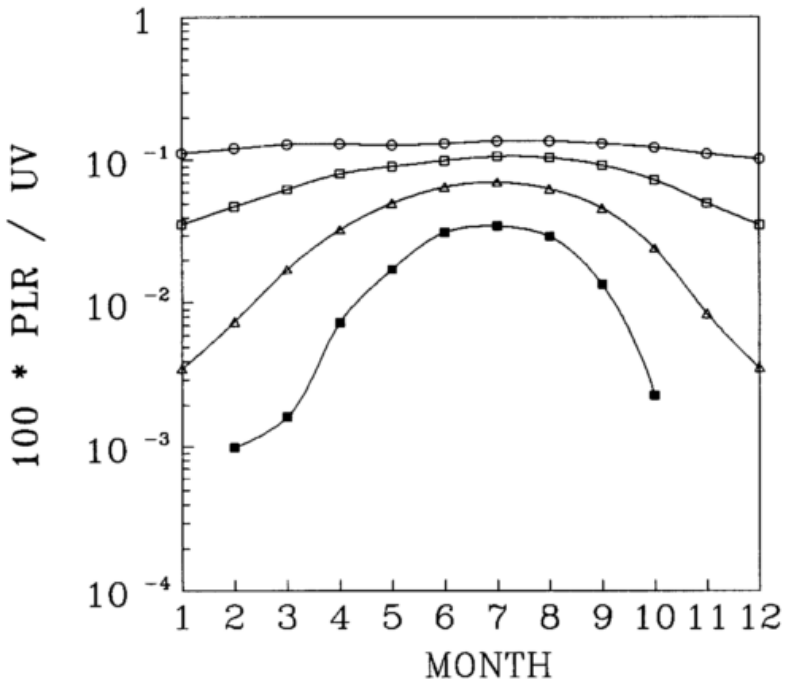

Fig. 23 Ratios between
a) plant damaging radiation and total UV radiation, and
b) erythemal radiation and total UV radiation
at 4 different latitudes

○○○ 15° N
□□□ 35° N
△△△ 55° N
■■■ 75° N

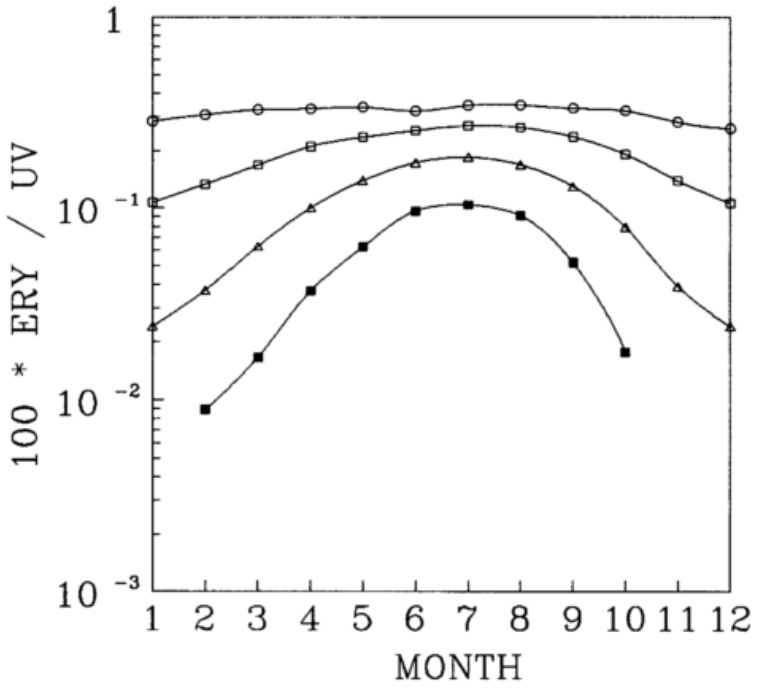

Wegen des Farbdrucks konnte die Reihenfolge der Abbildungen nicht eingehalten werden

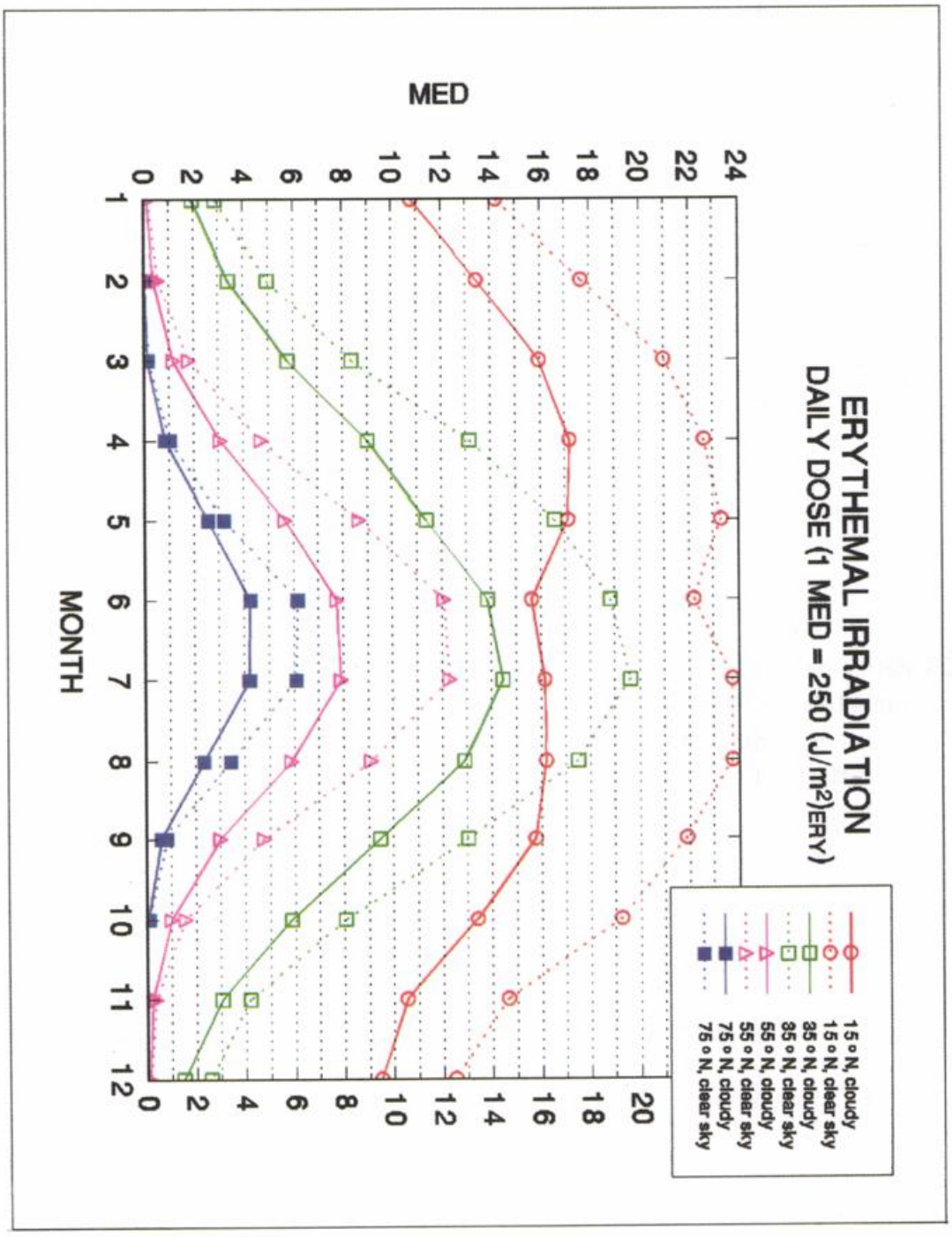

Fig. 22 b Seasonal course of the number of daily *M*inimal *E*rythemal *D*oses at different latitudes for clear sky and average cloudiness (1 MED = 250 (J m^{-2})$_{ERY}$)

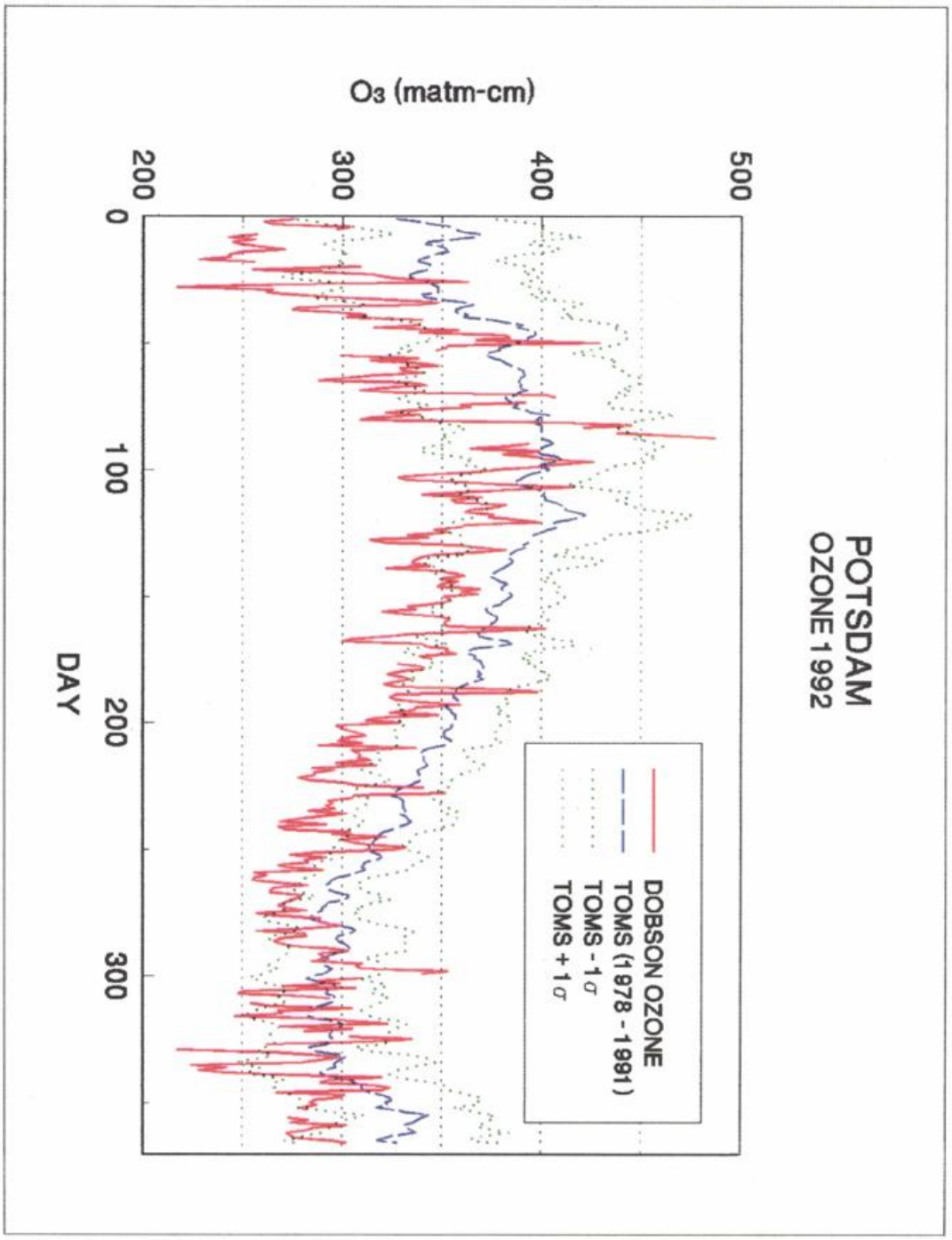

Fig. 26 Total ozone values from Dobson and Brewer measurements taken at Potsdam in 1992 (thick solid line). Long-term averages (dashed line) and $\pm$ 1 σ standard deviations (dotted lines) of TOMS satellite overpass data for the period 1978 to 1991 are shown for comparison.

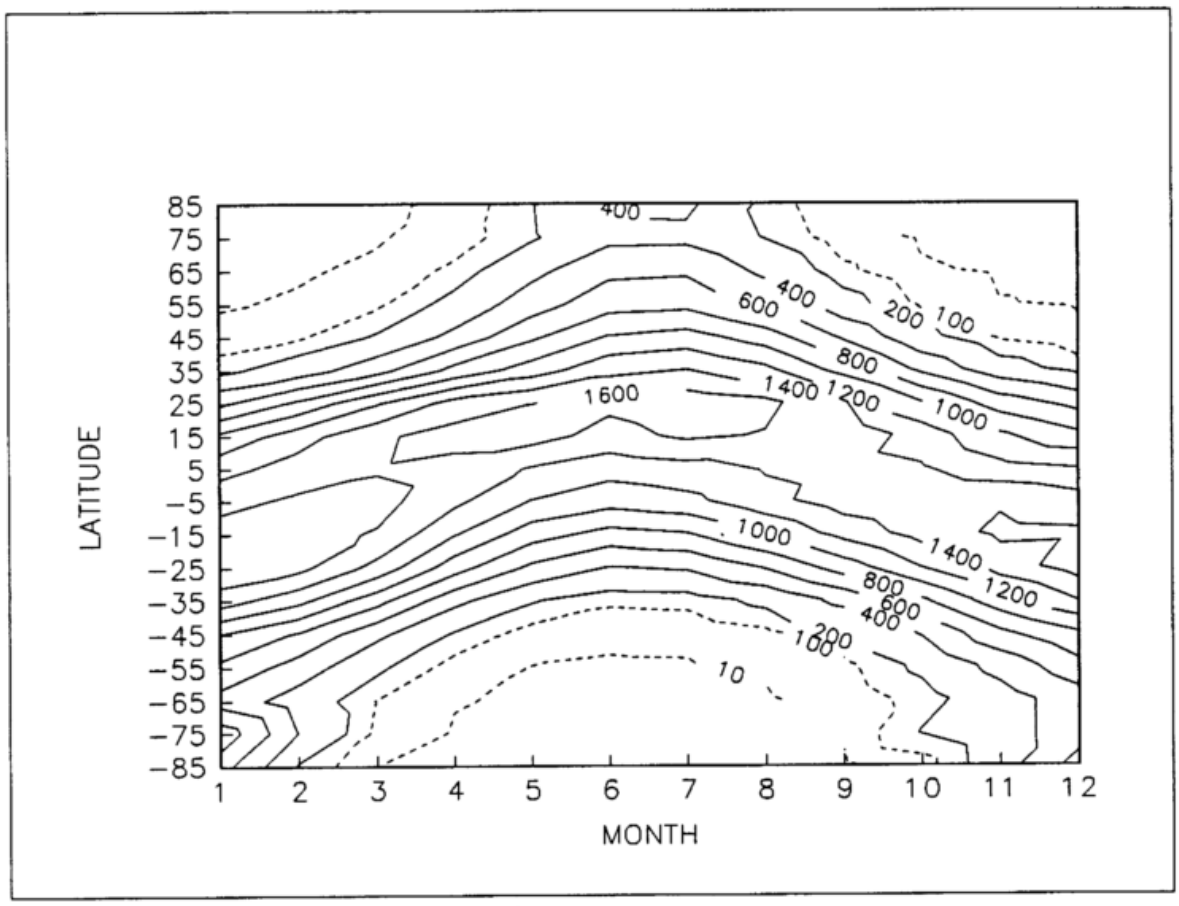

Fig. 24 Zonal and seasonal distribution of the effective global irradiation $(J\ m^{-2})_{PLR}$ producing plant response (CALDWELL 1971) modelled for average conditions of total ozone (natural levels) and cloudiness (see Fig. 20)

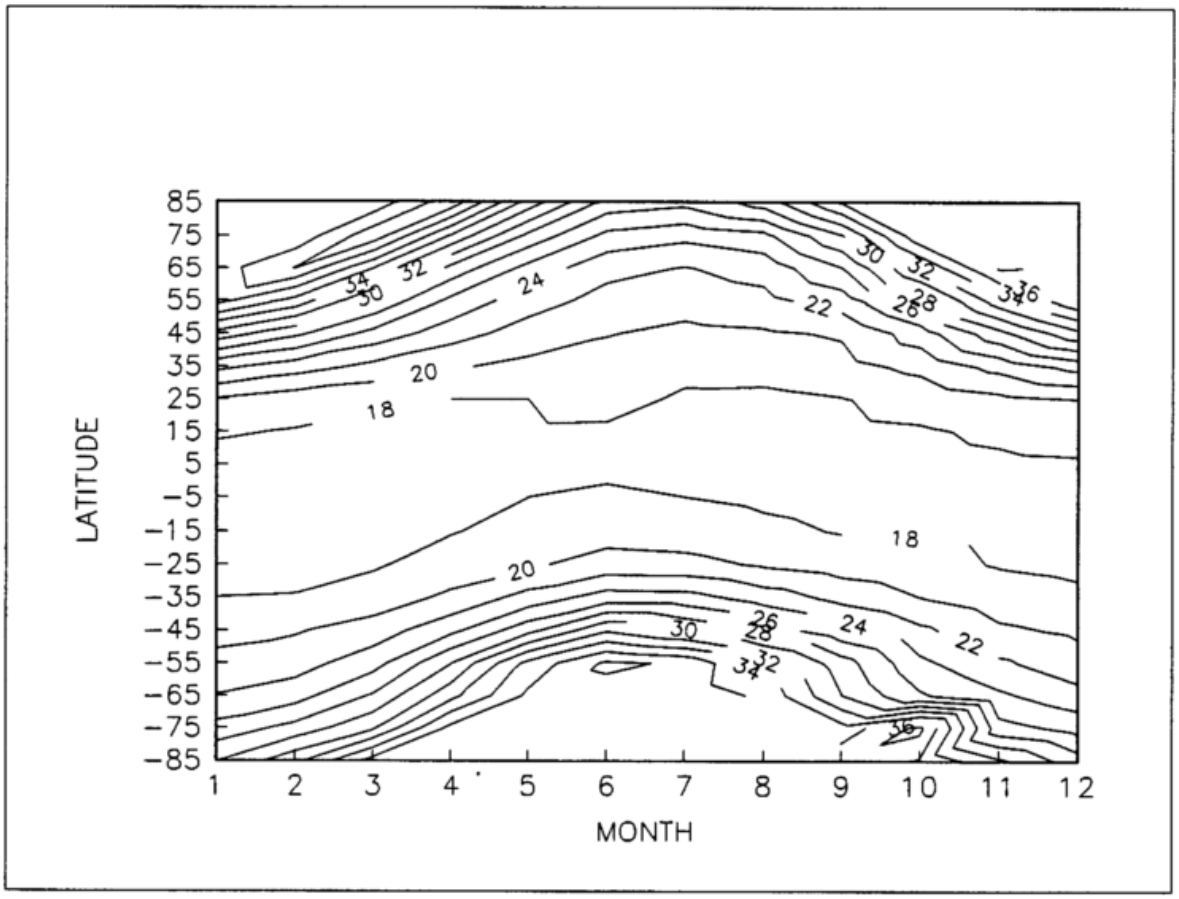

Fig. 25 Zonal and seasonal distribution of percentage changes in plant response for a reduction of total ozone by 10 %

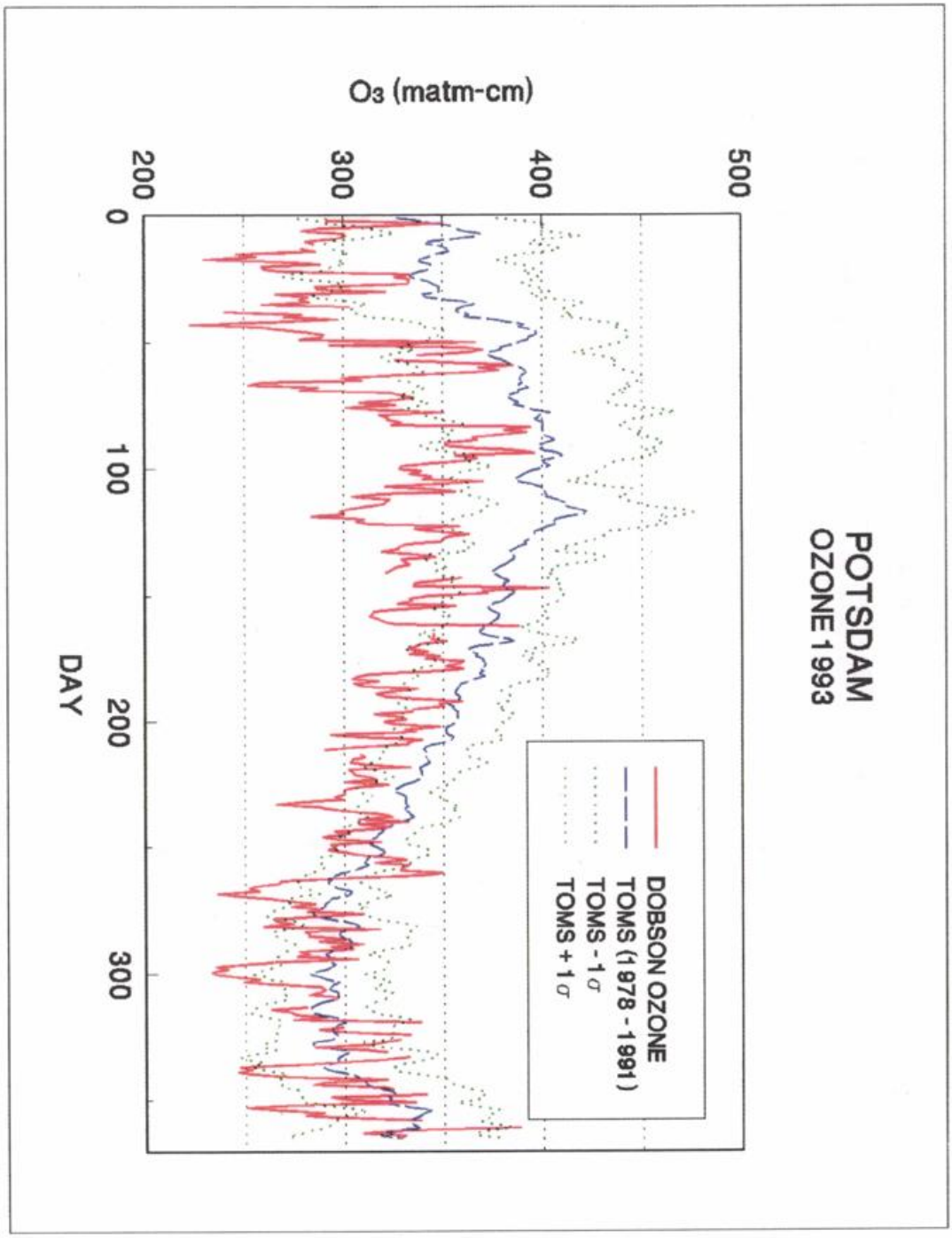

Fig. 27 As Fig. 26, but for 1993

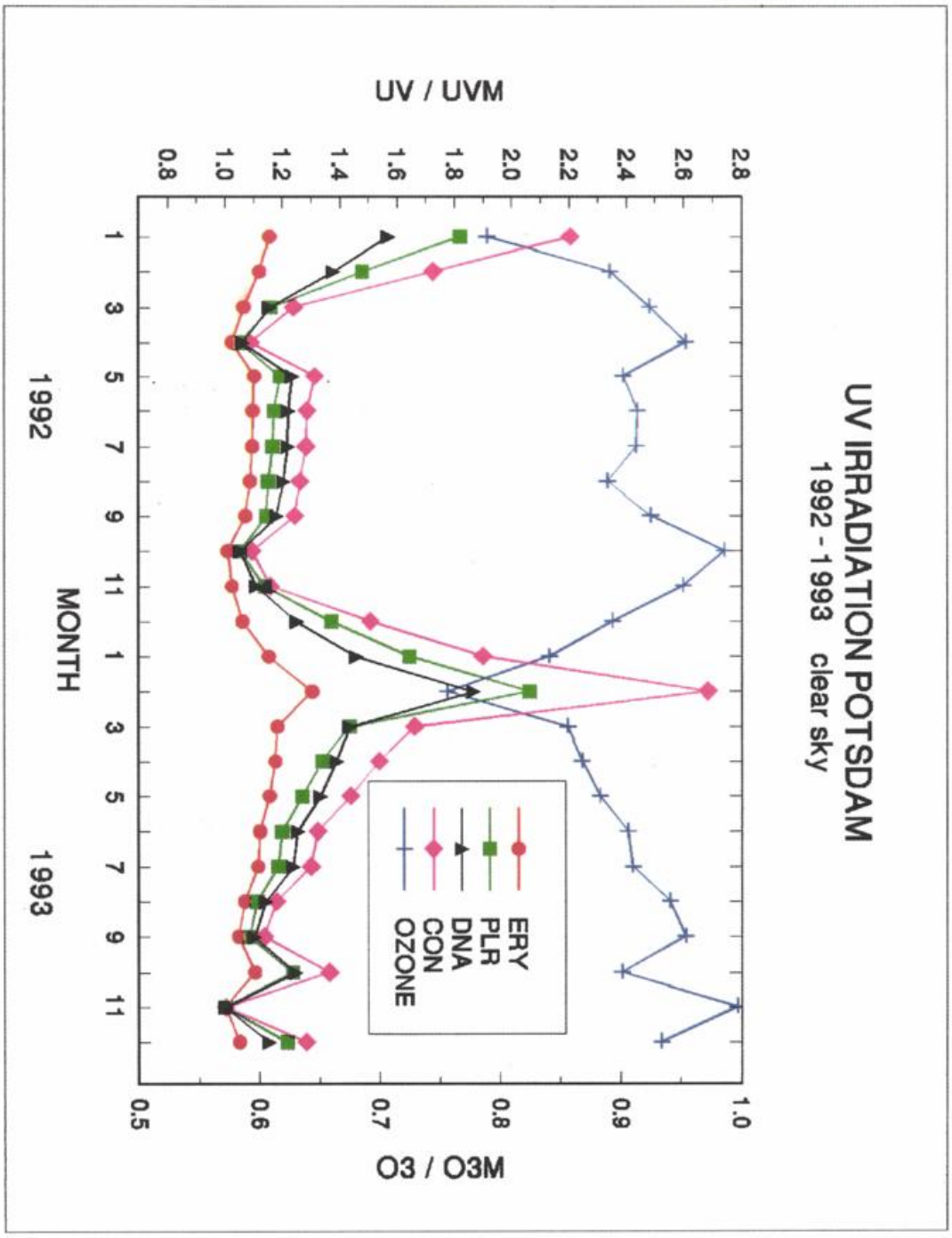

Fig. 28 Ratios between daily totals of effective UV irradiation (**clear sky**) modelled for monthly averages of total ozone at Potsdam in 1992/93 to the UV irradiation modelled for long-term averages of ozone (left-hand scale) and ratios of monthly averages of ozone measured in 1992/93 to the long-term averages of monthly means (determined from TOMS satellite data for Potsdam, version 6, 1978 - 1991, McPETERS 1992) (right-hand scale)

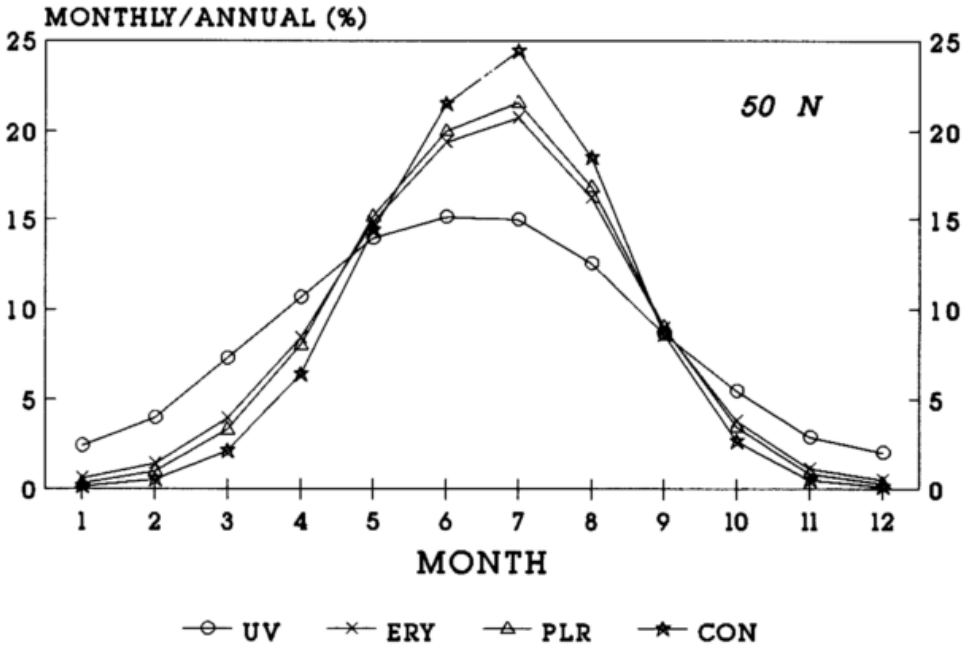

Fig. 29 Percentage contribution of monthly totals to the annual total UV irradiation modelled for 50° N, average ozone and clear sky

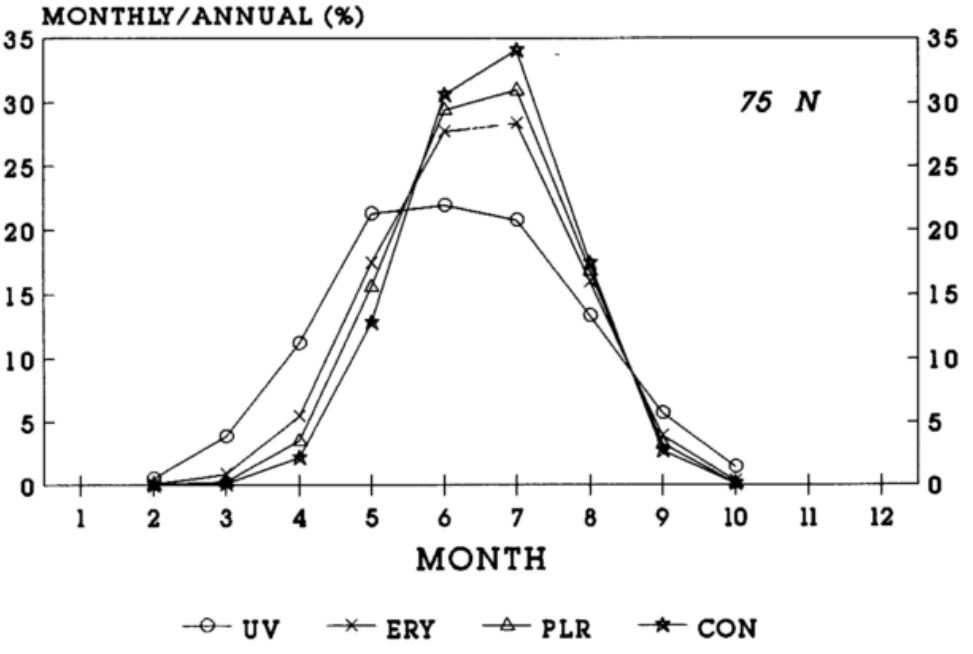

Fig. 30 As in Fig. 29, but for 75° N

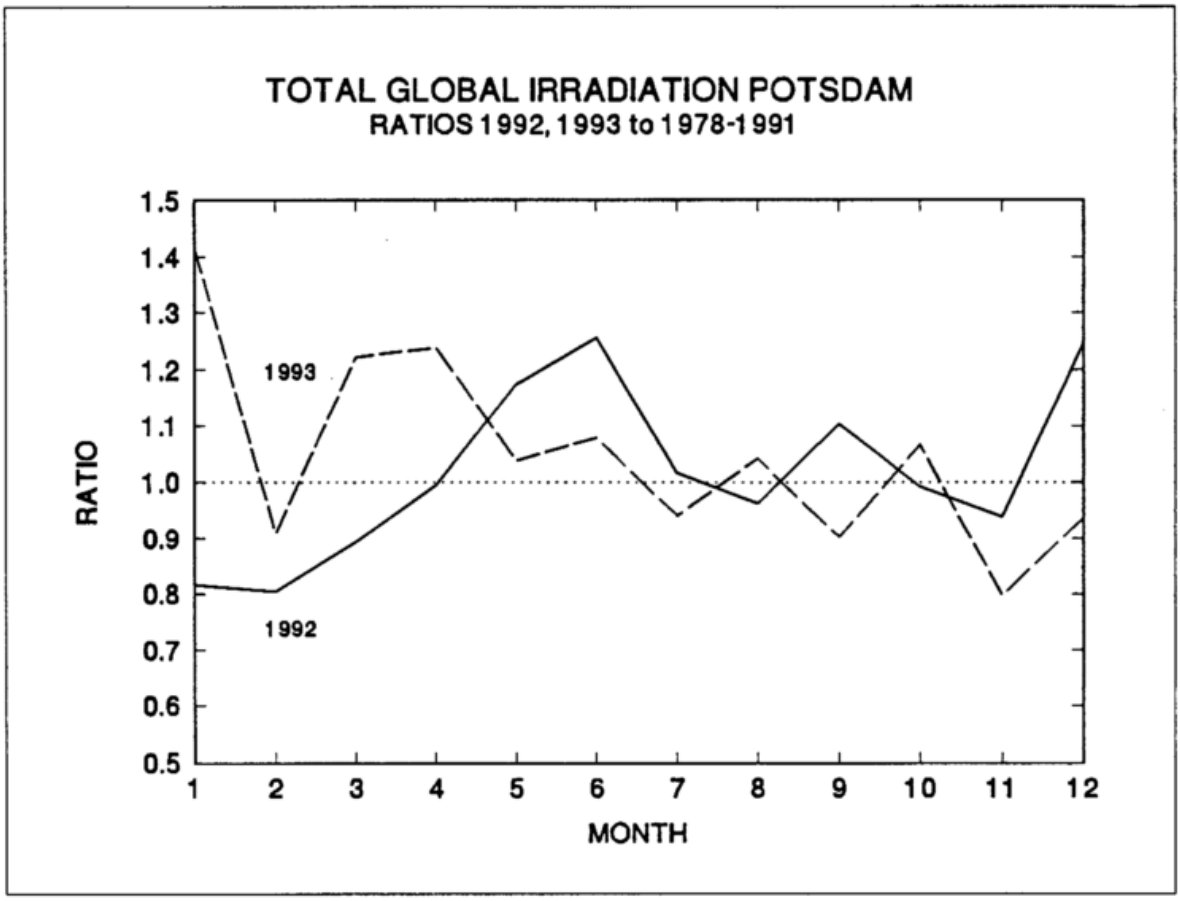

Fig. 31 Ratios between measured monthly totals of global irradiation (380 - 2800 nm) in 1992, 1993 and long-term mean values (1978 - 1991)

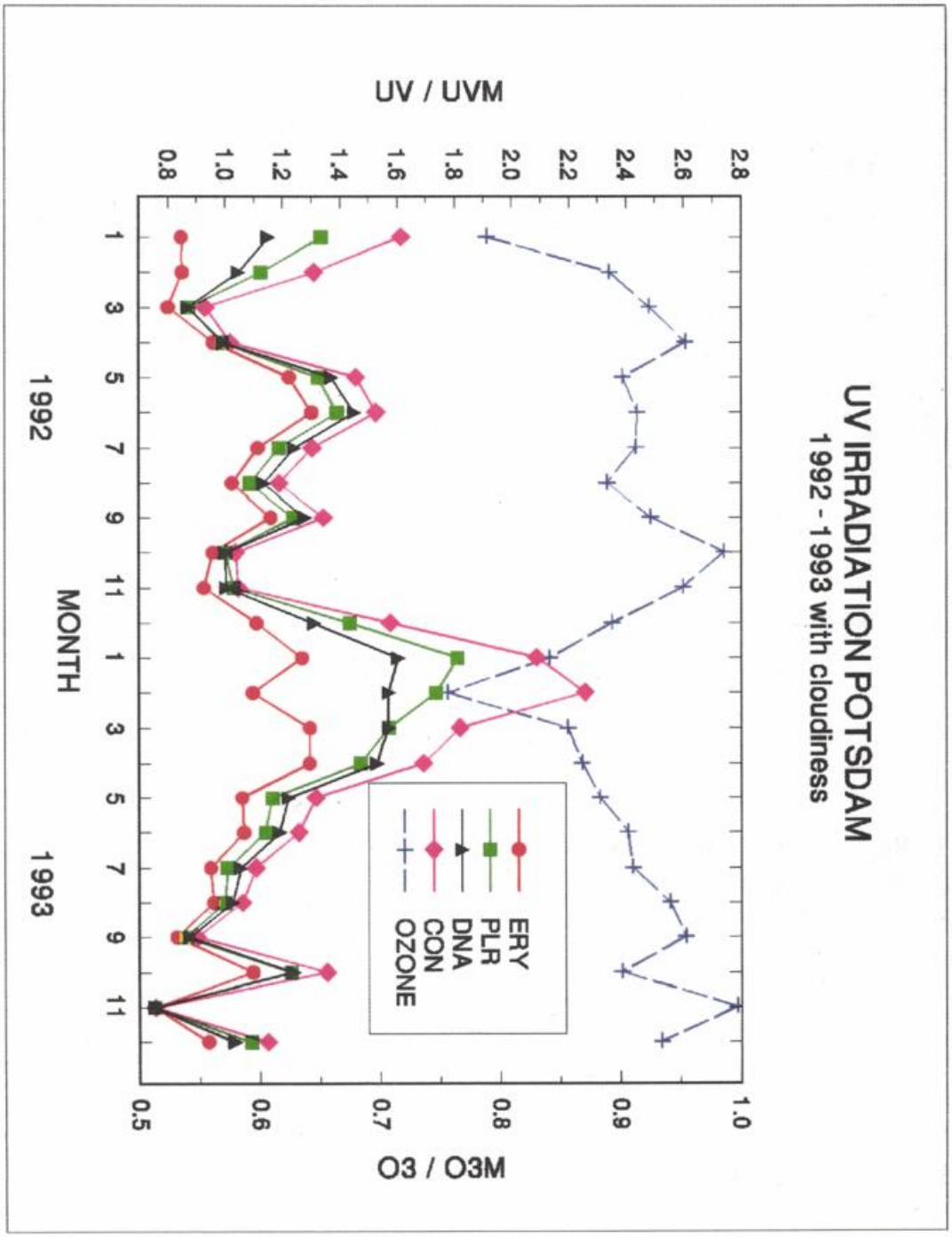

Fig. 32 Ratios between modelled effective irradiation for 1992, 1993 and the long-term averages of effective UV irradiation including the effects of changing ozone, cloud cover and aerosol load

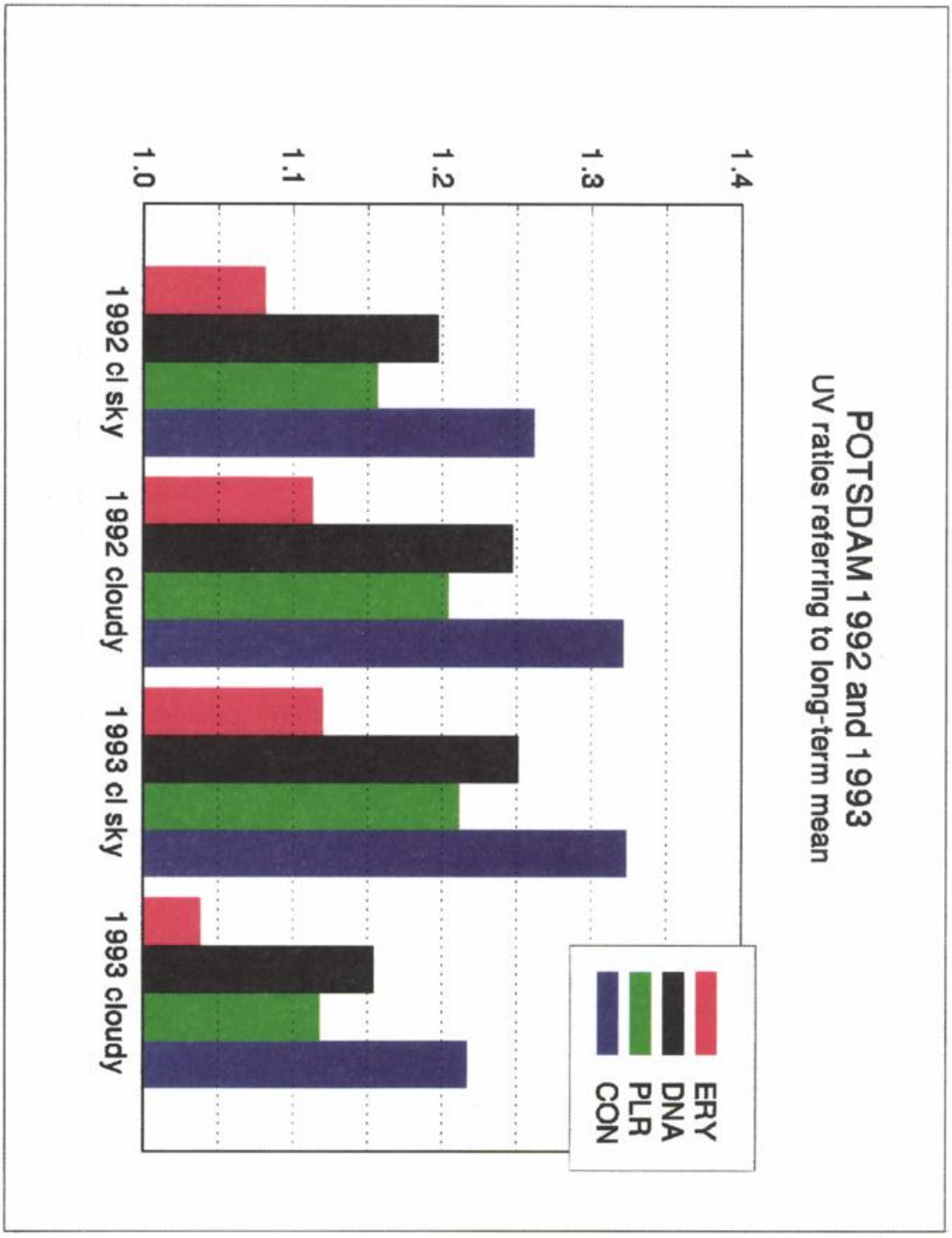

Fig. 33 Ratios between annual totals of effective UV irradiance in 1992 and 1993 referred to the long-term average 1978-1991

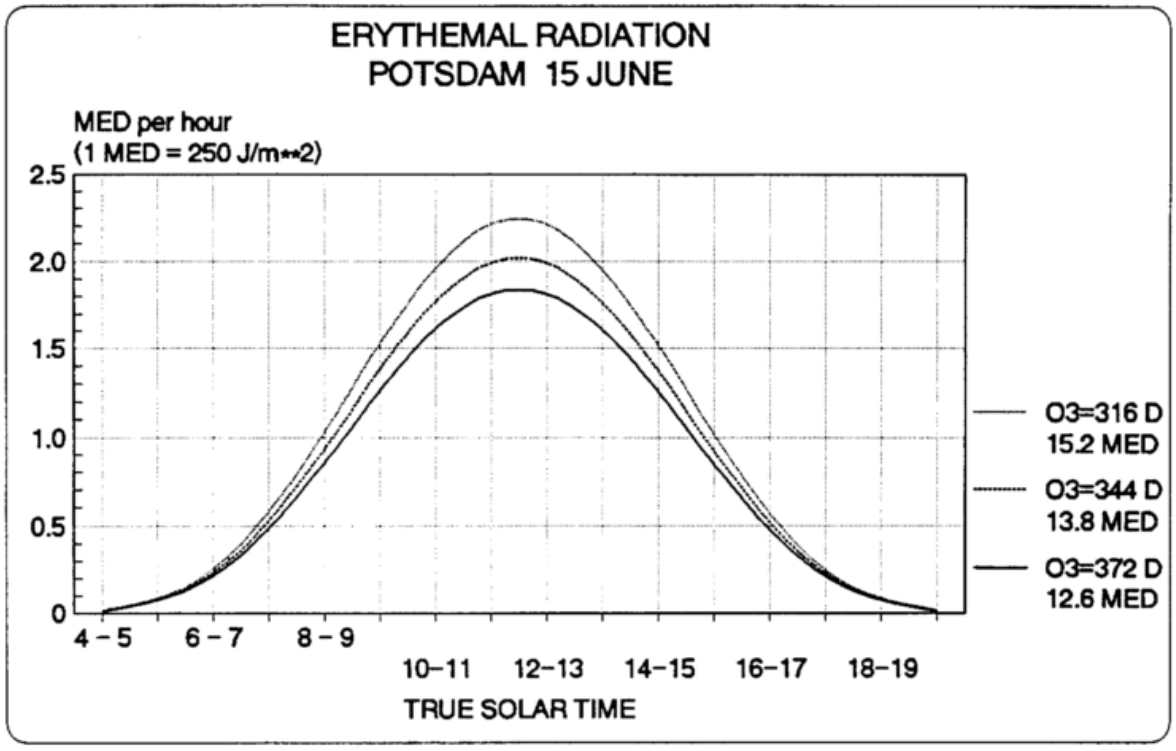

Fig. 34 Erythemal irradiation (action spectrum from CIE 1987) calculated for three different ozone values at Potsdam on June 15

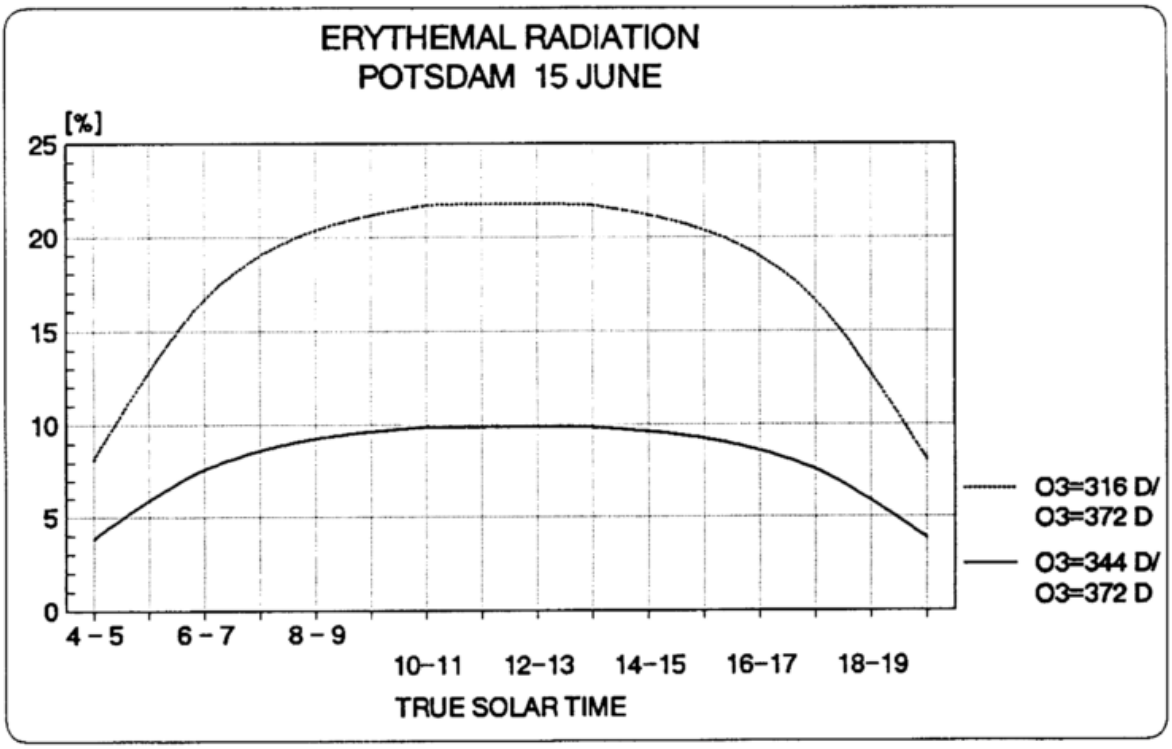

Fig. 35 Percentage ratios between irradiation modelled for ozone values diminished by 1 σ (344 D) and 2 σ (316 D) standard deviation of ozone, respectively, and irradiation modelled for the average ozone of 372 D in June at Potsdam

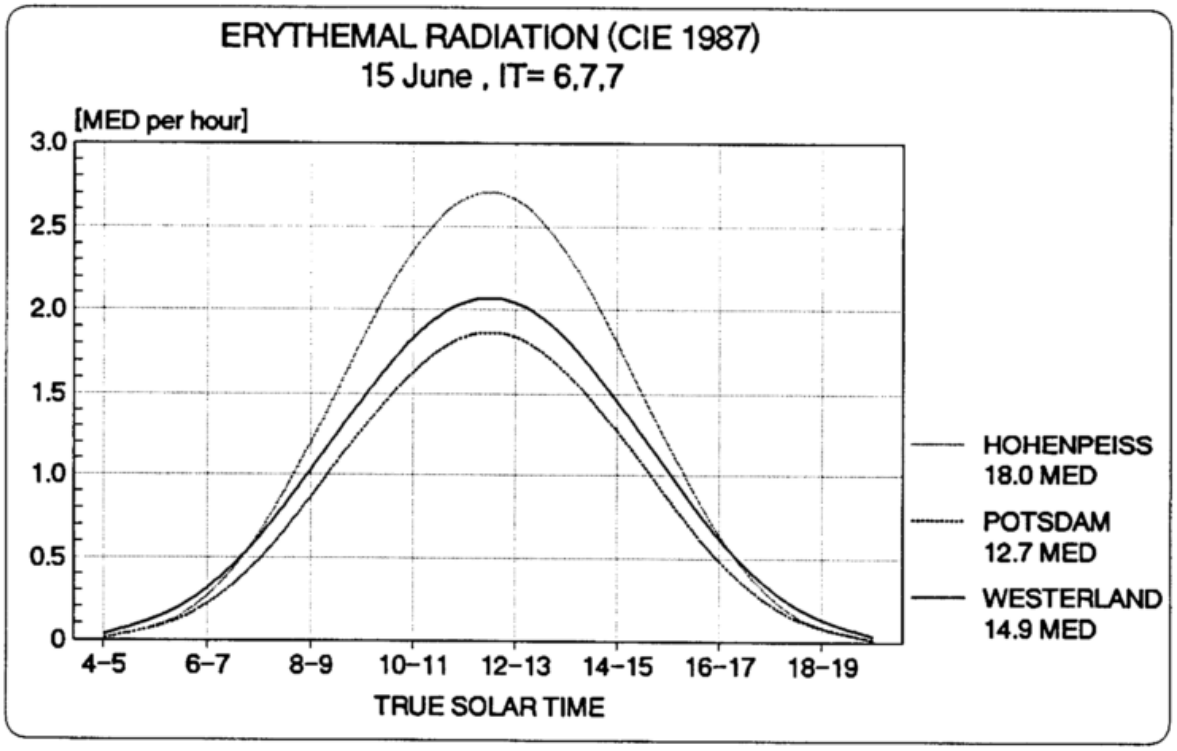

Fig. 36 Hourly totals of erythemal irradiation (action spectrum from CIE 1987) determined for Westerland (55° N), Potsdam (52° N) and Hohenpeissenberg (48° N) on June 15 for clear sky (1 MED = 250 $(J\ m^{-2})_{ERY}$)

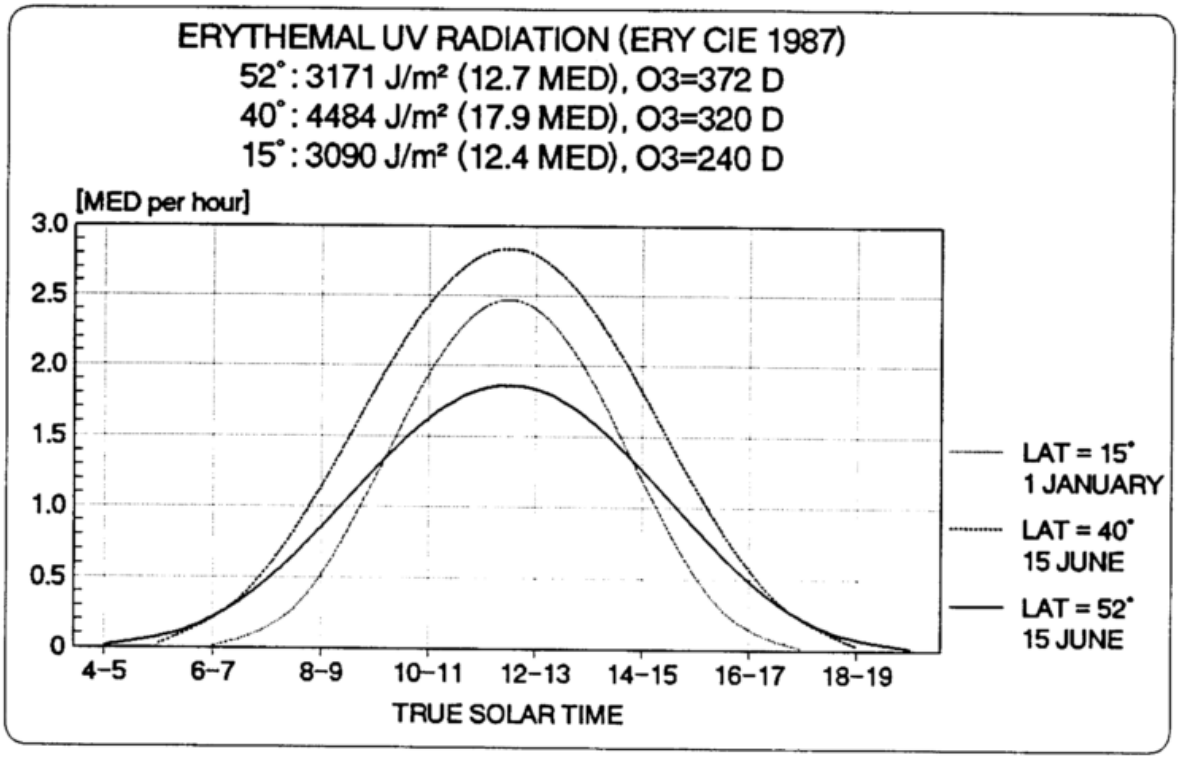

Fig. 37 Hourly totals of erythemal irradiation at three latitudes and dates

____	15 June,	52° N
-----	15 June,	40° N
.....	1 January,	15° N

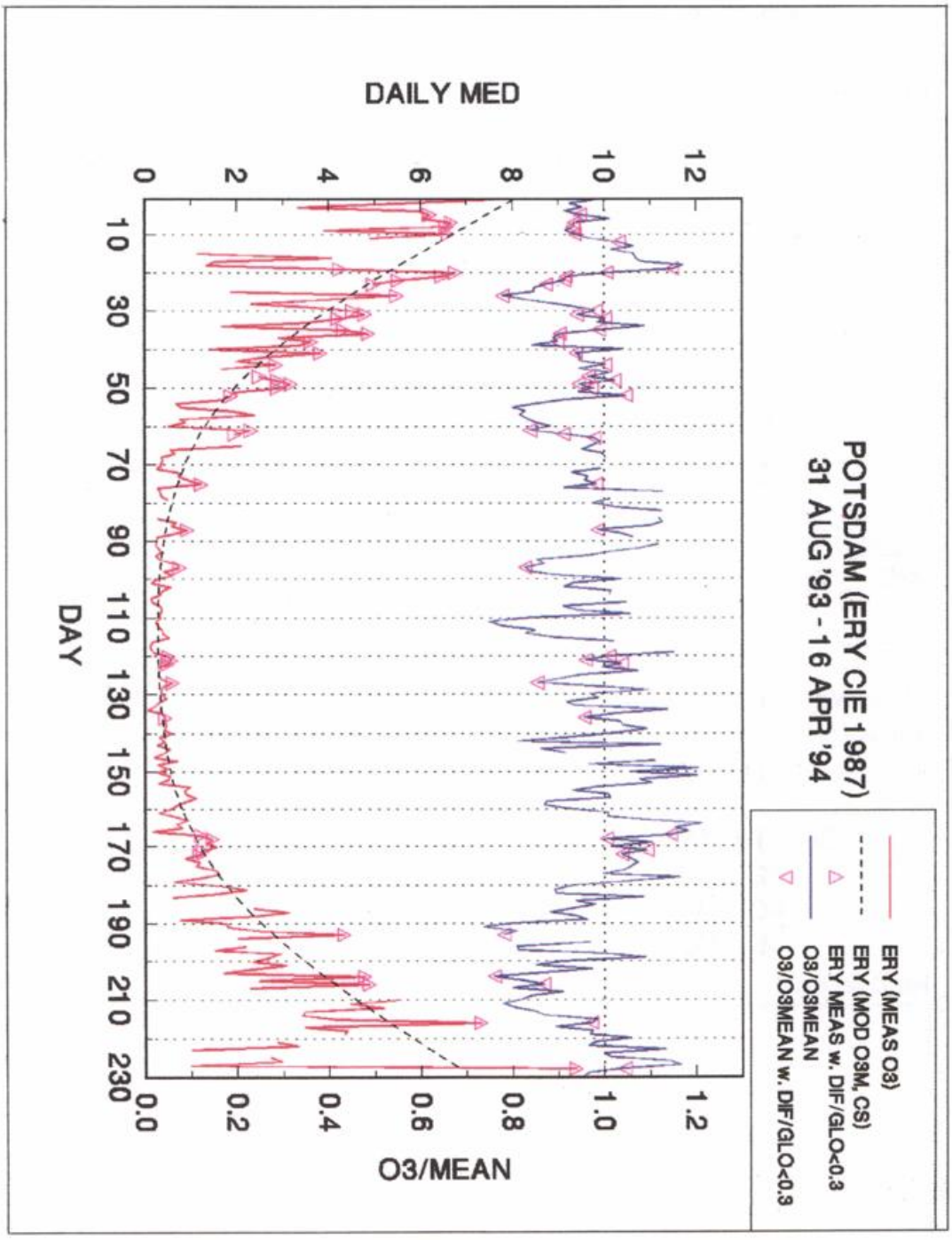

Fig. 38 Daily MED as determined from spectral measurements with the Potsdam Brewer spectrometer from 31 August 1993 to 16 April 1994. Spectra were folded with the erythemal action spectrum of CIE (1987). Multiplication with the erythemal threshold value of 250 $(J\ m^{-2})_{ERY}$ provides the erythemal irradiation. Days with ratios between diffuse and global total irradiation (380 - 2800 nm) less than 0.3 are designated by triangles. Ratios between daily mean ozone values as derived from observations with Dobson spectrophotometer #71, and long-term mean ozone values are shown on top (right-hand ordinate scale).

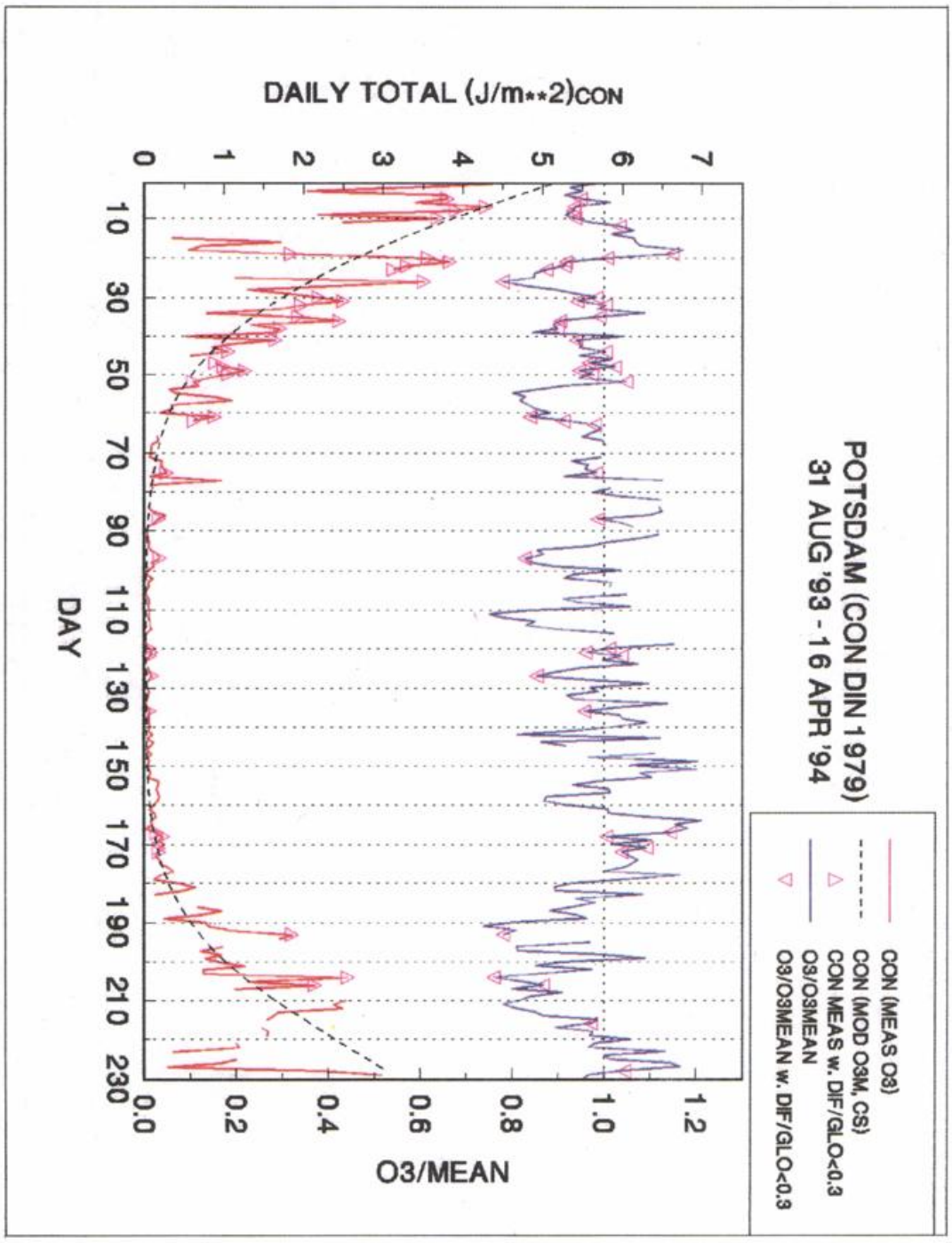

Fig. 39 Daily photoconjunctivitic irradiation as derived from spectral measurements with Brewer spectrophotometer #30 at Potsdam. Spectra were folded with the action spectrum of photoconjunctivitis of the eye (DIN 1979). Days with ratios between daily sums of diffuse and global total irradiation (380 - 2800 nm) less than 0.3 are designated by triangles. Ratios between daily mean ozone values as derived from observations with Dobson spectrophotometer #71, and long-term mean ozone values are shown on top (right-hand ordinate scale).